Dissertation
submitted to the
Combined Faculties for the Natural Sciences and for Mathematics
of the Ruperto-Carola University of Heidelberg, Germany
for the degree of
Doctor of Natural Sciences

presented by

BSc Cell and Molecular Biology Johanna Höög, 17th of July 2003, Oxford Brookes University

born in: Trollhättan, Sweden

Oral-examination:: .....

The 3D Architecture of Interphase Microtubule Cytoskeleton and Functions of Microtubule Plus End Tracking Proteins in Fission Yeast

Referees: Dr. Damian Brunner
PD Dr. Harald Herrmann-Lerdon

Summary

The microtubule (MT) cytoskeleton is important for establishing polar growth in the rod-shaped fission yeast (*Schizosaccharomyces pombe*). In these cells, MTs form an architectural scaffold of the cell by positioning organelles such as the nucleus and mitochondria.

Interphase MTs are arranged in bundles along the cell's long axis. The filaments start growing in the cell's middle in a zone of anti-parallel overlap, from which the more dynamic plus ends of MTs extend towards both cell ends.

After cell division the cell grows exclusively from the old end (away from the septum), where the growth machinery is still present from the mother cell. New end take off (NETO) occurs after about a third of the way through the cell cycle, when F-actin has moved into the new end. From this point onwards maintenance of polar growth is MT independent and occurs at both cell ends.

Guidance of the microtubules to the cell ends is performed by plus end tracking proteins (+TIPs), such as Tea1 and Tip1 (Clip-170). Tea1 is a landmark protein localizing to the cell ends. Tip1 is an anti-catastrophe factor that prevents MT depolymerization before the filament has reached the cell end. The delivery of Tip1 to MT ends is motors dependent and another +TIP, Mal3, anchors it at the MT end. Mal3 (EB1) stabilizes MTs, possibly by fortify its seem.

Here we describe a large-scale, electron tomography investigation of wild-type (WT) *S. pombe* cells, including the first 3D reconstruction of a complete eukaryotic cell volume. Sufficient resolution to show both how many MTs there are in a bundle and their detailed architecture was achieved. Most cytoplasmic MTs are open at one end and capped at the other, providing evidence about their polarity. Electron-dense bridges between the MTs themselves and between MTs and the nuclear envelope were frequently observed. Finally, we have investigated structure/function relationships between MTs and both mitochondria and vesicles.

Using the same approach, we then analyzed the bundle architechture in *tip1Δ* and *mal3Δ* mutants. MTs were half the length of WT in *mal3Δ* and a quarter the length of WT in *tip1Δ*. Further, there were less than half as many MTs in a bundle in *tip1Δ* then in WT. In contrast, *mal3Δ* bundles no difference in the amount of filaments in a bundle. However, structural differences of the MT lattice were observed in both mutants. The interaction between MTs and the spindle pole body was altered in both strains.

Our analysis shows that electron tomography of well-preserved cells is ideally suited for describing fine ultrastructural details that were not visible with previous techniques.

Zusammenfassung

Die Mikrotubuli üben bei der Etablierung des polaren Wachstums der stäbchenförmigen Spalthefe (*Schizosaccharmomyces pombe*) eine wichtige Funktion aus. Durch die Positionierung der Organellen wie Zellkern und Mitochondrien bilden sie außerdem ein architektonisches Gerüst für die innere Organisation der Zelle.

Sie wachsen durch Polymerisierung von Tubulinuntereinheiten an ihren Plusenden in Richtung beider Zellpole. Die Minus-Enden der Filamente befinden sich im Zentrum der Zelle in einer Zone antiparalleler Űberlappung.

Nach der Mitose wächst die neue Zelle ausschließlich an dem bereits existierenden Ende (gegenüber des Septums), an dem die Wachstumsmaschinerie der Mutterzelle noch vorhanden ist. Nach ungefähr einem Drittel des Zellzyklusses, nachdem das neue Ende durch Rekrutierung von F-Aktin stabilisiert worden ist, findet der sogenannte 'New End Take Off' (NETO) statt. Ab diesem Zeitpunkt ist die Aufrechterhaltung des polaren Wachstums unabhängig von den MT und tritt an beiden Zellenden auf.

Die Dirigierung der MT zu den Zellenden wird von den 'plus end tracking proteins' (+TIPs), wie zum Beispiel Tea1 and Tip1 (Clip-170), ausgeführt. Tea1 ist ein Markierungsprotein, welches an beiden Zellenden lokalisiert ist. Tip1 verhindert Depolymerisierung der MT bis diese das Zellende erreicht haben. Diese Faktor wird von Motormolekülen zu MT-Enden transportiert und dort von einem anderen +TIP Protein, Mal3, verankert. Mal3 (EB1) stabiliziert die MT, warscheinlich durch Verstärkung des Saums.

Hier beschreiben wir die Untersuchung von Wildtyp (WT) *S. pombe* Zellen mittels Elektronentomographie in grossem Maßstab einschließlich der ersten 3D Rekonstruktion eines vollständigen eukaryotischen Zellvolumens. Aufgrund der hohen Auflösung konnten sowohl die Anzahl der MT pro Bündel als auch ihre detaillierte Architektur gezeigt werden. Die meisten zytoplasmischen MT lagen an einem Ende offen und am anderen geschlossen vor, was Rückschlüsse auf ihre Polarität zuließ. Ausserdem wurden häufig elektronendichte Brücken zwischen den MT selbst sowie zwischen MT und der Hülle des Zellkerns beobachtet. Schließlich konnten Einblicke in die Struktur- und Funktionsbeziehungen von MT zu Mitochondrien und Vesikeln gewonnen werden.

Im nächsten Schritt haben wir in derselben Vorgehensweise die Bündelarchitektur von *tip1Δ* und *mal3Δ* Mutanten analysiert. Die MT waren im Vergleich zum WT in *mal3Δ* Zellen um die Hälfte, in *tip1Δ* sogar um drei Viertel verkürzt. Ausserdem bestand in *tip1Δ* ein Bündel aus weniger als halb so vielen MT als im WT. Im Gegensatz hierzu wurde in *mal3Δ* kein Unterschied bezüglich der Zahl an Filamenten pro Bündel festgestellt. Allerdings wurden in beiden Mutanten strukturelle Veränderungen des MT Gitters beobachtet. Auch die Interaktion zwischen MT und dem Spindelpolkörper war in beiden Hefestämmen gestört.

Unsere Ergebnisse zeigen, dass die Elektronentomographie von gut erhaltenen Zellen eine ideale Methode darstellt, um ultrastrukturelle Details zu erforschen, welche mittels früherer Techniken nicht sichtbar waren.

Chapter 1

Introduction

To keep different cellular components correctly positioned to each other is important for the proper function and division of all cells. Here, we are using the rod-shaped fission yeast (*Schizosaccharomyces pombe*) as a model organism for cell polarity and polar growth. Fission yeast grows in the cell ends, where actin and proteins important for maintenance of polar growth are found. The deposition of these proteins and the establishment of the growth axis is performed by bundles of microtubules (MTs). Thus, linear growth is MT dependent in these cells (Hayles and Nurse 2001; La Carbona et al. 2006; Sawin and Tran 2006).

The MT cytoskeleton organization and dynamics have been extensively studied using fluorescence microscopy. However, due to the limitation in resolution of light microscopy, important fine architectural details of these bundles are still unknown. Therefore we undertook a high resolution investigation of the interphase MT cytoskeleton using electron tomography.

The concept of electron tomography (ET) has existed since the 1970's, but has only recently been widely applied, mostly due to computers becoming capable to handle the huge data sets and complex calculations this process entails. In general, ET is a method to generate high resolution 3D reconstructions of a small sample (McIntosh et al. 2005). Here, we extended the limits of this technique, so that reconstruction of the first complete eukaryotic cell volume was possible.

At this high resolution, MT bundle architecture and MT importance in organelle positioning was readily seen. Even fine structures such as MT end morphologies and electron dense bridges between MTs could be visualized. Advantages of 3D reconstructions

were particularly obvious when intra-organellar measurements could be done. Our analysis shows that the combination of native cell preservation and electron tomography is ideally suited for describing fine ultrastructural details that were not visible with previous techniques.

We also applied this new methodology to two microtubule associated protein (MAP) deletion mutants, to further reveal these proteins' functions in MT arrangement. Finally, we imaged cells treated with a MT depolymerizing drug to expand our analysis of MT structure and function as well as organellear positioning in the fission yeast.

The fission yeast is a free living single-celled archiascomycete fungus that diverged from budding yeast (*Saccharomyces cerevisiae*), another commonly used model organism, over one billion years ago (Heckman et al. 2001). When its genome was sequenced in 2002 it was the sixth completed genome and the eukaryote with the fewest protein coding genes, (containing 4824 open reading frames) (Wood et al. 2002).

Kingdom:	Fungi
Phylum:	Ascomycota
Class:	Schizosaccharomycetes
Order:	Schizosaccharomycetales
Family:	Schizosaccharomycetacetae
Genus:	Schizosaccharomyces
Species:	*S. pombe*

We use this yeast as a model organism for microtubule (MT) dependent cell polarity because of its easily recognizable rod-shaped form and genetic tractability. Like budding yeast, the small genome ensures little overlap in protein function. Thus, deletion mutants often display clear phenotypes. However, fission yeast seems closer to mammalian cells than budding yeast in many ways. For example, many of the cellular organelles in fission yeast and mammalian cells are dependent on MTs for their intracellular distribution. In budding yeast, which is almost constantly in mitosis, the majority of MTs are intranuclear and cytoplasmic organelle distribution is often actin dependent.

Fission yeast is also a model organism for the cell cycle, and these studies, lead by Sir Paul Nurse, culminated in a shared Nobel Prize in physiology or medicine 2001.

Morphogenesis and Cell Polarity in Eukaryotes

1. Cellular Polarization and Cell Shape

A drop of oil in water forms a micelle. Similarly, a lipid cell membrane in aqueous media should create a micelle structure. However, cells commonly have different shapes, the typical examples being neurons and epithelial cells (Wilson 1997; Goldstein and Yang 2000).

Even round cells may be polarized when regions of membrane or cytoplasm are populated with a different set of, or proportions of, cellular constituents. This polarization is often vital for that cell's function and future divisions. A good example of this is the budding yeast. Although the mother cell has an approximately round cell shape, the previous division, in which a daughter cell budded off, has left membrane bound polarity markers. These will determine where the next bud will appear (Drubin and Nelson 1996).

2. General Principles of Polarization

Cell polarization is often a response to extracellular cues such as hormones, nutrients, attractants, repellants or pheromones. Cells also carry internal landmarks inherited from their parents that guide polarization without environmental input (Drubin and Nelson 1996).

In general, establishment of cell polarity can be conceptualized in four steps. First, determination of a site on the cell surface according to internal or external cues occurs. Second, this site is marked by a landmark protein. Third, small GTPases close to the site establish cell polarity. Fourth and finally, reorganization of the cytoskeleton and other polarized components leads to polarized cell growth (Drubin 1991; Pringle et al. 1995).

One well studied example, reviewed in (Chang and Peter 2003; Irazoqui and Lew 2004; Pruyne et al. 2004), is the previously mentioned asymmetrically growing budding yeast. Growth in these cells is largely restricted to the daughter bud. During G1 phase of

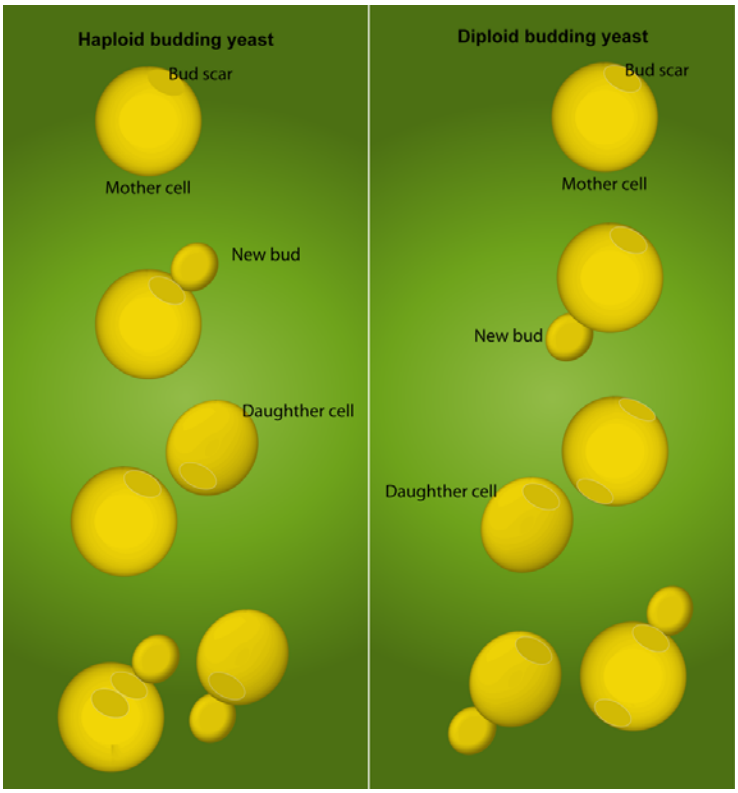

Figure 1 Budding patterns in *S. cerevisiae*. Haploid cells form new buds next to the old bud scar. Diploid cells bud at the opposing side of the last bud site.

the cell cycle, the round unbudded cell establishes the site of bud formation. In haploid cells the bud forms adjacent to the site of the previous cell division, the bud scar. This creates an axial budding pattern in both the mother and daughter cell. In diploid cells the new bud emerges opposite to the last bud scar in a bipolar budding pattern (figure 1). I give a short introduction to the mechanism of cell polarization in haploid budding yeast cells.

At the bud site, a large number of proteins get concentrated into a patch, approximately 0.5 µm in diameter. The size of this patch is thought to be regulated by the assembly of septin, a filament-forming GTPase, into a ring. Thus, the septin ring may be the first intracellular cue determining the site of polarization. Second, the septin ring

recruits the landmark proteins Bud3p, Bud4p and Bud10p to the bud site, which in turn recruit Bud5p. Bud5 then activates Rsr1p GTPase by phosphorylation. This triggers a cascade that establishes the axis of polarity through activation of the GTPase Cdc42p and its GEF Cdc24p. Finally, GTP-Cdc42 is thought to induce nucleation of actin cables in its vicinity, which then deliver secretory vesicles to the nucleation site, creating a cell wall distortion and the initiation of the bud (Li et al. 1995).

It is common that the cytoskeleton or parts of the cytoskeleton are involved in the establishment and maintenance of polar growth. Before describing polarity in fission yeast, I will give a short introduction to the cytoskeleton in general and to MTs in particular.

The Cytoskeleton

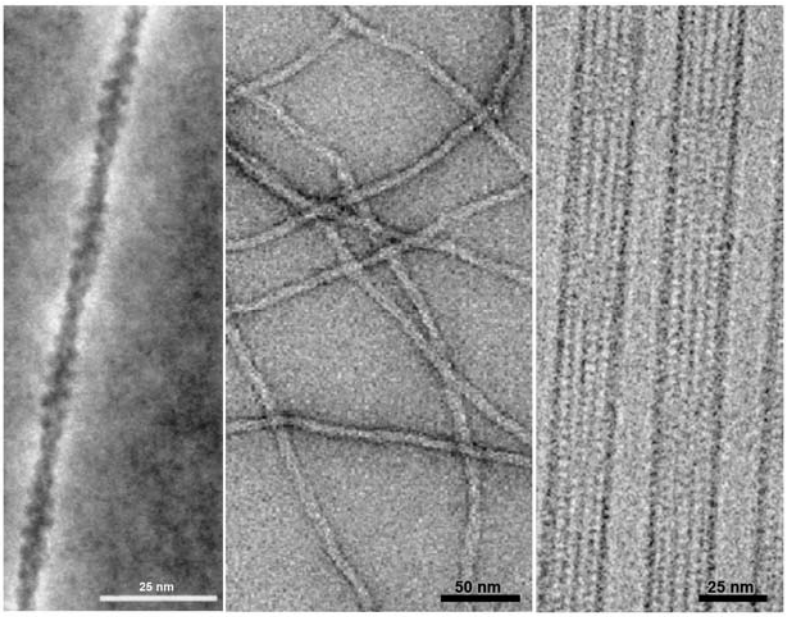

Figure 2 The cytoskeleton A) Negative stain of an actin filament (Steinmetz et al. 1997) B) Negatively stained vimentin intermediate filaments with a dimater of ca 12 nm (O'Toole et al. 2003; Goldie et al. 2006) C) Cryo-electron micrograph of an *in vitro* assembled microtubule. (Krebs et al. 2004)

The eukaryotic cytoskeleton has three filamentous components: actin, intermediate filaments (IFs) and MTs (figure 2).

In general, actin is found at the cell periphery and in the actin-myosin ring during cell division. Amongst other roles, actin is involved in endocytosis, intracellular transport and cell motility. IFs are usually found in the cytoplasm and the nuclear lamina, where they give physical support to the cell and the nucleus.

The last component, the MT network, is of particular interest to us, ad these polymers are important to support cell shape. During interphase, MTs are long filaments commonly radiating out from a point close to the nucleus toward the cell periphery. Some of MTs functions are intracellular trafficking and distribution of molecules and

organelles, and providing a mechanical support for the cell against stress and shear forces. During mitosis, MTs reorganize to a bipolar spindle responsible for segregation of the chromosomes into the daughter cells.

1. Actin

In polar cells, actin is localized in the growth zone, where it forms protrusions of the plasma membrane by pushing forces created when filaments in the network polymerize in the plus end and simultaneously depolymerize at the minus end. This process is called treadmilling and is also a behavior displayed by MTs.

Monomeric globular actin protein (G-actin) can form flexible filaments, 5-9 nm in diameter. The high resolution structure of the filamentous form (F-actin) is still unknown. However, lower resolution models have been suggested from actin fiber diffraction experiments, where actin is shown to be a right handed two stranded helix (Holmes et al. 1990). The polymer has an internal polarity, due to the head-to-tail assembly of the actin subunits, where the plus (barbed) end is more dynamic than its minus (pointed) end (Kabsch and Vandekerckhove 1992; Steinmetz et al. 1997).

However, G-actin structure is determined and shows a protein with two large domains connected by a hinge and a nucleotide binding site located in a cleft between the domains (Klenchin et al. 2006). The nucleotide, ATP, is hydrolyzed into ADP following polymerization into F-actin, probably inducing a structural change to the actin molecule (Page et al. 1998).

The dynamic assembly and disassembly of filaments and the formation of larger scale filament structures are crucial aspects of actin's function. Therefore, nucleation, capping, stabilizing, severing, depolymerizing, cross-linking, bundling, sequestering or delivering of monomers or promoting nucleotide exchange are processes tightly regulated by numerous actin binding proteins (ARPs) (Ayscough and Winder 2004).

The first stage in *de novo* filament formation is nucleation. So far, three different groups of nucleators have been identified - the arp2/3 complex, the formins and the spires, as reviewed in (Zigmond 2004; Kerkhoff 2006). In budding yeast it is thought that the formins nucleate the long actin cables required for cell polarity, and that arp2/3

complex initiates the branched actin patches found for example at sites of endocytosis (McCollum et al. 1996; Feierbach and Chang 2001).

2. Intermediate Filaments

In contrast to actin and tubulin, which are found in all eukaryotes, IFs are mostly found in metazoans. However, a budding yeast protein important in organelle positioning has been shown to form IFs *in vitro* (McConnell and Yaffe 1993), and long coiled coil proteins are commonly found both in yeast and plants (Rose et al. 2004). Thus, these proteins may be present in more organisms and important in multiple processes within these cells.

The best understood function of IFs is to provide a scaffold that maintains cell and tissue integrity (Omary et al. 2004). They are composed of different coiled coil proteins (~60 diverse proteins in humans only), that are expressed tissue-specifically. Common IFs are keratins, the main component in hairs and nails, neurofilaments, which are deposited during axon growth and which determine the thickness of axons, and vimentin, which is expressed in endothelial cells and fibroblasts.

This group of coiled coil proteins share a tripartite domain structure; an N-terminal head, a central rod consisting of mostly α-helices, and a C-terminal tail (reviewed in (Herrmann and Aebi 2004). The sequence identity is low but there are two conserved IF consensus motifs, one in each of the N- and C-terminal domains.

The rod forms a dimer with a parallel molecule, which in turn associates with an anti-parallel dimer, creating the basic tetramer. These proteins are insoluble in buffers of physiological pH and ionic strength. It is thought that this insolubility causes the formation of rope like filaments, where 6-10 tetramers are gathered in each cross section. This fluctuation of filament thickness is also seen within a filament built of the same protein, therefore the filament width varies from 8-12 nm.

IFs also differ from tubulin and actin by being non-polar and currently no molecular motors are known to travel along this cytoskeletal element. Nevertheless, these fibers are thought to be highly dynamic structures within the cell and several reports have shown transport of IFs along MTs, as reviewed in (Helfand et al. 2004).

Interest in IFs is increasing rapidly as more and more diseases caused by mutations in the polymerizing proteins are found (reviewed in (Magin et al. 2004; Omary et al. 2004) and new model systems emerge as in the hag fish slime, consisting of micron thick IFs (Fudge and Gosline 2004).

3. Microtubules

Formatted: Bullets and Numbering

A. The Structure and Polarity of Eukaryotic Tubulin and MTs

MTs are vital for the establishment of cell polarity, motility, vesicle trafficking and formation of the mitotic/meiotic spindles. Tubulin, the protein forming MTs, is one of the most conserved eukaryotic proteins and is essential in all eukaryotic cells. Even though prokaryotes do not have a tubulin homologue, a conserved prokaryotic protein, FtsZ, of a remarkably similar structure that also creates filaments has been discovered (Lowe and Amos 1998).

MTs are hollow cylinders with a diameter of 25 nm. These cylinders consist of tubulin α-,β-dimers that connect in a head-to-tail fashion to form protofilaments, which in turn associate laterally into MTs. Most MTs *in vivo* consist of 13 laterally associated protofilaments (Tilney et al. 1973). *In vitro* the number of protofilaments in a MT can fluctuate between 10 and 16, thus the cylinder diameter may vary between filaments (Desai and Mitchison 1997). The head-to-tail arrangement of the tubulin heterodimers creates a polarized filament where the α-tubulin subunit is exposed at the MT minus end and the β-tubulin subunit at the opposing plus end.

The α- and β-tubulin encoding genes share 40% sequence identity and, as expected, their structures are very similar (Nogales and Wang 2006b; Tuszynski et al. 2006). Both tubulins are 4 nm long and have a nucleotide interaction site, which binds a GTP molecule when in the unpolymerized state.

Even though the MT lattice has been shown to have some flexibility as it changes confirmation upon kinesin binding (Krebs et al. 2004), most changes in MT structure occur at the filament ends, in a process called dynamic instability (Mitchison and Kirschner 1984).

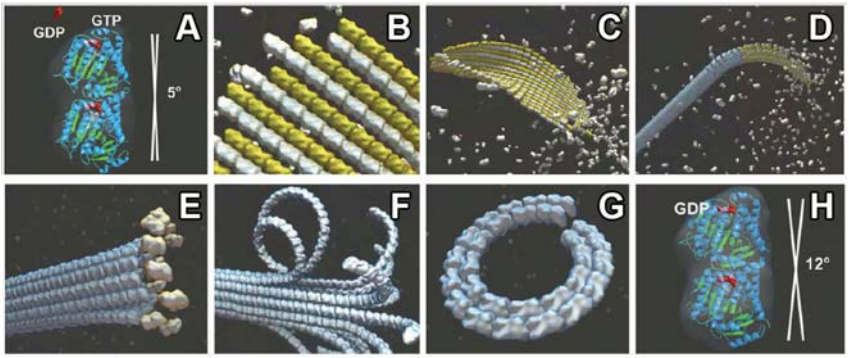

Figure 3 Dynamic instability Microtubule assembly: A) The straight GTP-tubulin dimer B) GTP tubulin self assembly into sheets or ribbons C) Closing of the sheet into a cylinder D) zipping of the sheet into a microtubule.
Microtubule disassembly E) Loss of GTP cap F) Protofilament peeling G) ring disassembly intermediate H) GDP dimer in the relaxed curved state (the lines indicate the axis of the two monomers within the dimer) (Nogales and Wang 2006a).

B. The MT Dynamic Instability Model

Formatted: Bullets and Numbering

MTs undergo cycles of rapid growth and disassembly in a process known as dynamic instability. This has been extensively studied both *in vitro* and *in vivo* (Mitchison and Kirschner 1984).

The GTP molecule bound to the β-tubulin in the α,β-dimer is hydrolyzed to GDP after MT polymerization. Dimers still bound to a GTP molecule have a straight structure which forms a GTP cap on the growing end of the MT (Chretien et al. 1995; Nogales et al. 1998; Chretien et al. 1999; Lowe et al. 2001; Nogales and Wang 2006a). Upon hydrolyzation, the tubulin conformation changes to a curved state that destabilizes the lattice (Howard and Timasheff 1986; Melki et al. 1989; Mandelkow et al. 1991; Hyman et al. 1995; Muller-Reichert et al. 1998).

The straight conformation of the GTP tubulin in growing MT ends enables the formation of tubulin sheets *in vitro*. These sheets are thought to close up into a cylinder that is then zippered up into a MT (figure 3) (Erickson 1974; Kirschner et al. 1975; Simon and Salmon 1990; Chretien et al. 1995). Studies in *Xenopus* extract showed that these MT end structures also exist in a physiologically more relevant environment (Arnal et al. 2000). However, it is still not known how a growing MT end looks like *in situ*.

Similarly, studies of depolymerizing MTs *in vitro* have shown curling 'rams-horn' structures created by individual protofilaments curling back from the MTs due to the loss of the GTP cap (Mandelkow et al. 1991; Muller-Reichert et al. 1998). MT growth is regulated by many factors, such as the concentrations of free tubulin and microtubule associated proteins. A decrease or increase of one or more of these factors can cause an environmental change more favorable for MT shrinkage or growth. A transition from MT growth to shrinkage is called 'catastrophe'. 'Rescue' occurs when the MT returns to growth after a shrinking phase. The dynamic instability model enables a thorough description of the MT dynamics based on four key parameters: growth and shrinkage speed, catastrophe and rescue frequency (Walker et al. 1988).

Most of this dynamic instability occurs on the MT plus end *in vivo*, since the minus end is often capped by the nucleating γ-tubulin ring complex normally found near centrosomes.

C. MT Nucleation by Centrosomes and other MTOCs

Formatted: Bullets and Numbering

Most cells contain a site that controls the organization of MTs. This is commonly referred to as the MT organizing center (MTOC). In the majority of animal cells, MTs grow with their minus ends anchored at a perinuclear positioned centrosome, with their plus ends radiating out towards the cell periphery (Ou and Rattner 2004).

A centrosome is composed of a pair of centrioles and a surrounding fibrous matrix, the pericentriolar material. Five further members of the tubulin protein superfamily – γ-, δ-, ε-, η- and ζ can be found on the centrosome or basal bodies (Tuszynski et al. 2006). Sequence identity of the γ-, δ-, ε-, ζ- and η-tubulin are well conserved between species, although yeasts and plants do not appear to have clear homologues of all tubulin variants.

The γ-tubulin protein is the best characterized of the centrosomal tubulins (Wiese and Zheng 2006). It is part of the 2.2 MDa γ-tubulin ring complex (γ-TURC) that nucleates new MTs around the centrosomes and other MTOCs by acting as a ring template (Keating and Borisy 2000; Moritz et al. 2000; Wiese and Zheng 2000). This makes MT nucleation possible at the low concentrations of free tubulin that are found in cells (figure 4).

However, the cellular function of the centrosome is debated. Previously it was believed to be essential in the mitotic spindle, where it gathers the MTs minus ends at the poles. Supporting this, cancer cells often show multiple centrosomes, causing chromosome missegregation (Fukasawa 2005). However, studies in *Xenopus* extract have shown that mitotic spindles can form in the absence of centrosomes (Heald et al. 1997). Furthermore, whole flies can develop into adults without centrosomes, showing that the centrosome can be dispensable during cell division (Basto et al. 2006). Plants and yeast have also no conventional centrosomes, but still have highly organized MT arrays (Murata et al. 2005).

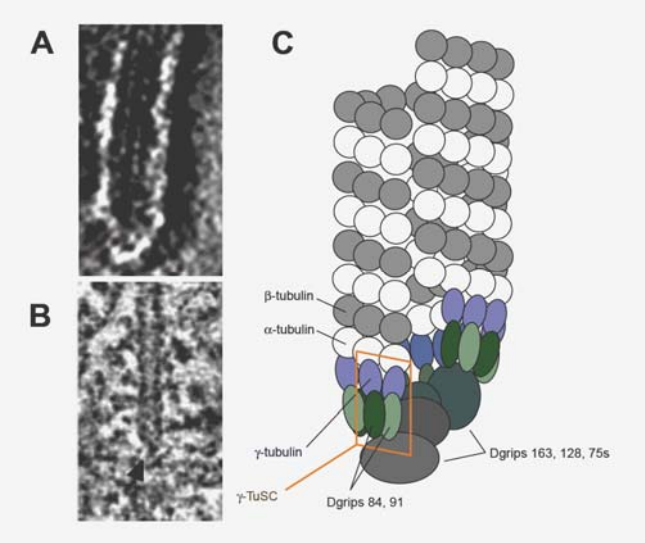

Figure 4 Tomography of the gamma tubulin ring complex A) γ-TURC in complex with MT **B)** Slice from a capped MT in a *C. elegans* mitotic centrosome **C)** Model of MT nucleation by the template action of the γ-TURC (Moritz et al. 2000; O'Toole et al. 2003)

D. Structure of Centrosomes and SPBs

Formatted: Bullets and Numbering

The basic structure of a centrosome has been described as two centrioles (the mother and an orthogonally growing daughter), and the pericentriolar material (PCM). The PCM is a fibrous matrix in which one can find the γ-TURCs. Centrioles are 100-150 nm wide and 100-400 nm long barrel structures with nine fold symmetry of singlet, doublet or triplet MTs (Pelletier et al. 2006).

As previously mentioned, plants and fungi have no conventional centrosomes. However, in fungi there is a centrosome equivalent called a spindle pole body (SPB), the structure of which varies between species (figure 5). The layered SPB of *S. cerevisiae* has

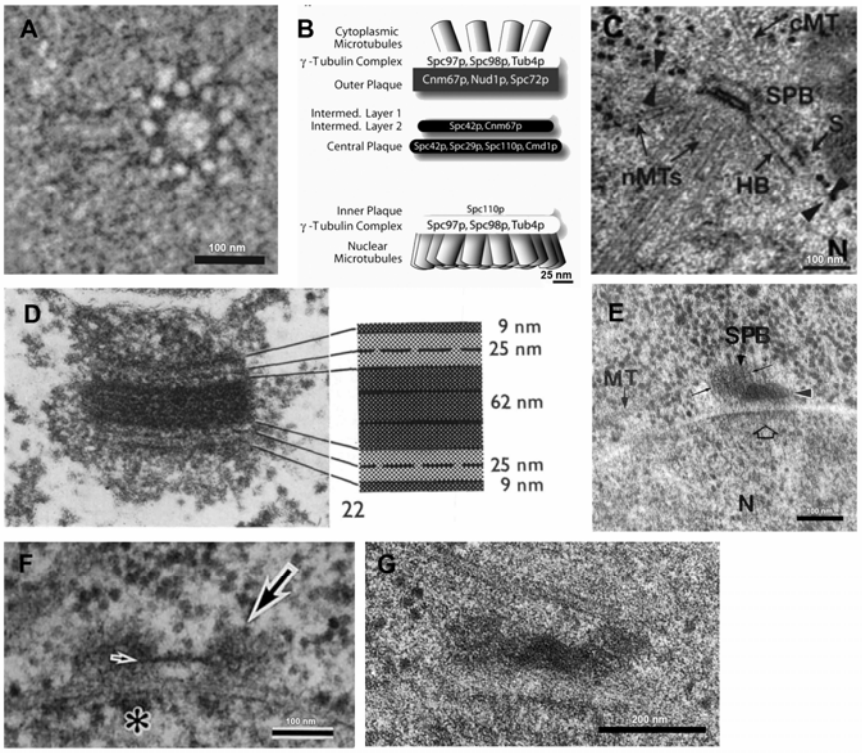

Figure 5 Centrosomes and SPBs A) Centriole pair in C. elegans, that has nine singlet MTs (Pelletier et al. 2006).**B)** Schematic diagram of the layered *S. cerevisiae* SPB shows the proteins and the layers where they are located (Muller et al. 2005).**C)** Thin section of S. cerevisiae SPB, which is embedded inside the nuclear envelope (arrowheads) and nucleates MTs both towards the cytoplasm and nucleoplasm (N). The halfbridge (HB) has an associated satellite (S) (Jaspersen and Winey 2004). **D)** The MTOC in the slime mold *Polysphondylium violaceum* has a layered structure (Roos 1975). **E)** S. pombe SPB located outside the nuclear envelope, with the central plaque (thin arrows), the central bridge (arrowhead) electron dense material inside the nuclear envelope (open arrow) (McIntosh and O'Toole 1999). **F)** A duplicated SPB (large arrow) including the connecting central bridge (small arrow), sitting on the nuclear envelope in the pathogenic yeast. * marks electron dense material below the NE (Yamaguchi et al. 2002). **G)** A duplicated S. pombe SPB with cytoplasmic MTs.

the most thoroughly described structure. It is duplicated in G1 phase and sits inserted into the nuclear envelope, where it nucleates MTs from both the cytosolic and nucleoplasmic face (O'Toole et al. 1999). It has six layers, including a central layer containing the coiled coil protein Spc42 that forms the crystalline core of the SPB (Donaldson and Kilmartin 1996; Bullitt et al. 1997; O'Toole et al. 1999). Recently a complete map of protein organization within the SPB has been suggested by

mathematical modeling and fluorescence resonance energy transfer experiments (Muller et al. 2005).

Other layered MTOCs exist in the cellular slime molds *Polysphondylium violaceum* and *Dictyostelium discoideum* (Roos 1975; Daunderer et al. 1999). However, most SPBs have a less distinct structure, like the ones found in *S. pombe* and the pathogenic yeast *Exophiala dermatitidis*. These yeasts have a disk-shaped electron dense structure with an even more dense central plaque in the middle sitting on the outside of the nuclear envelope during interphase. The disk has a small appendix called the central bridge, from which the daughter SPB derives in a yet unknown process before mitosis occurs (Ding et al. 1997; Yamaguchi et al. 2002; Uzawa et al. 2004).

E. Local Regulation of MT Dynamics in the Cell

Formatted: Bullets and Numbering

The cell has many ways with which it can regulate MT dynamics to enable the different cellular roles of MTs. Local changes of tubulin concentration can be a limiting factor for MT growth in small cellular compartments such as a neuronal growth cone (Janulevicius et al. 2006). However, as with actin, a whole range of MT associated proteins (MAPs) regulate the dynamics of MTs as well (Maccioni and Cambiazo 1995). A combination of these factors can cause the MT cytoskeleton to behave differently in different regions of the cell or during the cell cycle.

For example, MTs have been shown to be much more dynamic during mitosis (Rusan et al. 2001). During mitosis, MTs should connect to the kinetochores of the centrosomes and separate the two sisters into individual daughter cells. The increased dynamism of the MTs during this time might increase the chances of encountering a kinetochore where it would then be stabilized.

Similarly, increased catastrophe and rescue events at the cell periphery keep MTs growing and shrinking in this region, indicating another form of local MT regulation (Komarova et al. 2002). This combination of dynamic instability and local stabilization of MTs, where and when necessary, is called the ‘search and capture model’ (Holy and Leibler 1994).

Polarity and Morphogenesis in the Fission yeast

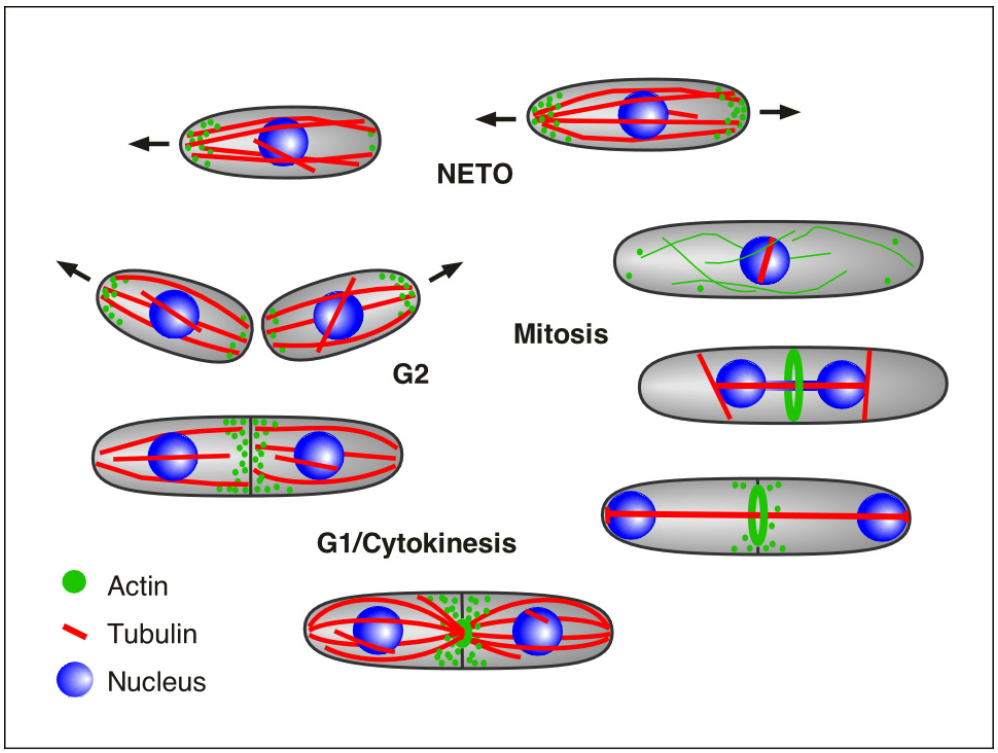

Figure 6 The fission yeast cell cycle. The different stages of the cell cycle are shown in clockwise order. After division cells grow monopolar at the 'old end'. 'NETO' initiates bipolar growth which lasts until the cell has doubled its length, when mitosis is started. G1 and S phases occur during cytokinesis. Courtesy of Damian Brunner.

1. The Fission Yeast Growth Cycle

Fission yeast is an excellent model organism for cell polarity because of its symmetrical cylinder shape that allows for easy recognition of morphology mutants (Snell and Nurse 1994; Verde et al. 1995). This yeast grows in a linear manner with growth zones at the cell ends and in optimal growth conditions, cells divide every three hours. Directly after division, cells are around 7-8 µm long (1.11x the length of the

mother cell divided by two; figure 6) (Mitchison and Walker 1959). Initially, growth only occurs at the old end (away from the septum), where actin and growth markers are already present since the last cell cycle. Bipolar growth is initiated with the new end take off (NETO). NETO occurs during G2 and is cell length dependent (it occurs at around 9.5 µm cell length) (Mitchison and Nurse 1985). Subsequently, the cell grows linearly at both ends until it is 13-15 µm long, when it undergoes mitosis.

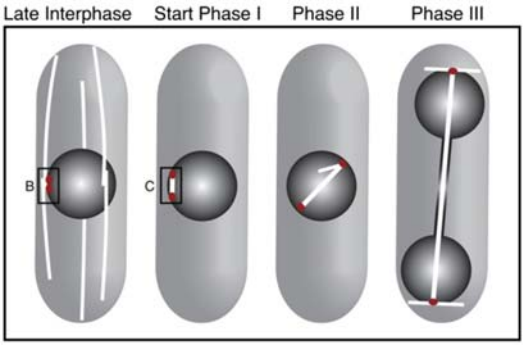

Figure 7 Phases of closed mitosis in *S. pombe* (Vogel et al. 2007)

Mitosis is initiated with a rearrangement of MTs into the nucleus (figure 7) and consists of three phases: phase I - spindle formation, phase II - constant spindle length and phase III - spindle elongation (Nabeshima et al. 1998). Again, division by medial fission produces two equally long daughter cells.

2. The Growth Zones

Yeast cells grow by incorporating new material into their plasma membranes and cell wall. The cell wall in fission yeast is formed by a meshwork of glucans. Excretion of new cell wall and membrane occurs at the cell ends and is actin dependent (Marks et al. 1986; Konomi et al. 2000; Takagi et al. 2003; Kamasaki et al. 2005).

If the cell wall is removed, the cells form a round protoplast. The protoplast will not regain its form before the cell wall has reformed, which makes the cell wall an essential component of cell polarity (Osumi et al. 1989). The cell ends are also the region of endocytosis (Gachet and Hyams 2005). Here, the plasma membrane around the growth sites contains ergosterol-rich domains (Wachtler et al. 2003). These domains are held in place by the fission yeasts myosin 1 homologue, myo1 (Takeda and Chang 2005). Myo1 also stimulates actin nucleation at the cell ends (Lee et al. 2000).

This kind of polarized growth resembles the growth of hyphae in filamentous fungi (Harris 2006) and that of root hairs in plants (Sieberer et al. 2005).

3. The Establishment of Growth Zones

The cellular growth machinery has to be targeted to the correct location, which in interphase fission yeast is the cell ends. The landmark protein Tea1 (tip elongation aberrant 1) is carried on the plus ends of MTs to the cell cortex, where it is deposited (figure 8) (Snell and Nurse 1994; Verde et al. 1995; Mata and Nurse 1997; Behrens and Nurse 2002). Tea1 is then anchored at the cortex by Mod5, a protein containing a prenylation site suggesting a membrane attachment (Snaith and Sawin 2003; Snaith et al. 2005). However, Tea1 is in turn essential for Mod5's well-defined localization to the cell ends. Therefore, the two proteins seem to be dependent on each other for their targeting and attachment to the correct part of the plasma membrane (Snaith and Sawin 2003).

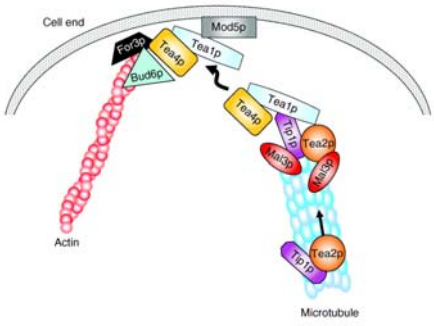

Figure 8 Polarity markers are delivered to the cell end by the cytoskeleton (Lansbergen and Akhmanova 2006)

Tea1 is thought to guide the MTs to grow parallel to the long axis of the cell by depolymerizing them when they reach the cell end (Mata and Nurse 1997). It is also required for targeting other polarity factors, such as the kinase Pom1, Bud6 and the formin For3 to the cell end (Bahler and Nurse 2001; Glynn et al. 2001; Feierbach et al. 2004). Bud6 and For3 are actin binding proteins, which establish a link between the MT delivered polarity markers and the actin cytoskeleton as reviewed in (La Carbona et al. 2006).

In fission yeast, actin is encoded by the *act1* gene. F-actin assembles into patches at the sites of cell growth, as well as into actin cables that run along the cell's long axis (figure 9) (Marks et al. 1986; Arai et al. 1998). The filament's plus ends point towards the membrane at the cell end (Kamasaki et al. 2005). The patches are nucleated in the cell ends, then transported along actin filaments away from the cell ends and the septum (Pelham and Chang 2001).

The organization of MTs by the polarity proteins will be introduced thoroughly in 'The Fission Yeast Microtubule Cytoskeleton' section.

The Fission Yeast Microtubule Cytoskeleton

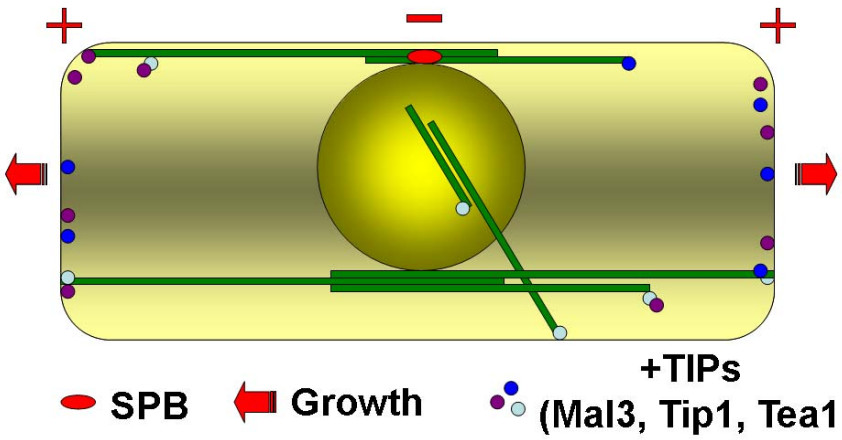

Figure 9 Fission yeast microtubule cytoskeleton Microtubules are mostly aligned with the long axis of the cell. Proteins important for polar growth are carried on microtubule plus ends to the cell ends where they get deposited. The proteins shown are just some examples of the many proteins being carried on MT plus ends.

1. The Interphase MT Cytoskeleton is involved in Cellular Morphogenesis

Establishment of linear growth in fission yeast is dependent on MTs, in contrast to budding yeast where polar growth is actin dependent. If the MTs are too short, as in the absence of stabilizing proteins, these polarity factors will be delivered to the wrong position on the plasma membrane. Subsequently, the growth machinery is misplaced causing cells to grow bent or T-shaped (figure 10) (Toda et al. 1983; Radcliffe et al. 1998; Sawin and Nurse 1998; Nakayama et al. 2003). Thus, MTs play an essential role in positioning the growth sites in a manner that ensures rod-shaped growth. However, once polarity is established, polarity maintenance is MT independent (Sawin and Snaith 2004).

A MT that starts growing in an axis other than the cell's long axis will be oriented when reaching the plasma membrane, as it will continue to grow until it reaches the cell end. This is a process dependent on the presence of the anti-catastrophe factor Tip1 (Brunner and Nurse 2000). This guidance is important for growth site positioning of

MTs, because the polarity proteins such as Tea1 travel on MT plus ends and deposited at the cell ends (figure 9) (Mata and Nurse 1997; Behrens and Nurse 2002; Snaith and Sawin 2003; Feierbach et al. 2004; Snaith et al. 2005).

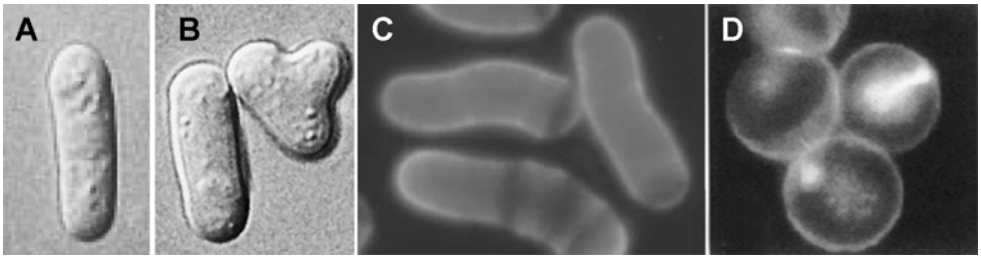

Figure 10 Fission yeast morphology mutants A) Wild type **B)** mal3Δ branched cell **C)** of bent cells of tip1Δ D) orbital mutants of orb6 (Verde et al. 1995; Beinhauer et al. 1997; Brunner and Nurse 2000)

2. Interphase MTs Extend From the Nucleus Toward Both Cell Ends

During interphase MTs in fission yeast are organized as cytoplasmic bundles oriented along the cellular log axis (Hagan 1998). The number of MT bundles in a cell varies with time, but is commonly between two and six (Carazo-Salas et al. 2005). Fluorescence studies have shown that the MT minus ends are gathered in the middle of the cell and their more dynamic plus ends point towards the cell ends (Drummond and Cross 2000). MTs nucleated away from the nuclear region get pulled there by a molecular motor (Carazo-Salas et al. 2005; Janson et al. 2007). An antiparallel bundle with a middle region of MT minus end overlap is established in this way. Only one of these bundles is associated with the SPB. The others originate in the central overlap region, which therefore is called the interphase MTOC (iMTOC). The iMTOCs are attached to the nuclear envelope, which enables MTs to position the nucleus in the middle of the cell (Tran et al. 2000; Tran et al. 2001). However, MTs bundles are able to form without such connections to the nucleus and the SPB (Carazo-Salas and Nurse 2006; Daga et al. 2006b).

From fluorescence intensity it has been suggested that only one MT extends the full length of the bundle to the cell end (Sagolla et al. 2003). Here, the MT is growing slowly for about one minute before it undergoes catastrophe (D. Foethke personal

communication). In wild type cells, catastrophe almost exclusively occurs at the cell end (Brunner and Nurse 2000; Drummond and Cross 2000; Busch and Brunner 2004). Furthermore, almost no rescue occurs before the MT has depolymerized all the way back to the iMTOC region (Busch and Brunner 2004). Thus, MT interphase bundle dynamics in *S. pombe* consist of growth, slower growth (or stalling) at the plasma membrane followed by catastrophe.

3. Fission Yeast MT Organizing Centers

The yeast equivalent of the centrosome is the spindle pole body (SPB). In fission yeast this is an electron dense oblate ellipsoid 90-180 nm long, positioned on the cytoplasmic side of the nuclear envelope during interphase (figure 5) (Ding et al. 1997). In contrast to the layered appearance of the budding yeast SPB, fission yeast SPB is an amorphous structure layered by a single electron dense central plaque (Ding et al. 1997; McIntosh and O'Toole 1999; Muller et al. 2005). However, over 200 proteins localize to the fission yeast SPB, indicating a complex network of protein interactions within this structure (Matsuyama et al. 2006). Furthermore, it takes at least one and a half cell cycle for the SPB to fully mature, as shown by the delay in ability to bind the NIMA kinase Fin1 (Grallert et al. 2004).

There is some controversy as to when the SPB duplicates in preparation for mitosis. Originally, duplication was shown to occur in late G2 (Ding et al. 1997). More recently, it was claimed that duplication occurs during the G1/S transition, hence before cytokinesis is complete (Uzawa et al. 2004). At the onset of mitosis, these SPBs enter the nuclear envelope and nucleate MTs into the nucleoplasm, where they form the mitotic spindle (Ding et al. 1993; Ding et al. 1997). Another MTOC is found at the division site where the equatorial MT organizing center (eMTOC) nucleates a ring of MTs (Hagan and Hyams 1988; Heitz et al. 2001; Zimmerman et al. 2004).

MT nucleation sites in interphasic fission yeast are not restricted to the SPB but are also found at the nuclear envelope and on MTs themselves (Sawin et al. 2004; Zimmerman et al. 2004; Janson et al. 2005; Zimmerman and Chang 2005). The γ-tubulin protein (Gtb1), and the γ-tubulin complex components Alp4 and Alp6 are essential for MT nucleation and thus, cell viability (Horio et al. 1991; Vardy and Toda 2000). Three

more proteins, Gfh1, Alp16 and Mod21 have been found to belong to the γ-tubulin complex. These proteins are not essential for nucleating MTs but deletion of their genes cause aberrant interphase MT cytoskeletons (Fujita et al. 2002; Sawin et al. 2004; Venkatram et al. 2005; Anders et al. 2006).

4. MT Organization During Closed Mitosis

As in budding yeast, chromosome segregation occurs inside a closed nuclear envelope in fission yeast. The kinetochores of the three chromosomes lie in the direct vicinity of the SPB during interphase but lose this association in beginning of mitosis (Funabiki et al. 1993).

During metaphase, the spindle consists of pole-to-pole MTs and shorter MTs, including three pairs of kinetochore MTs. As mitosis proceeds, the amount of MTs from each pole decreases and the pole-to-pole MTs disappear completely. However, the length of the spindle almost yields a duplication in the total amount of polymerized tubulin during mitosis (Ding et al. 1993). The chromosomes are separated upon MT depolymerization (Grishchuk and McIntosh 2006).

MT's Role in Organelle Positioning

1. Positioning of the Nucleus and the Site of Cytokinesis by MTs

Fission yeast cells have a nucleus positioned in the geometric centre of the cell. There, the nucleus determines the site of the septum formation by emitting the protein Mid1 that forms a band around the middle of the cell (Tran et al. 2000; Daga and Chang 2005; Tolic-Norrelykke et al. 2005). Mid1 is thought to be excluded from the cell ends by the kinesin Pom1 in the non growing half of the cell and an unidentified protein is likely to have the same function in the growing end (Celton-Morizur et al. 2006; Padte et al. 2006). The importance of proper nuclear positioning is demonstrated when its location is shifted (centrifugation after MT depolymerization or pushing using optical tweezers). The septum is then misplaced, causing unequal division of the cellular material during cytokinesis (Daga and Chang 2005; Tolic-Norrelykke et al. 2005).

This central position of the nucleus is maintained by asymmetric pushing forces exerted by MTs (Hagan and Yanagida 1997; Tran et al. 2000; Daga et al. 2006a). Although several MAP deletion mutants (i.e. *tip1Δ* and *mal3Δ*) fail in centering the nucleus, this is most likely an indirect effect of short MTs. It has been shown that the force applied on MTs reaching the cell end, and the subsequently induced depolymerization, are sufficient to correctly position the nucleus (D. Föthke personal communication).

2. Golgi and Mitochondria Morphology is MT Dependent

In *S. cerevisiae* the Golgi apparatus and mitochondria distribution is dependent on actin. The Golgi is found as individual cisternae in the cytoplasm (Rossanese et al. 2001). In contrast, fission yeast resembles mammalian cells, with the stacked Golgi cisternae and mitochondria's distribution dependent on MTs. This makes the fission yeast a more suitable model organism to elucidate the positioning mechanism of these organelles.

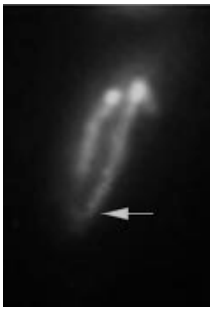

Figure 11 Fission yeast mitochondria (Yaffe et al. 2003)

However, fission yeast Golgi have a dispersed cytoplasmic distribution, whereas the mammalian Golgi is close to the MTOC. In mammalian cells, the Golgi apparatus is dispersed in the cytoplasm upon MT depolymerization (Robbins and Gonatas 1964; Wehland et al. 1983; Rogalski and Singer 1984). Similarly, fission yeast Golgi was found to unstack into single cisternae when MTs were depolymerized using the drug TBZ (Ayscough et al. 1993). Therefore, it has been concluded that Golgi stacking in fission yeast as well as in mammals needs intact MTs.

Fission yeast mitochondria have an elongated and tubular shape and have been seen in close proximity to MTs (figure 11) (Kanbe et al. 1989). Fluorescence microscopy confirmed this intimate association when mutations in the *atb2* (α-tubulin 2) gene lead to aggregated and unevenly distributed mitochondria (Yaffe et al. 1996). When fluorescence live imaging became feasible, it was shown that mitochondria grow and shrink with MTs, and that this movement requires a previously unknown linker protein named Mmd1 (Yaffe et al. 2003; Weir and Yaffe 2004).

3. Most Intracellular Vesicle Trafficking is Performed by Actin

Endocytosis, exocytosis and intracellular trafficking between membrane bound organelles inside the cell involve functionally distinct trafficking vesicles adapted to dock and fuse with defined target membranes. These vesicles are commonly transported along MTs, and mediate the regulated delivery of vesicle content and membrane components (Lippincott-Schwartz 1998; Bonifacino and Glick 2004; Takamori et al. 2006). However, during yeast endocytosis actin patches are formed at the sites of internalization and have been seen around vesicles in EM studies (Kanbe et al. 1989; Takagi et al. 2003; Gachet and Hyams 2005; Kaksonen et al. 2005). These actin patches and late secretory vesicles are transported within the cell along actin cables (figure 12) (Feierbach and Chang 2001; Pelham and Chang 2001; Huckaba et al. 2004). In fission yeast, MTs might play a role in

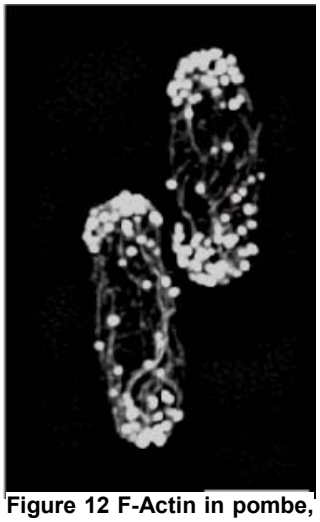

Figure 12 F-Actin in pombe, in patches and cables (Pelham and Chang 2001). Bar 5 µm.

Golgi to endoplasmic reticulum (ER) membrane recycling through the kinesin-like protein Klp3, as well as in stacking Golgi cisternae (Ayscough et al. 1993; Brazer et al. 2000). However, secretion is not affected by the loss of MTs (Ayscough et al. 1993).

MT-Associated Proteins in the Fission Yeast

1. MT Plus-End Tracking MAPs Regulate MT Dynamics

Plus end tracking proteins, or +TIPs are a highly diverse group of MAPs, including both MT dependent motors and non-motor proteins. These proteins accumulate at the dynamic plus end of MTs in one or a combination of several of the following ways:

i. Specific binding affinity for a structure of the polymerizing MT end, i.e. tubulin sheets or the GTP cap.
ii. Actively transported by plus end directed motors to the growing MT end.
iii. By binding to other +TIP proteins already localized at the plus end.
iv. By co-assembly with tubulin dimers and subsequent release.
v. Preferential dissociation from the older part of the MT.

+TIPs can regulate MT dynamics though influencing their structure or accessibility to other proteins. Many +TIPs (e.g. Clip-170 and EB1) stabilize the MTs by decreasing catastrophe rates, increasing the number of rescues or by promoting MT elongation in other ways (Brunner and Nurse 2000; Busch and Brunner 2004).

The plus ends of MTs are highly populated in fission yeast, and almost all of these MAPs play an important role in the establishment of polar growth (figure 8) (Lansbergen and Akhmanova 2006). Two of the klps, Klp2 and Tea2, belong to the +TIPs (Browning et al. 2000; Browning et al. 2003; Busch et al. 2004; Janson et al. 2007). Tea2 transports Tip1 (the fission yeast CLIP-170 homologue) to the MT plus end. Once at the end, Tip is retained there by Mal3 (the EB1 homologue) (Busch et al. 2004). Mal3 also recruits the kinesin Tea2 to the MT (Browning and Hackney 2005).

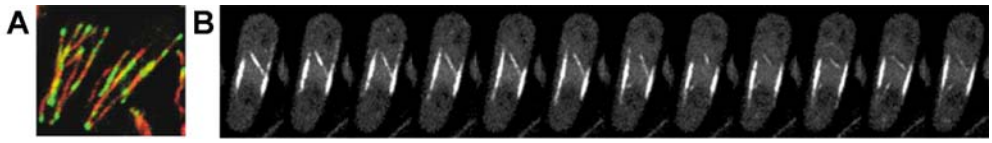

Figure 13 Mal3 localizes to microtubule ends and stabilizes microtubules A) Immunofluorescence staining of methanol fixed cells. Anti- tubulin staining is in red, anti-mal3p staining in green. **B)** Movie sequence of full projects of GFP-tubulin in *mal3Δ*. (Busch and Brunner 2004)

A. The EB1 Protein Family and Mal3

End binding protein 1 (EB1) is a small conserved protein that is usually found as a dimer (MW ~60kDa). It was first described in a screen identifying adenomatous polyposis coli (APC) interactors (Su et al. 1995). It has subsequently been found to interact with almost every +TIP protein described, and has been shown to recruit some of them to the growing MT ends (reviewed in (Morrison 2007)).

The protein consists of three domains. The N-terminal part is basic and contains a calponin homology domain, which is thought to mediate MT binding (Hayashi and Ikura 2003). The second domain is a flexible linker region that joins the N- and C-termini. The last domain is the C-terminus, which contains the EB1-like sequence motif, specific to the EB1 family of proteins. This motif is part of coiled-coil region which enables protein dimerization and interaction with other +TIP proteins. The C-terminal also has a sequence of acidic amino acid residues (Bu and Su 2003; Honnappa et al. 2005).

EB1 is thought to be autoinhibitory, with the C-terminus preventing effective MT binding. EB1 interacting proteins release this inhibition and increase EB1's MT affinity (Hayashi et al. 2005).

In fission yeast, Mal3 (EB1) was identified in a screen for minichromosome loss. *mal3Δ* cells are sometimes bent and branched. When the MT bundles were studied, they were found to be half the length of WT bundles (Beinhauer et al. 1997; Busch and Brunner 2004). Mal3, like its human counter part, localizes preferentially to MT plus ends (figure 13). The GFP tagged Mal3 left the MT ends before catastrophe (Busch and Brunner 2004). Therefore, it has been concluded that Mal3 is important for stability of growing MTs.

Recent *in vitro* electron microscopy studies revealed a preferential binding of Mal3 to the MT seam. It was suggested that Mal3 works as a molecular zipper of the MT lattice, stabilizing the MTs by strengthening their weakest point (Sandblad et al. 2006).

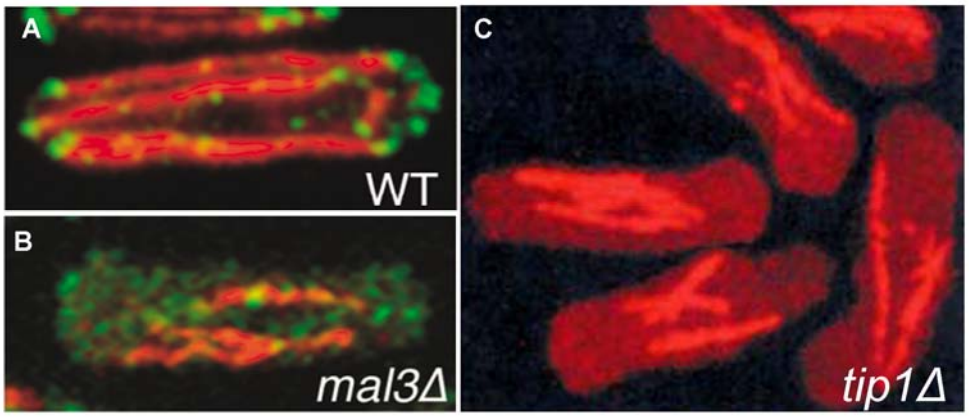

Figure 14 Tip1 localizes to microtubule plus ends in a Mal3 dependent manner and *tip1* deletion cause short microtubules. Immunofluorescence staining of fixed cells using the anti-tip1p antibody (green) and the anti-tubulin antibody (red) (Brunner and Nurse 2000; Busch and Brunner 2004)

B. The Clip-170 Family and Tip1

Cytoplasmic linker protein 170 (Clip-170) is the prototype +TIP protein (Rickard and Kreis 1990). It has been shown to mediate the interaction between MT ends and kinetochores, endocytotic vesicles and the leading edge of migrating cells (Pierre et al. 1992; Schuyler and Pellman 2001; Tanenbaum et al. 2006).

The protein consists of two CAP-gly domains in the N-terminal part, followed by a long coiled-coil region which ends in two zinc fingers in the C-terminal part (Pierre et al. 1994). The protein is auto-inhibited by a head-to-tail fold where the N-terminus and the first zinc finger of the C-terminus interact (Lansbergen et al. 2004).

Mammalian Clip-170 treadmills on the MT ends by binding tubulin heterodimers and copolymerizes with tubulin into the MT (Diamantopoulos et al. 1999; Perez et al. 1999; Folker et al. 2005). It has been shown that phosphorylation of the serine residues in Clip-170 inhibits MT binding (Rickard and Kreis 1991). Therefore, phosphorylation may be the mechanism by which the Clip-170 disassociates from the MT lattice.

However, both Bik1 (Clip-170 in budding yeast) and Tip1 (in fission yeast) are delivered to the plus ends of MTs by the kinesins Kip2 and Tea2 respectively (Busch et al. 2004; Carvalho et al. 2004). This gives these kinesins a new mechanism to influence

MT stability and an alternative mechanism of Clip-170 plus end association. Once at the MT plus end, Tip1 is anchored there by Mal3 (figure 14).

In fission yeast, MT bundles continue growing when they contact a cell wall. Consequentially, bundles align with the cell's long axis. MTs then continue to grow until they reach the cell ends where they deliver the polarity markers and undergo catastrophe (Brunner and Nurse 2000).

In cells where Tip1 is deleted, MT catastrophe is no longer restricted to the cell ends, but also occurs in the middle of the cell. Therefore, MTs are short and cells grow bent or T-shaped. This local influence of MT dynamics performed by Tip1 guides the MTs to deliver the polarity markers at the cell end (Brunner and Nurse 2000). However, much still remains to be elucidated about the function of +TIPs at MT plus ends.

C. +TIPs as Centrosomal Proteins

Recently, more and more evidence shows that EB1 and other +TIPs such as XMAP215 and dynein are also centrosomal components (Wang and Huffaker 1997; Popov et al. 2001; Ma and Chisholm 2002; Rehberg and Graf 2002; Cassimeris and Morabito 2004). EB1 has been implicated in MT anchoring at the centrosome (Askham et al. 2002; Yan et al. 2006).

Bim1 (EB1) and Kar9 (APC-related protein) localize to the SPB in *S. cerevisiae*. This localization is necessary for the correct alignment of the spindle (Liakopoulos et al. 2003). Interestingly, in budding yeast as well as in human cells, EB1 localizes to the old centrosome/SPB (Hwang et al. 2003; Liakopoulos et al. 2003; Maekawa et al. 2003).

2. Molecular Motors

Kinesins are molecular motors that move along MTs in an ATP dependent manner. There are 14 different families of kinesins described today (Lawrence et al. 2004; Miki et al. 2005). Kinesins are important for MT organization and the transport of cargo along MTs. They can also actively stabilize or depolymerize MTs (Howard and Hyman 2007). The genome of *S. pombe* encodes nine kinesin-related genes and one cytoplasmic dynein (Wood et al. 2002).

The dynein is cortically anchored and necessary for nuclear oscillation during meiosis (Yamamoto et al. 1999; Niccoli et al. 2004; Yamashita and Yamamoto 2006). Of the nine kinesin like proteins (KLPs), seven proteins have been characterized and only one, Cut7, was found to be essential. All seven characterized proteins have an impact on MT organization in fission yeast (table 1).

Table 1 The kinesin like proteins in fission yeast (Hagan and Yanagida 1990; Brazer et al. 2000; Browning et al. 2000; Troxell et al. 2001; Jeong et al. 2002; Busch et al. 2004; Browning and Hackney 2005; Carazo-Salas et al. 2005; Rhee et al. 2005; Janson et al. 2007)

Protein	Kinesin family	Interphase function	Mitosis function
Pkl1 (Klp1)	14	Not known	Stabilizing interdigitating MTs
Klp2	14	Minus end directed sliding of MTs +TIP tracking	Shortening MTs at the kinetochores
Klp3	1	Recycling of Golgi cisternae	Not known
Tea2	7	Transporting Tip1 to MT plus ends; recruiting Mal3 to MTs	Not known
Cut7	5	Not known	Stabilizing interdigitating MTs
Klp5 & 6	8	Not known	Depolymerize MTs

3. MT Bundlers

Since MTs in fission yeast are bundled, it is likely that some molecular linkers are holding the filaments together. The yeast PRC1 homologue, Ase1, bundles MT minus ends to form a midzone of crosslinked antiparallel MTs close to the nucleus where Ase1 is localized (Loiodice et al. 2005; Yamashita et al. 2005). However, a small amount of bundling can also occur in the absence of Ase1 (Daga et al. 2006b).

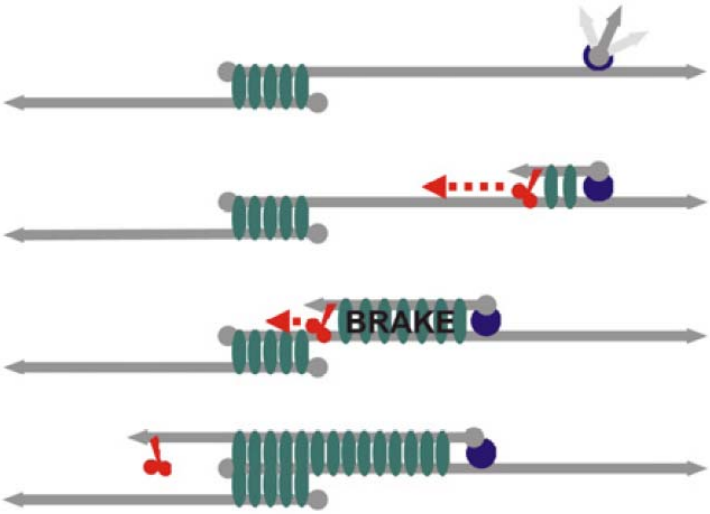

Figure 15 Model of microtubule bundling in fission yeast Microtubule plus ends are indicated by arrow heads, minus ends by spheres. MT nucleation along interphase bundles occurs from MT-bound nucleation complexes (blue). After nucleation, MTs are stabilized in the antiparallel configuration by polarity-specific Ase1 (green). The minus-end-directed kinesin-14 Klp2 (red) subsequently transports MTs to the bundle midzone. As the new MT grows, additional Ase1 binds, increasing the friction against a length-independent number of motors at MT plus ends. Consequently, the speed of transport decreases and finally becomes zero when motors lose contact with antiparallel MTs. (Janson et al. 2007)

MT nucleation outside the nuclear region occurs at the satellite MTOCs (Janson et al. 2005). The plus end tracking motor Klp2 slides the MTs so that their minus ends can be found in the overlap region. Here, Ase1 acts as a molecular break to prevent further sliding and is thereby it focuses MT minus ends in the iMTOC (figure 15) (Janson et al. 2007).

Tomography

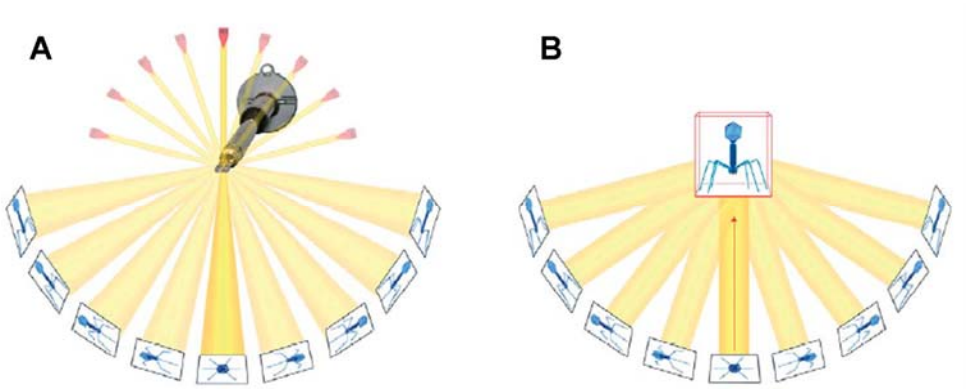

Figure 16 The principle of electron tomography A) A series of 2D pictures of the sample is acquired from different angles **B)** The resulting series of 2D images is back-projected to a digital 3D reconstruction of the original sample. (McIntosh et al. 2005)

1. 3D Reconstruction of Cells Using Electron Tomography

Electron microscopy studies of cells and of macromolecular complexes within cells are currently undergoing a huge transformation. The recent improvements of both the methods and the instrumentation for electron microscopy are now allowing subcellular structures and organelles to be characterized in 3D with unprecedented detail and reliability (O'Toole et al. 1999; McIntosh et al. 2005). This is the contribution of cellular electron tomography (ET), a method which can produce 3D reconstructions of fixed and plastic embedded cells or frozen hydrated samples (Frank 1992; Baumeister et al. 1999).

In principle of electron tomography consists in taking many 2D images of one object from varying angles. These pictures are then combined into a 3D volume *in silico* by a method called weighted backprojection (figure 16) (McIntosh et al. 2005). The resolution one can achieve depends on many factors, but viewing a sample in vitreous ice by cryo-tomography can yield up to 20 Å resolution, enough to study individual protein

structures (Sandin et al. 2004). However, in a sample embedded in resin and stained with heavy metals, the resolution could never reach higher than 50 Å. This is due to the metal coat applied on the sample's proteins (McIntosh et al. 2005).

2. MT End Structure can show MT Polarity and Dynamics

Microtubule bundles have traditionally been studied by thin serial section reconstructions of pictures taken from MTs imaged in cross sections. This method provided us with an unreliable picture of interphase MTs in *S. pombe* since these cytoplasmic fibers, in contrast to mitotic spindles, are not arranged in parallel bundles (Ding et al. 1993). The interphase MT arrays of fission yeast bend and diverge; consequentially they are very hard to track by the serial section reconstruction method. We have found that electron tomography gives a more accurate picture of the cytoskeletal arrangement when one is working with such irregular structures.

Additionally, electron tomography provides more detailed information than serial thin sections, since its 3D resolution is essentially isotropic, while that of serial thin sections is limited along the dimension perpendicular to the image by the section thickness (usually > 40 nm).

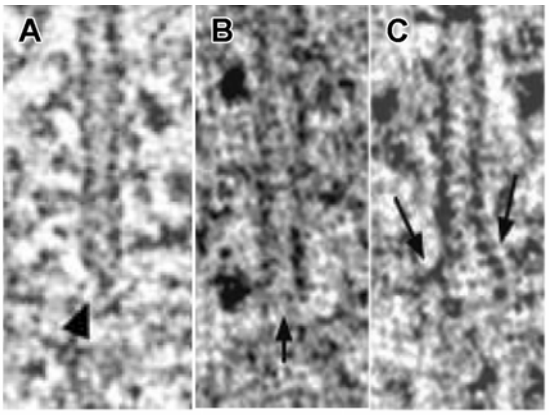

Figure 17 Microtubule end structures in *Caenorhabditis elegans* A) capped end **B)** blunt end **C)** flared end (O'Toole et al. 2003)

As described in "The MT Dynamic Instability Model" chapter, the MT end morphology changes when it undergoes catastrophe or rescue. MTs that depolymerize have protofilaments curling backwards from their ends, growing MTs have a 'sheet' and metastable MTs have a blunt end. Furthermore, the γ-TURC complex is thought to nucleate MTs, and is then left as a 'cap' on the minus ends (figure 17).

These morphological differences can be seen with tomography and have been used to determine the polymer's polarity (capped versus open end), as well as its dynamic

state at the time of freezing inside cells (O'Toole et al. 1999; O'Toole et al. 2003). Furthermore, the MT lattice structure can also be studied in the cellular context using resin embedded and heavy metal stained samples for tomography (Srayko et al. 2006). Finally, interactions between MTs and other organelles, or indeed any ultrastructural feature, can be studied in the resulting tomograms (Marsh et al. 2001). Thus, the labor spent, though significant, yields a lot of valuable information about the entire cell architecture.

Chapter 2

Materials and methods

Table 1 Steps in producing a large tomogram reconstruction (white boxes) and the software needed (black boxes)

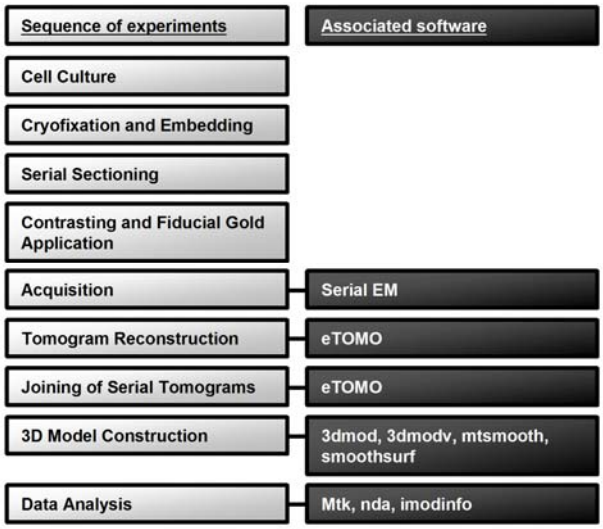

Summary

The various steps of the complete procedure to reconstruct and model large cell volumes by electron tomography can be divided into three main parts (see also table 1):

1. Sample preparation: The first step involves handling cell cultures and performing cryo-immobilization of cells using a high pressure freezer. This is followed by freeze substitution in acetone and plastic infiltration to generate blocks of embedded samples. From these, thick sections collected in ordered series are cut, contrasted and fiducial gold particles are added to later facilitate a precise alignment of the projections in the tilt series.

2. Electron microscopy: The second step requires a transmission electron microscope (200-300 kV) equipped with a CCD camera and controlled by appropriate acquisition software. This is used to acquire a series of 2D projections at various orientations (tilt series). Montaged images in the x/y plane can be made in order to cover the full area of interest at each angle during acquisition.

3. Computation: The final reconstruction includes alignment of all images from the tilt series with high precision helped by the fiducial markers. Lastly, all tomograms in the series are calculated and joined in the z-axis to create a large volume. A 3D model is then created from contours of features of interest. These can be painted in the tomogram using the slicer tool. Quantitative measurements can then be performed on these models using various IMOD programs.

Methods

Sample preparation

1. Cell culture

Fission yeast strains are best maintained by well-established methods that have been already described (Moreno et al. 1991). Briefly, yeast cells can be stored in a glycerol-containing medium at –80^{o}C for years, then awakened by cultivation on a plate of rich medium and incubated at 25-32ºC for 1-4 days. A liquid pre-culture (10 ml) of a standard rich medium (YE5S) is then inoculated with a small amount of cells from the initial plate. This pre-culture is placed at 25-32ºC in an incubator with constant agitation. The pre-culture is then used to inoculate a larger culture, taking into account the generation time of the strain that will be studied (usually about 3h). The optical density (OD) is checked (at 595 nm) and should be between 0.25 and 0.75 for cells to be in log-phase growth. Cell cryo-immobilization is best performed when the culture has an OD between 0.5 and 0.75, since this higher density gives better performance during the harvesting of cells for rapid freezing, thus optimizing freezing quality (see below). Cells can also be cultivated in the defined Edinburgh Minimum Medium. However, cells usually grow more slowly in defined media, and they often show some morphological alterations, e.g., more vacuolar structures within the cells.

2. High Pressure Freezing (HPF)

As ET of subcellular organization is a multi step procedure (i.e., expensive and time-consuming, see table 1), it is of great importance that specimens are initially preserved as well as possible. Thus, cryo-immobilization by HPF is highly recommended when possible. HPF freezes biological specimens up to several hundred microns thick under a pressure of over 2000 bar. This instrument works well for the preservation of fission yeast when employed as described below and for us it was the method of choice. At the time of freezing, 15 ml of cell culture at OD ~0.5 (at 595 nm) is filtered to a paste

using a Millipore 15 ml filtration set-up with 25 mm polycarbonate circular filter (0.4 µm pore size). Cells are then gently scraped from the filter using a toothpick and the paste is loaded into a specimen carrier for the HPF that is available (Baltec 200 µm deep carriers or Leica slot carriers). A syringe needle bent at 45 degrees is used to flatten the cell paste contained within the carrier. The carriers are then closed and mounted on the specific specimen holder of the HPF machine and frozen.

3. Freeze substitution

Freeze substitution (FS) is a valuable and common way to process biological samples following HPF cryo-immobilization (Steinbrecht 1987). During FS the water is slowly substituted for an organic solvent at low temperature (around –90ºC) for a long time (2-3 days). This method performs cell dehydration with minimal cellular damage (Steinbrecht 1987; Steinbrecht 1993; Giddings et al. 2001). Shrinkage or collapse of cell structures would inevitably occur at room temperature. Yeast cells are best freeze substituted in acetone supplemented with some fixatives (McDonald and Morphew 1993). The water content of the cells is extracted in the FS solution at -90ºC for 48-72 h in a Leica AFS device (see Material section).

The advantage of FS is that the fixatives can diffuse into the cryo-immobilized cells at a very low temperature (–90ºC) and are therefore already present in all subcellular compartments when the temperature rise brings them over the efficacy threshold for the fixatives. Thus, following cryo-immobilization the carriers containing the frozen fission yeast are placed into a dehydrated acetone FS solution supplemented with 0.1% dehydrated glutaraldehyde (GA), 0.25% uranyl acetate (UA) and 0.01% osmium tetroxide (OsO_4). This mixture gave good results for visualizing MT arrays in yeast cells (Muller-Reichert et al. 2003), however, the composition of the FS solution can be varied to some extent as we also obtained very good SPBs and MTs preservation in fission yeast using a FS solution made of 0.5% dehydrated GA, 0.5% UA and 1% OsO_4. Surprisingly membrane contrast can be well improved by adding 1% water, or more, to the freeze substitution solution (Walther and Ziegler 2002).

After the dehydration step the temperature is progressively raised to –45ºC with an increment of 5-10ºC/h. The carriers are then rinsed at this temperature with pure

dehydrated acetone and then placed together with their container within the chamber of a cryo-ultramicrotome set at –45ºC in order to proceed at the separation of the pellets from the carriers with a needle from a syringe. Using a cryo-ultramicrotome for this operation makes this step more comfortable, as one can benefit from the microscope on the cryo-attachment. The free pellets are then placed back into the plastic tubes which are transferred back into the AFS machine and further processed by progressive infiltration with resins. In the case of lowicryl (HM20) embedding, several steps are required to start the infiltration at –45ºC: acetone/lowicryl 3:1 for 60 min, 1:1 for 2-3h, 1:3 for 2-3h, pure lowicryl 2 times for 60 min, then overnight. Finally, a last resin change is made before starting polymerization by the action of UV light. For the preparation of epon blocks, the resin is infiltrated in the same way after rinsing with pure acetone, but this is done around –30ºC or even at RT.

Lowicryl polymerization is started at –45ºC for 48h and is continued during the rise of temperature (10ºC/h) up to room temperature, where the blocks are left for another 12h under the UV lamp. For epon blocks the polymerization is made over night in an oven set at 60ºC.

4. Choice of FS resin

Advantages of acrylic resins, like lowicryl (HM20), include their low freezing point as well as their low viscosity, even at low temperature. HM20 has a water-like viscosity even at -35ºC. Therefore, embedding can be started at very low temperatures when the proteins are best stabilized and the samples are optimally preserved (Griffiths 1993). The resulting blocks have very good sectioning properties when one uses a diamond knife with a 35º included angle. Epon shrinks with around 30% when exposed to the electron beam (Braunfeld et al. 1994). In our study we found the shrinkage of lowicryl to be around 10% in the z-axis, and as such, more stable than epon (see also Carlemalm, 1982). Further, we have found lowicryl to be slightly less electron dense and, as such, permit thicker sections for ET. It was therefore our resin of choise. However, epon is the standard embedding medium in most labs. This resin gives very good contrast and is much less harmful for the health of the microscopist, compared with lowicryl resins.

5. Serial sectioning

Serial sections 200-250 nm thick are ideal for tomography when using a microscope that operates at 200 or 300kV. A plastic block is trimmed to make the block face a trapezoid with a low height (base= ~300μm and h= ~100μm). Serial sections are cut from the plastic block on an ultramicrotome using a 35º diamond knife. In case the consecutive sections do not attach to each other to form a consistent ribbon, a solution made from a droplet of rubber cement dissolved in xylene (circa 1:20 dilution) may be applied to the block face. After this adhesive is dry, newly made sections should attach to each other better. Chloroform vapors (from a small ball of cotton moved over the sections) help the sections to flatten if they have wrinkles.

As the large volume approach requires serial sections, slot grids with a large central hole (1x2 mm) are preferable. These grids will be coated with a rather thick film of formvar (90-100 nm thick, which shows a golden interference color); this provides adequate section stability over the entire hole in the grid. Fresh formvar coated grids should be made and should not be carbon-coated, as the films are more fragile when old and carbon coated.

Preparing the grid and finding the right cell are the largest hurdles when wanting to reconstruct a full cell volume. A perfect grid has 25 or more serial sections straight down the middle of the slot. To fit many serial sections in the 2 mm slot one has to trim the block to a very small surface. The grid edges will appear in the picture at high tilt and make tomogram acquisition impossible if the cell of interest is far from the center of the formvar film. Therefore, centering the serial section ribbon is crucial.

To align the sections to the middle of the grid we recommend attaching a long hair diagonally across the knife boat. One end of the hair is attached with tape to the knife's external wall; the other end is attached at the middle of the back edge of the pool. As ribbons of sections come off the knife's edge, they can be parked along the hair, gently aligned with the axis of the slot grid, and therefore easily picked up from underneath. This allows the microtomist to place the ribbon in a precise and controlled way on the grid.

6. Contrasting and application of fiducial markers for tilt alignment

Lowicyl sections are contrasted by staining grids with 2% UA in 70% methanol for four minutes, followed by a lead citrate stain (Reynolds solution) for one minute. Longer staining darkens the cells within the sections without an increase in their contrast. For epon sections methanolic or aqueous UA contrasting solutions are suitable, and these can be applied to the sections for a longer time (up to 15 min). Lead citrate contrasting is again required, as with lowicryl sections.

To make a tomogram one needs a series of images of the same area of the specimen, taken over a wide range of tilts, typically $\pm 60^{o}$ in increments of 1^{o}. These images must then be accurately aligned. To facilitate this process, gold particles are applied to both sides of the grid after contrasting; these can act as fiducial points to bring the multiple tilted views into alignment. Depending on which magnification is used for acquiring the images (14,500 – 25,000X), the colloidal gold particles should be 10-15nm in diameter. The issue is to have the image of the gold particle large enough on the CCD camera used for image recording that there are ~10 pixels across the diameter of each particle. To put the particles onto the sample, grids are floated on 5 µl droplets of a solution of colloidal gold (15 nm in diameter, OD=4) for 3 minutes on each side. The grids are then quickly rinsed on water droplets and dried by blotting.

Tomogram acquisition

1. Large scale adaptations

In yeast cells the cytoplasm is filled with electron dense ribosomes that obscure the MTs in a semi-thick section, like ones used for tomography (figure 1a). Thus, the selection of cell sections to image must occur “blind”. The importance of choosing the right cell must be stressed, since the time spent acquiring and aligning the images and in calculating the tomogram is so considerable that the number of cells studied is usually very low. We developed two methods to tackle this problem. First, a quick screen to

examine the content of a section was designed; second we developed a large volume approach that should include MTs, regardless of their position in the cell. In both cases image resolution was compromised to achieve the largest possible volume, but our compromises leave MTs still clearly visible (figure 1b).

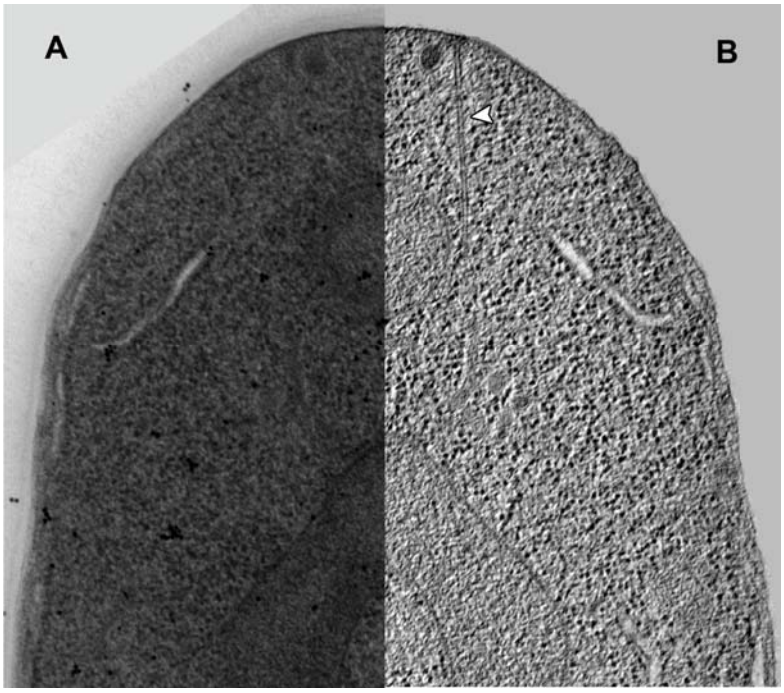

Figure 1: Microtubules are not visible in the dense cytoplasm of yeast semi-thick sections A) A zero angle projection of a 250 nm section **B)** a section of the tomographic reconstruction of the same cell with a MT clearly visible (white arrowhead; picture has been rotated horizontally to create a mirror image).

The alignment of interphase MTs almost parallel to the axis of the fission yeast cell (see figure 2a) made it possible to choose cells that would be favourable for whole-cell MT reconstruction using images from only a single axis of tilt. We chose to image cells that were oriented with their long axis parallel to the tilt axis, with the results that we had good resolution and contrast of MT walls, even with single axis tomography (figure 2b). Though dual axis tomograms provide the more isotropic resolution and contrast (Mastronarde 1997), our strategy provided reconstructions with adequate quality,

even though they were based on only half the data, a serious issue when large volume reconstructions are considered.

Our first approach to picking favourable cells is based on producing a preliminary, or "screening" tomogram by acquiring pictures in which the pixels are

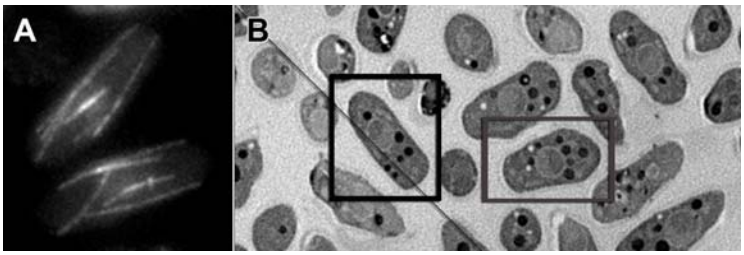

Figure 2 Linear arrangement of microtubule interphase arrays in fission yeast enables single axis tomograms to give the resolution required A) fluorescence picture with GFP-tubulin. (Courtesy of Dr. Damian Brunner). **B)** A suitable, well embedded, short cell (black square) aligned along tilt axis (black line) in low magnification. In this orientation IMAs should have ideal resolution in single axis tomograms. Cell not suitable for single axis tilt series is shown in grey square.

binned to ~ 2 nm and images are collected at 4° increments over ± 60°. These data are used to build a tomogram using cross-correlation to align the tilted views without fiducial alignments. The resulting tomogram provides a low-resolution 3D image of the contents in the section studied. When these reconstructions revealed MTs lying flat within the section, we collected the data necessary for a serious reconstruction (1.5° increments over ± 60-65° tilt, 1.526 nm pixel). The MT bundles could then be followed through the serial sections.

The second approach was made possible by the ease with which one can acquire montaged images, using the SerialEM acquisition software (see http://bio3d.colorado.edu for details). Short cells (7-9μm) in the right orientation were found and tracked through serial sections (see figure 3a). To find a cell that is present in all sections and preferable do not have dust covering any sections is difficult. By initiating the search for a cell that looks cut through the middle in the mid-section of the ribbon, one increase chances to find all serial sections within the sections on that grid.

Searching for the right cell was simplified by the newly developed Navigator software, which works within SerialEM. Navigator makes a low magnification montage of the whole EM grid. The resulting map can be used to identify promising areas and to zoom up in magnification, seeking a cell that looks well preserved, then zoom out and make sure one can follow the cell through the serial sections. Each cell that is suitable can then be marked with a colored point (figure 3b) and can be relocalized automatically by the computer-controlled stage, even after the grid has been removed from the microscope, thanks to the use of four registration points. Only when a cell was traceable through many sections (5-16) did we go on to acquire montaged image from each section, covering the whole cell length at a resolution appropriate for reconstruction (figure 3c and 3d; 1x3 montage, 1.5^{o} increment, ± 60-65˚, 1.526 nm pixel). Serial sections were then joined in z to reconstruct a *S. pombe* cell that is around 4 μm in diameter. Thus, reconstruction of large parts or even whole cells was achieved and the MT bundles could be partially or even completely reconstructed (figure 3e).

2. Image Acquisition

Tomograms are 3D reconstructions of samples that have been imaged from many directions. The more directions of view included and the higher the total range of the angles of view, the better resolved are the internal content of the section. Therefore, special high-tilt holders have been developed to allow for angles of tilt to up to ±75˚. For the optimal usage of these holders the specimen must be placed centrally on the EM grid.

When the electrons hit the plastic-embedded sample, shrinkage is induced (Luther et al. 1988). This shrinkage causes problems during the subsequent image alignment so it is important to minimize the shrinkage during acquisition of a tilt series. If a pre-illumination step is added, most shrinkage has occurred before the first picture is taken. During this “pre-burn” the electron beam is spread to include a large area around the sample, to have a uniformity of the shrinkage in the whole area, and left there for around five minutes.

Several programs are available to facilitate the collection of data for tomography; the choice of which to use is determined by the application and which hardware is available. Some examples are TOM, TVIPS and SerialEM. We used SerialEM, which is

specially adapted to the FEI Tecnai series and has proven very useful for MT studies, especially when large volumes and montaging are necessary (Mastronarde 2005).

Tilt increment and angular range desired are entered into the software which then undertakes a repeated macro of tilting the specimen holder, tracking the sample, focusing, final exposure, and saving the image to file. For work with stained, plastic embedded samples that seeks about 5 nm resolution, pictures are usually taken with about 0.2 µm defocus for optimal result.

Tomogram calculation and 3D model reconstruction

1. eTomo and tomogram calculation

After a series of tilted 2D projections of the specimen has been taken it must undergo a set of processes to generate the final tomogram. Also here there are several software packages available, depending on the application and nature of your data. IMOD is the only software, to our knowledge, with integrated ability to calculate montaged tomograms (Mastronarde 1997; Sandberg et al. 2003). Further, it has a graphical user interface, eTomo, and a large set of programs designed specially for dealing with microtubules once the tomogram has been generated. For an in-depth introduction and a tutorial to this software see the webpage (http://bio3d.colorado.edu/).

The first step towards a high quality tomogram is to remove camera defects as well as extremely bright pixels that were created during image acquisition by x-rays. This can best be done by replacing any markedly deviating pixels with the average values from surrounding pixels in a sort of interpellation process. The IMOD package includes a program called *ccderaser* to do this job.

Tomograms are generally calculated by a weighted backprojection of the 2D projections acquired, though other methods are available (Frank, 1992). For the best possible resolution in the final tomogram all the projections must be carefully aligned to one another. If one uses the IMOD program suite, the images are first aligned coarsely, using cross-correlation (programs: *xcorr, prenewst*). Large deviations in this alignment can be fixed in the manual alignment program, Midas. Then a selection of fiducial

particles (the colloidal gold from both sides of the sample) is used to refine the alignment. This is most easily accomplished if the particles are evenly spread over the specimen. These gold particles are then tracked through all of the projections and a model that represents all of these points is visually scrutinized to identify points that are out of place. It is important to ensure the best possible alignment of the tilted views. Fiducial alignment is a time consuming process because corrections are made in cycles with increasing accuracy. On montaged tomograms around 40 fiducials per frame are chosen and local alignment is used. Local alignments separate the image stack into smaller regions by choosing areas that include a certain amount of fiducials on each side of the section (default is 8 on one side and 3 on the other but this is flexible). These region's distortions are then separately considered by the algorithms that estimate the position of the gold fiducial, which greatly improves the estimates. Hence, one has to consider that the larger the imaged area the higher the distortions, therefore local alignments matter even more with large areas such as image montages.

Once the alignment is as good as possible, three quick tomograms corresponding to the top, middle, and bottom of the volume are created (*sample*) and viewed along an axis parallel to the plane of the section, e.g., the y-axis. By doing this, the section thickness, the angle around the x- and y-axes, and z position of the section within the tomogram become obvious. Then, by drawing boundary lines at the bottom, and top of the three tomograms a small model is created which gives numerical values for these parameters. In IMOD, the program *tomopitch* assures that the image stack is finally aligned and positioned so that the 3D volume created is as small as possible. In the final alignment step it is recommendable to use linear interpolation or the 2D image filtering option for optimal reconstruction quality.

The next step is the actual calculation of the tomogram, which is followed only by a final trimming of the volume, the conversion of pixels to bytes, and adjustment of contrast.

2. Joining of serial tomograms

To create reconstructions of large volumes, it is essential to join tomograms of serial sections. While one might imagine that a greater volume could be reconstructed

simply by imaging a thicker section, in our hands this leads to poorer image resolution and a reduction in the visibility of cellular detail, so objects like yeast MTs, which are surrounded by a dense distribution of darkly staining ribosomes, become invisible. Recently the procedure for joining serial tomograms with IMOD has been greatly simplified by a new function in the eTomo graphical user interface. The joining consists of three steps: set up, alignment, and join.

Set up includes defining the slices from each tomographic reconstruction that should be used for the visual alignment of the serial sections. These slices should be chosen so that organelles and the cell's plasma membrane are clearly visible, but they should still be as close to the top or bottom of the reconstructed volume as possible (figure 4 b and c). Furthermore, the sections that will be used as the first and last in the actual joining must be chosen. These should normally be the first and last section of the tomographic stack, so as not to lose any of the biological information available (figure 4 a and d).

The alignment step is crucial for the generation of a large serial tomogram from which it will be possible to generate a precise 3D model. Using eTomo there is an initial automatic alignment, which then can be manually improved, if necessary, with Midas. The transforms that will bring about proper alignment are saved in a text file that is then utilized in the final join step. Here the serial section tomogram reconstructions are stitched together into one large image file. To ensure the best possible result, a test join option is available in the software. This option creates an image stack with every *n*th picture (so the file is not too big for rapid calculation and display); this can easily be opened and scrutinized before the final join is submitted. It is often necessary to do iterative steps of trial joins and alignments for the best final joined tomogram possible.

3. Taking a snapshot from the tomogram

It is often useful to prepare 2D images that are slices from the tomogram. To create snapshots in IMOD, there are simple key commands that will save either the full screen or a selected part of it as either a "tif" or an "rgb" file. Since these forms of the data are useful for presentation, one must make sure that the contrast is ideal before

storing such an image. If the image is to be used for publication, one has to acquire a montaged snapshot, which can provide the resolution appropriate for such a use.

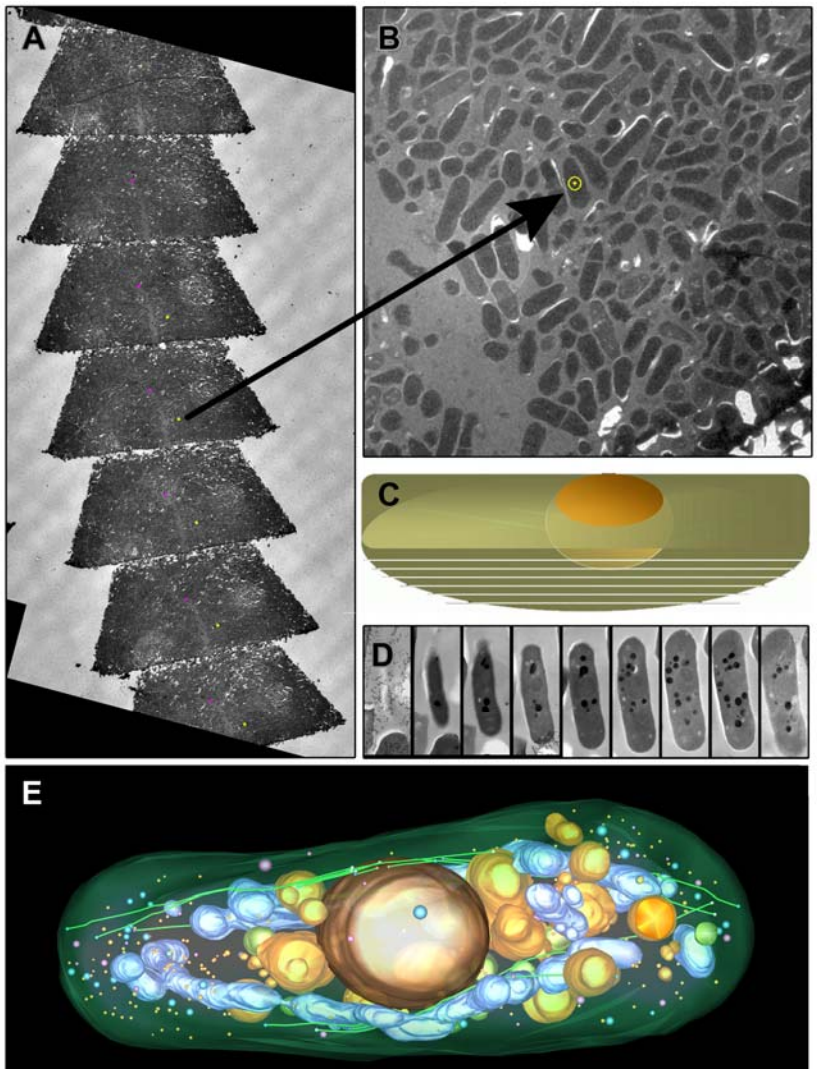

Figure 4 Principle of choosing sections for tomogram joining A) and **D)** are sections that are used for the actual join. Ideally, they are the top and bottom sections of the tomogram (red lines in E). **B)** and **C)** are used for alignment since intracellular detail is clearer (green lines in E). **E)** Tomogram flipped around the x-axis, so that we see the depth of the section. **F)** Unaligned sections from top (green) and bottom (magenta) of adjacent serial sections, **G)** sections in F) have now been aligned, **H)** side view of an image file containing nine joined serial tomographic reconstructions.

A snapshot from a tomogram is often the image data from a single tomographic slice, which is usually only 1-2 nm thick. Often one can make a more useful and pleasing image by averaging the 2D information in several adjacent tomographic slices. In IMOD this can be accomplished with the slicer tool. Slicer can also be used to change the orientation of the sample that is cut from the tomogram, so it will best display a feature of interest, like a cytoskeletal fiber.

4. Construction of a 3D model

A. Tracking MTs and other filaments using 3dmod

Segmentation of the image data in 3D reconstructions is sometimes necessary to clearly visualize and display the organization of a feature of interest, like the MT bundles. Segmentation can create graphic objects that represent features of interest without the complexity that is caused by tomographic imaging of well-fixed cytoplasm. A model can then be built from these graphic objects, which simplify structure interpretation and can be used for measuring distances between organelles. Still, one must remember that making a model is an interpretation of the data. Thus, it should not be used instead of snapshots of the real tomogram unless such simplification is necessary. The program suite called IMOD includes the program *3dmod*, which allows a choice of closed or open contours to represent objects on each plane in the tomogram. These contours can subsequently be used to define a graphic object that accurately represents the cellular structure of interest.

A major advantage of having a computerized 3D reconstruction to study is that modeling is greatly facilitated. For example, if one is studying MTs in the bundle, one can cut the reconstructed volume at any angle. In *3dmod* one can use the slicer option to extract from the tomogram a slice that contains a MT's axis. This greatly facilitates tracking the MT because one can follow the polymer through the reconstructed volume by placing the cursor in its lumen (figure 5a) and adjusting the orientation of the slice until the MT is laying flat in the field of view. One can step through tomographic slices to find the middle of the MT (when it looks the widest) and then draw a line (an open contour) down the middle of the fiber (figure 5b). Since MTs are flexible, the line that represents their axis will often curve, and realignment along the way is almost always

necessary. Once the end of the MT is reached, one can represent the end structure with a simple label, such as a point that is color-coded to represent a feature of interest, such as whether the end is open/closed or skirted/blunt/sheet/closed, etc. (figure 6). By keeping track of MT end morphology, we have learned that cytoplasmic MTs in *S. pombe* are often open at one end and capped at the other. This manifestation of structural polarity is likely to be of physiological significance, so we have represented it in all our models of fission yeast MTs. As one works, one should make a new contour for each new MT.

When drawing a contour to represent each MT, it is important to make sure that each fiber is represented in the model once and only once. In IMOD we have found it easy to do this if each point is highlighted with a circle (choose circle in the edit, object, type menu). The MTs being tracked is then represented fully by using the computer to place a circle on each tomographic slice. This is accomplished by the function "fill in Z" in the edit menu (figure 5c).

When a MT bundle passes through serial plastic sections it is sometimes not immediately clear how the contours on one section connect with contours on the next. The process of making these connections accurately can be simplified by modeling each of the MT fragments individually (separate contours), filling them in z, and then studying both the model and the model superimposed upon the tomogram to decide which two contours to connect. Once these determinations have been made one can join the two contours together. In IMOD this employs the "join" function in the edit contour menu. Equally, if two contours have been falsely connected they can be broken again by the "break" function in the same menu. It is also possible to go back to a contour already created and add more modeling points. One must simply start by highlighting the last point created. If one wishes to add at the end that was first digitized, it is easiest to invert the contour before adding more points or toggle the modelling direction.

The contours are shown in the model as lines, which are not very similar to real MTs. To provide a more realistic 3D image the contour can be meshed to form a tube whose diameter represents that of an actual MT. In IMOD this uses the program *imodmesh* and –t option for making a tube. If the MT appears kinked at the site of a join between sections, the program *mtsmooth* can help to take that out. Note that the MTs need to be remeshed before the smoothing is apparent. However, use of mtsmooth should

be conservative; since you change the original trajectory of the MT. it is therefore not advisable before measuring distances between the fibre and a second object such as the mitochondria.

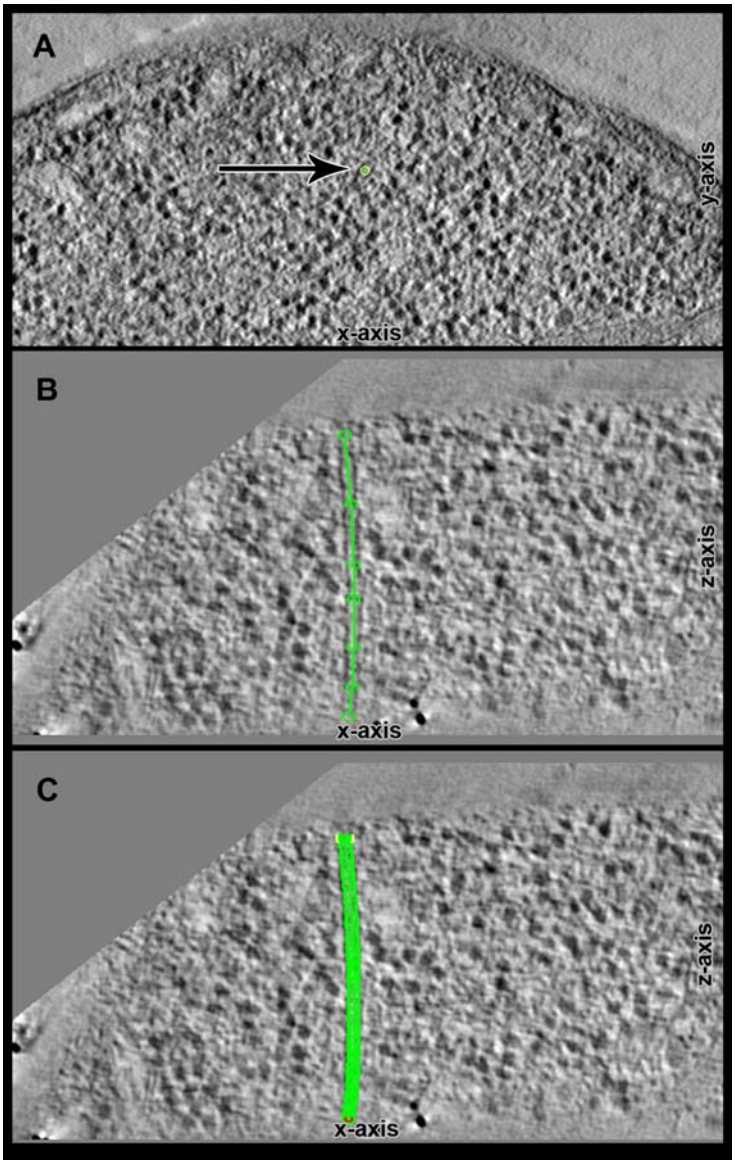

Figure 5 Modeling of MTs A) Zap window with a green modeling point in the lumen of a MT **B)** same MT properly oriented and modeled in the slicer window **C)** the MT has been 'filled in Z' which simplifies tracking and modeling of MT bundles in the Zap and slicer windows.

B. Modeling nucleus, PM and other membrane-bound organelles in 3dmod

Membrane bound organelles should be modeled as surfaces that display the position and shape of the membrane in space. *3dmod* allows a choice of closed contours, which will always connect the last point digitized with the first. This is ideal for representing membrane-bounded structures where in general there are no free edges. If one is using *3dmod*, the digitization of membranes is conveniently done directly in the Zap-window. To outline membrane-bound organelles in the tomogram, e.g., to show the cell's shape, it is not necessary to place a line around the structure of interest in every tomographic slice. Every third, fifth, or even tenth section is usually sufficient as long as there is not a significant change in the shape of the organelle. If there is, smaller increments between contours are required. The ghost function (under the edit, contour, type menu) simplifies drawing a smooth surface by showing the last contour you painted as a shadow on the sections near it.

If the surface still needs some smoothing after careful drawing this can be performed using the *smoothsurf* program. To skin the objects use the *imodmesh* program.

5. Analysis of 3D data

A. Measuring within a model

When a plastic embedded sample is in the electron microscope the beam vaporizes some of the plastic material, causing the sample to shrink anisotropically (Luther et al., 1988). This shrinkage is mostly in the axis perpendicular to the section plane, so the resulting distortions must be accounted for when making measurements in the volume. In 3dmod this may be done in an approximate manner by changing the z-scale in the edit model header menu to a number found by following formula:

z-axis = a/(n*p) where

a = Thickness of section(s) at sectioning (as defined by the microtome setting or better by the interference color of the section, or better still by interference microscopy)

n = number of tomographic slices in reconstruction

p = pixel size in nm

If the image file consists of many serial tomograms, this formula can sometimes overestimate the shrinkage, and after its application the organelles look stretched along the z-axis. An alternative is to find the z-scale factor by trial and error until the nucleus or appropriate small vesicles appears round. The error in using the equation is probably a result of the a-term, which is dependent on the precision with which one could measure section thickness before putting it into the EM.

Once the tomogram has been made isotropic, all volumes, lengths and areas can be measured readily. In IMOD this is accomplished with the *imodinfo* program. If the pixel size has been entered in the header menu, the *imodinfo* file will give the measurements in the unit entered, otherwise the output is in pixels.

B. Quantifying feature proximity in IMOD

There are existing programs within the IMOD suite that allow the analysis of 3D models of cellular structure. Our study of MT bundles in interphase of *S. pombe* is greatly facilitated by these programs. For example, the average distance of MTs from one another can be determined using *nda* (neighbour density analysis). This distance can then be used in *mtpairing* to see which MTs are placed relative to one another by this characteristic distance, or something close to it. This can help in deciding when a MT is in a bundle and how long the actual bundle is. Clearly, such decisions are to some extent matters of definition, but with proper quantification, one can be explicit about how such decisions were made.

Preferred distances between 3D objects (i.e. membrane-bound organelles) and MTs can be determined using *mtk* (MT "kissing" program) (Marsh et al. 2001). It defines the distances of closest approach between MTs and any chosen surface. The program displays the frequencies of such distances as the number of objects per cubic micrometer at the given distance. Thus, one can examine whether a given organelle is positioned relative to MTs in a way that departs from randomness. The departure from random can, in turn, be taken as evidence for some level of interaction between the two objects. For more MT analysis and processing programs see Materials.

Light microscopy

Cells expressing different fluorescently labeled SPB proteins (table 2) were grown in EMM media (see 'Cell Culture' section) and attached with 1 µl of 2 mg/ml lectin to glass bottom microwell dish. Unattached cells were removed with a medium wash after 10 minutes of sedimentation. Cells were imaged in 2 ml of EMM medium.

Stack of eight slices (0.5 µm distance between planes) was maximum projected and the amount of fluorescent particles was quantified manually.

Materials

1. Cells and media

S. pombe strains (see table 2) was grown in suspension culture at 32ºC on yeast extract with five amino acid supplements (YE5S; i.e. adenine, histidine, leucine, uracyl and lysine, for details, see Moreno et al., 1991) until they reached midlog-phase growth. Alternatively, cells were grown in the defined Edinburgh minimal medium (EMM).

Table 2 Strains used in this study

Strain	Genotype	Source
Tomography:		
PN972	h-	P Nurse
DB518	h- *mal3Δ::his3 ura4-D18 leu1-32 his3-D1 ade6-M210*	I Hagan
DB 392	h+ *tip1Δ::KanR ade6-M210 leu1-32 ura4-D18*	D Brunner
LM:		
DB1219	h- *cut12-GFP::ura-4 leu-1-32 ura4-D18*	I Hagan
DB1037	h- *cut12-GFP::ura mal3Δ::his3 ura4-D18 leu1-32 ade6-M210*	This study
DB1222	h- *pcp1-GFP::KanR ade6-M210 leu1-32 ura4-D18 his-*	T Davis
DB1234	h+ *pcp1-GFP::KanR mal3Δ::his3 his- ade6-M210*	This study
DB1326	h- *cdc11-GFP::KanR ura4-D18 leu1-32 ade6-M210*	K Gould
DB1376	h- *cdc11-GFP::KanR mal3Δ::his3 his3-D1*	This study
DB1324	h- *sid4-GFP::KanR ura4-D18 ade6-M210 leu1-32*	K Gould
DB1374	h+ *sid4-GFP::KanR mal3Δ::his3 his3-D1*	This study
DB1325	h+ *spg1-GFP::KanR ura4-D18 ade6-210 leu1-32*	K Gould
DB1382	h+ *spg1-GFP::KanR mal3Δ::his3 ura4-D18 ade6-210 leu1-32 his3-D1*	This study
DB1203	h+ *tip1Δ::KanR lys1+::nmt1-GFP- α-2tub*	D Brunner
DB1405	h- *ura4-d18 lys1+::nmt1-GFP- α-2tub*	D Brunner
DB1591	h- *nmt1-mcherry-α-tubulin KanR cut12-GFP:: ura4 ura4-D18 or ura4-06*	This study
DB1610	h- or h+ *tip1Δ::KanR nmt1-mcherry-α-2tub KanR cut12-GFP:: ura4 leu-1-32 ura4-D18*	This study

2. High pressure freezer, freeze substitution, resins

Both the BAL-TEC HPM 010 high pressure freezer (Bal-Tec, Balzers, Lichtenstein) and the Leica EMPACT-1 (Leica-Microsystems, Vienna, Austria) were used to freeze yeast cells (McDonald 2006). The advantage of the BAL-TEC machine is that a rather large volume can be loaded in the carrier (2 mm in diameter and 200 μm in depth). Therefore, one can process a large pellet of cells, which, once embedded in plastic, can be cut in several smaller blocks using a fine saw. With the Leica EMPACT-1 device (Studer et al. 2001) we mostly used home-made carriers (2 mm of diameter and 1mm thick containing a sample cavity 200 μm in depth and 1.2 mm in diameter).

The slot carriers (Leica) were advantageous as they provide a larger pellet, which was easier to handle than the flat carriers (Leica). With the latter, pellets do not easily come off as a single object upon rinsing the carriers with acetone at the end of the FS run. Moreover, we had variable quality of freezing using these carriers.

Freeze substitution was always performed in a Leica EM AFS device (Leica Microsystems, Vienna, Austria) using the special perforated plastic tubes, which greatly facilitate the solvent and resin exchange.

Lowicryl HM20 (Polysciences, Warrington, PA, USA) was mixed in dehydrated acetone during the progressive infiltration steps.

3. Microscope hardware

Tilt series were taken on the FEI Tecnai TF20 transmission electron microscope (TEM), operating at 200 kV. The images were collected on a Gatan Ultrascan 890 digital camera as well as on a Gatan Ultrascan 895 digital camera (4 port readout, 15 μm/pixel). The latter camera was about three times faster in acquiring tomograms; therefore it was particularly profitable when montaging of many serial sections was required upon tilt series acquisition.

A FEI Tecnai TF30, operating at 300 keV was used when thicker sections were employed. A Gatan Megascan 795 camera was mounted on this TEM.

The tilt series were acquired over ± 65˚, using a Gatan 670 high tilt holder, a Fischione 2020 high tilt holder, or a Gatan 650 high tilt-rotate holder. The preferred holder was the Fischione holder which had the best range where high tilts could be achieved so that larger area of the grid could be used. Thus, it was easier to find many serial sections of the cell to image. The Gatan 650 high-tilt rotate holder had a complex grid attachment system, which made the slot grids more prone to break during specimen changes. Further, the area on the grid where high tilts were possible was comparatively small. However, this holder had the advantage that a well-preserved cell could be turned into the right orientation for optimal resolution with single axis tomography without the removal of the grid.

4. Microtome

The plastic semi-thin sections were cut at a thickness between 210-250 nm using a Leica-Reichert Ultramicrotome (Leica Microsystems, Vienna, Austria). We used diamond knives with a 35º included angle (Diatome, Biel, Switzerland). The sections were collected on copper palladium slot grids (2x1 mm) freshly coated with Formvar (1% polyvinyl formal in chloroform). We used cationic gold particles (15 nm) (British BioCell International, UK) as fiducial markers.

5. Computers

Sun opteron computers running the Fedora operating system and the IMOD software package were used to calculate tomograms. The IMOD software works only with upper-end Nvidia graphic cards. The large file sizes produced demands of 4-16 GB of RAM. All data were stored on a 2 TB network server, therefore only standard size local hard drives were necessary. Further, a three-buttoned mouse is essential.

6. Software package IMOD ©

IMOD is a software package containing around 140 different programs for image processing, tomographic reconstruction, modeling and display (Kremer et al. 1996). As described above, it includes features that facilitate 3D reconstruction of EM serial sections, and it can be used for optical sections as well. Most commonly the display

programs *3dmod* and *3dmodv* are used. *3dmod* displays pictures stored in the mrc or tif format; they can then be modeled and displayed in 3D using *3dmodv*.

In addition to all the programs required for tomogram reconstruction there are several programs developed specially for research on MTs. Here is a short list of the MT related programs that are the most important when working with tomograms:

mtoverlap – this program is used to display and measure overlaps of microtubules coming from two distinct foci, like the poles of a mitotic spindle.

mtpairing – this program determines when MTs are paired and the length of this region of pairing. Further, this program can recolor MTs depending on their polarity (based on the positions of their end points in z).

mtk – MT kissing is a program to analyze the distance in 3D between microtubules and other objects, such as mitochondria or the nuclear envelope (Marsh et al. 2001).

nda – neighbour density analysis is a program to measure the preferred distance between MTs in a bundle. To use this program, a model must first be converted using *resamplemod* (Mastronarde et al. 1993).

mtsmooth – this program smooths the trajectory of open contours, such as MTs, to improve their presentation. It should not be applied to models that will subsequently be analyzed by *nda* or *mtk*.

resamplemod - some of these programs were developed for serial section 3D reconstruction. This program was developed to convert a 3D model built from a tomogram into a model by turning it 90^{o} about the y-axis and resectioning it.

For more information on these and other programs, visit the website http://bio3d.colorado.edu/ (here, there is a listing of all programs available in the IMOD software package, which is downloadable at no cost).

7. Light Microscopy Hardware

To image live cells, images were taken on a Coolsnap HQ digital camera (Roper Scientific, Tuscon, AZ) on an Axiovert 200 M microscope (Carl Zeiss, Göttingen, Germany) with a Plan_Apochromat 100x NA objective (Zeiss). We used glass bottom dishes (MatTek, Ashland, MA) coated with lectin from Sigma, St. Louis, MO).

8. Light Microscopy Software

We used Metamorph 6.2r6 to acquire pictures that were processed using ImageJ 1.37v. A plug in package created by Kota Miura, EMBL, was used for particle tracking.

Chapter 3

Organization of interphase microtubules in fission yeast analyzed by electron tomography

Introduction

Cells are seldom round or symmetric. Classic examples of cells with differentiated shapes include neurons and epithelial cells, but small cells, like yeasts and bacteria, also show growth polarity (Drubin and Nelson 1996). In such polarized cells the MT cytoskeleton and its associated proteins (MAPs) are fundamental elements that support cell shape generation and maintenance. Thus, it is not surprising that fission yeast has become an important model organism for studies on the role of MTs in cell morphogenesis (Hayles and Nurse 2001; La Carbona et al. 2006; Sawin and Tran 2006).

Cytoplasmic MTs in fission yeast have been extensively analyzed by light microscopy (LM) and in a few studies by conventional EM techniques, but knowledge of the precise structural arrangement of these MTs has been lacking. LM analysis has described the fission yeast interphase MT cytoskeleton as three to six MT bundles arranged along the long axis of the cell. These bundles appear to meet as pairs in the middle of the cell, forming a narrow zone of antiparallel overlap between MTs, whose plus ends extend towards opposite ends of the cell (Drummond and Cross 2000; Tran et al. 2001; Sagolla et al. 2003). MT growth has been seen to slow down for some time at the cell ends before the MTs undergo rapid depolymerization (Drummond and Cross 2000; Tran et al. 2001; Grallert et al. 2006). During this period, tea1p and tip1p are deposited at the cell tip. If production, delivery or anchoring of these proteins is inhibited, the cells show abnormal growth patterns, creating branched or bent cells (Mata and Nurse 1997; Brunner and Nurse 2000; Behrens and Nurse 2002; Snaith and Sawin 2003; Feierbach et al. 2004).

The minus ends of MTs are less dynamic than their plus ends (Mitchison and Kirschner 1984). In fission yeast these are localized in the nuclear area of MT overlap, also called the interphase MT organizing center (iMTOC). Until now iMTOCs have not been defined as discrete structures in fission yeast. MT minus ends are thought to be stabilized with a γ-tubulin ring complex (γ-TURC) that caps the MT tip (Keating and Borisy 2000; Moritz et al. 2000; Wiese and Zheng 2000). γ-tubulin and other components of the γ-tubulin ring complex (γ-TURC) localize to the SPB (Ding et al. 1997) and to moving particles, referred to as satellite MTOCs (Sawin et al. 2004; Zimmerman et al. 2004; Janson et al. 2005; Zimmerman and Chang 2005). Some of these satellite MTOCs are thought to actively nucleate MTs whilst moving bidirectionally along existing MTs (Janson et al. 2005) but most are concentrated in the iMTOC region (Sawin and Snaith 2004; Zimmerman et al. 2004). iMTOCs also appear to attach to the nuclear envelope, although the mechanism of this attachment is still not known (Tran et al. 2001).

Electron microscopic (EM) serial section studies have shown that a variable number of MTs are laterally bound to each interphase SPB (Ding et al. 1997; Uzawa et al. 2004). Since it is not possible to identify the polarity of MTs in such conventional EM analysis, Ding and co-workers suggested that the variability of MT number could be due to MT nucleation, or possibly MTs nucleated elsewhere and ending in this region. Recent evidence suggests that the *S. pombe* ASE1/PRC1/MAP65 homologue, ase1p, bundles interphase MTs and also facilitates the maintenance of MT minus ends at the overlap region. A model in which ase1p forms bridges between antiparallel bundles has been proposed (Loiodice et al. 2005; Yamashita et al. 2005), but ase1p is probably not the sole MT bundler in fission yeast (Carazo-Salas and Nurse 2006; Daga et al. 2006b). It has been shown that klp2, a minus directed kinesin-like motor protein, slides MTs of opposite polarity (minus ends out) away from the cell periphery and towards the iMTOC (Carazo-Salas et al. 2005).

Correct positioning of organelles is essential for cell division and often depends on MTs. Here, we analyzed the function of MTs in organelle positioning by measuring the 3D association between MTs and mitochondria or vesicles respectively. Mitochondria in fission yeast are organized as large, branched networks that shrink and grow together

with MT (de)polymerization (Yaffe et al. 1996; Yaffe et al. 2003). We present here the first high resolution study confirming this interaction.

Endocytosis, exocytosis and intracellular trafficking between membrane bound organelles inside the cell involve functionally distinct trafficking vesicles adapted to dock and fuse with defined target membranes. These vesicles are commonly transported along MTs, and mediate the regulated delivery of membrane components, as well as vesicular content in multi-step transport (Lippincott-Schwartz 1998; Bonifacino and Glick 2004; Takamori et al. 2006). However, during yeast endocytosis actin patches are formed at the sites of internalization and have been seen around vesicles in EM studies (Kanbe et al. 1989; Takagi et al. 2003; Gachet and Hyams 2005; Kaksonen et al. 2005). These actin patches and late secretory vesicles are transported within the cell along actin cables (Feierbach and Chang 2001; Pelham and Chang 2001; Huckaba et al. 2004). In fission yeast, MTs might play a role in Golgi to endoplasmic reticulum (ER) membrane recycling through the kinesin like protein klp3p, as well as in stacking Golgi cisternae (Ayscough et al. 1993; Brazer et al. 2000). However, secretion is not affected by the loss of MTs (Ayscough et al. 1993). In this study we examine the role of fission yeast MTs in vesicular trafficking based on an ultrastructural analysis by electron tomography.

Moreover, we illustrate the three dimensional bundle architecture and distribution of cytoplasmic interphase MTs. For this purpose we have developed a large-scale ET approach that yields reconstructions of significant parts of cells and even whole cell volumes at a resolution where MTs and their end structures are clearly visible (Höög and Antony *in press*). The number of MTs in a bundle has been quantified and MT polarity identified; we also describe links between MTs and bridges between MTs and other cytoplasmic components. This work opens a new window on the study of cellular architecture at high resolution.

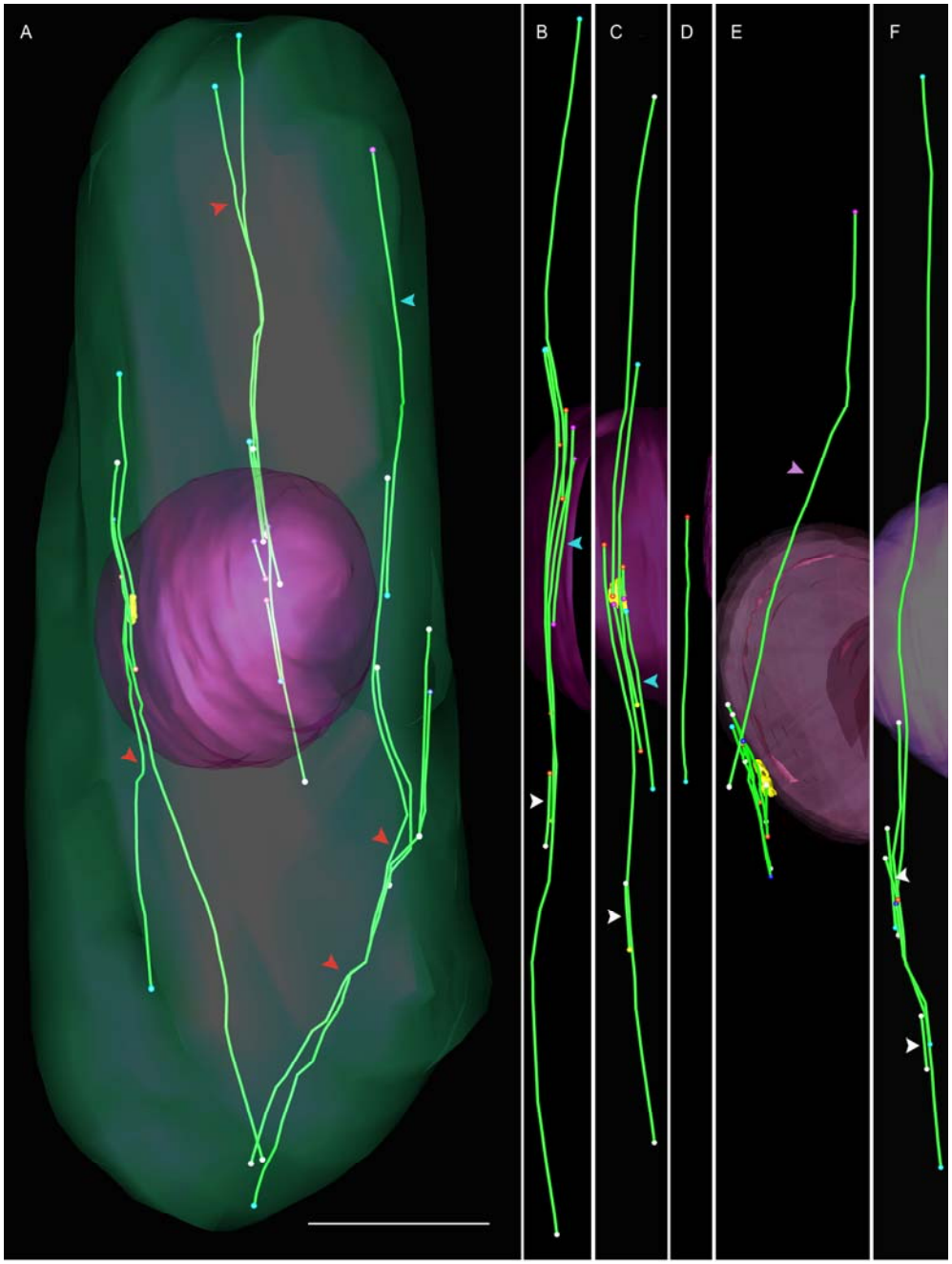
A
B
C
D
E
F

Figure 1 3D model of interphase MT bundles
MT end structures are indicated by colored caps: red (capped end), turquoise (flared end), blue (blunt end) and white (ambiguous end). The NE is shown in transparent pink. **A)** A reconstruction of a complete cell volume that contains three interphase bundles (green) and a total of 16 MTs. Splaying of MT bundles is marked with red arrowheads. **B)** A typical example of a larger MT bundle. Short MTs detached from the nuclear region are marked with white arrowheads. Turquoise arrowheads mark MTs where both ends are open. **C)** SPB (yellow) bundle with a typical MT arrangement. **D)** A single MT not associated with the NE. **E)** One MT (pink arrowhead) attached to the NE and crossing an SPB-associated MT bundle. **F)** An unusual example where the bundle is not attached to the NE and the overlap region is shifted closer to the cell's tip. White bar = 1 μm.

Results

Spatial organization of microtubule bundles and quantification of tubulin polymer

We cryoimmobilized cells in log phase growth by high pressure freezing, then fixed them by freeze-substitution, and embedded them in acrylic resin. Plastic embedded cells were sectioned into 250 nm thick slices from which tilt series were acquired (±60-65˚, 1.5˚ increment). Large volumes were reconstructed by tomography on 17 different wild type cells; one of these was reconstructed completely. Using the 3D imaging capabilities of ET, we tracked the MTs through serial sections and measured their lengths. Short interphase cells (7-9 μm; pre-"new end take-off") were chosen to exclude the cells that could have been preparing for mitosis.

In the whole cell volume, reconstructed from 15 montaged serial tomograms, we found 16 MTs arranged in three bundles (figure 1A; supplementary movie 1). The cumulative length of polymerized tubulin in this cell was 34.5 μm. Due to the exact measurements of MTs and cell volume in this full cell reconstruction, we could calculate the concentration of polymerized tubulin. Assuming 13 protofilament MTs, since the diameter of *S. pombe* MTs is 25 nm (Schwartz et al. 2003), the total concentration of polymerized tubulin was 2.78 μM in this cell (total volume 33.5 μm^3 of which nucleus was 3.16 μm^3, mitochondria 1.23 μm^3 and vacuoles 2.21 μm^3).

We selected 4 cells (all pre-new end take-off) for further analysis and found that most MTs are short, with an average length of 1.64±1.43 μm (n=70; figure 2). (N.B. the high SD is due to the large variation in MT length; the longest MT was almost 6 μm and

the shortest only 70 nm). No single MT extended the length of the whole cell. From the exponential fit (figure 2F), we found that the average MT length was 22% of the cell length.

Average length of a MT bundle was 4.97±1.39 μm (supplementary table 1). In the region around the nucleus, bundles contained several MTs, consistent with this region being the iMTOC region. However, only a few single MTs extended from this region towards the cell ends. This organization was characteristic of larger bundles (figure 1B-C; supplementary movie 2). The average numbers of MTs in a bundle was 4.4±2.6 (n=28 bundles), but MTs were often found singly or in pairs (6 of 28 bundles). Most of the single MTs were lying by themselves in the cytoplasm (figure 1D), and in this analysis only two out of six showed a connection to the nuclear envelope (figure 1E). We suggest that these single MTs might arise through separation from other bundles, from cytoplasmic nucleation or de-attachment from the nucleus, as described in live cells (Carazo-Salas et al. 2005; Carazo-Salas and Nurse 2006; Daga et al. 2006b).

The shortest cell we studied showed a distinctive organization with two bundles not connected to the nucleus and very long MTs that connected to the cell's tips (figure 1F and 2A). It is possible that this cell had not yet completely established its interphase array after cytokinesis.

Microtubule polarity can be determined by polymer end structure

In previous tomography studies, based on specimen preparation techniques like those used here, MT end structures that correlate with polymer polarity could be identified (O'Toole et al. 1999; O'Toole et al. 2003). Five representative end structures and simplified representations of them are shown in figure 3A-F. In O'Toole et al's studies, capped or closed MT ends, were adjacent to the SPB or centrosome, where the minus end resides. Open end structures are commonly found at the MT plus ends, although some have also been found at MT minus ends near the centrosome (O'Toole et al. 2003). We also found MTs with two open ends, confirming this finding (turquoise arrows in figure 1) and implying that there is a sub-population of MTs with dynamic minus ends.

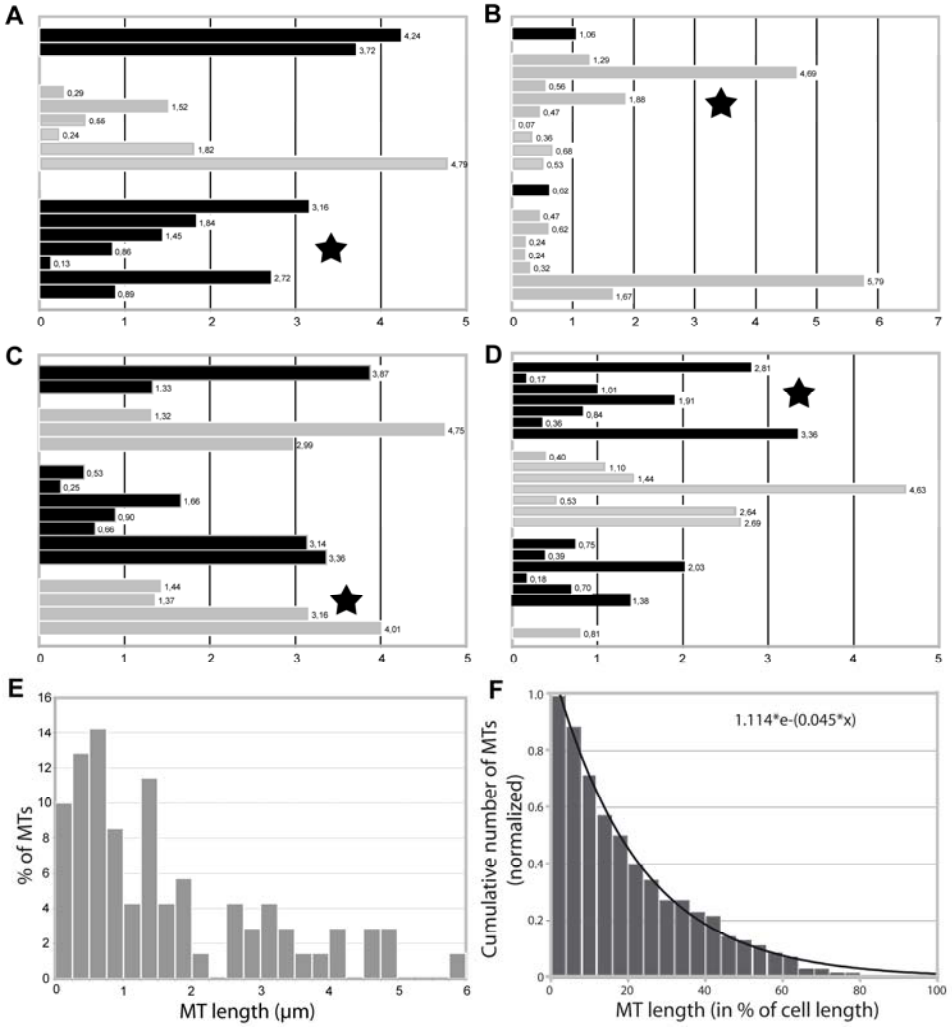

Figure 2 MT lengths
A-D) Bundles of MTs from four different cells are depicted as groups of black and grey bars, where each bar represent one MT. The bundle associated with the SPB is marked with a star. Cells that are: **A)** 6.7 µm, **B)** 7.4 µm, **C)** 7.7 µm (full cell volume), and **D)** 7.9 µm in length. **E)** Histogram of MT lengths (all MTs in A-D pooled) showing that most MT are 0-1 µm long. **F)** The line shows an exponential fit to the cumulative number of MTs per length interval, where each interval (bar) represents 4% of the cell length. Each bar contains all MTs that are longer than the x-value of that bar. The sum of square errors of the fit was 0.011.

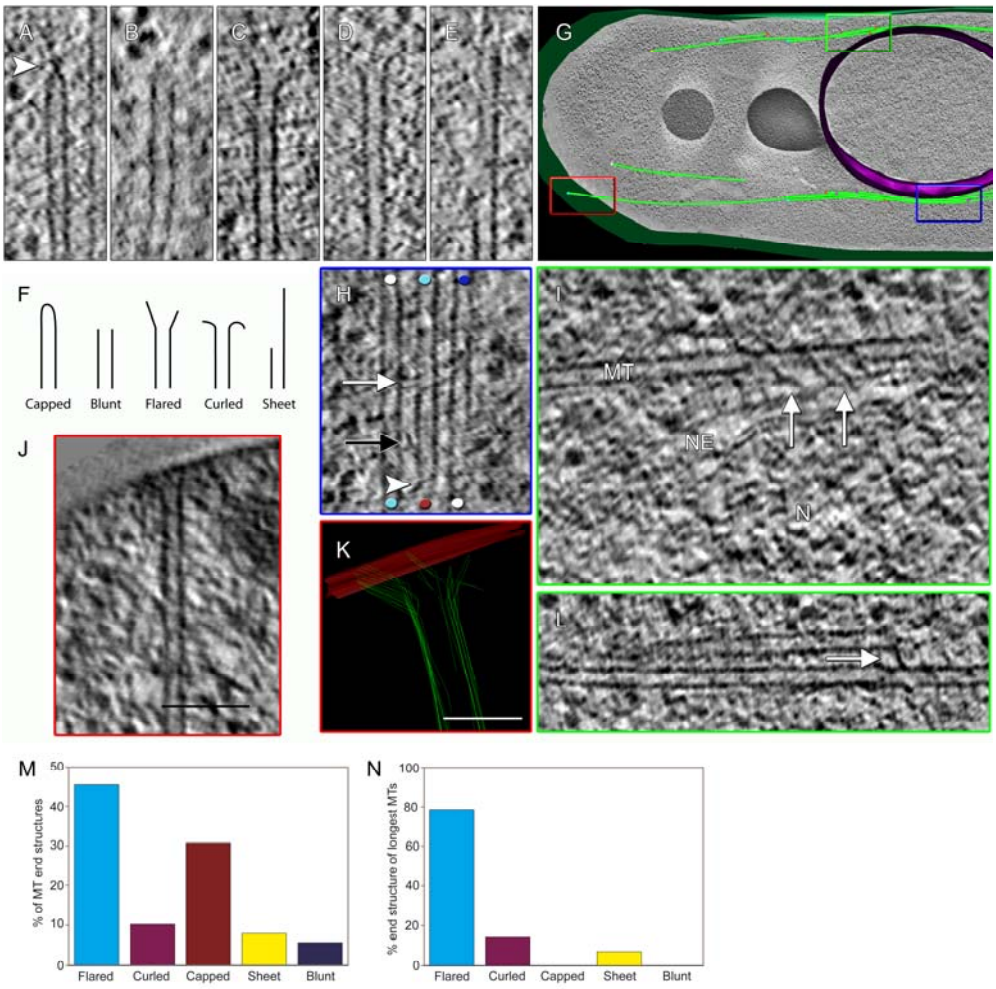

Figure 3 MT end structures and interactions
A) A capped MT end with attached filaments (white arrowhead). **B-E)** open MT ends; B) Blunt C) Flared D) Curled E) Sheet. **F)** Cartoon of MT end structures. **G)** Tomographic slice with the 3D model projected on top. The highlighted squares show the regions studied in H-L, where MTs are in close association with nuclear envelope (green), have bridges between themselves (blue), or touch the plasma membrane (red). **H)** MTs with interconnecting electron-dense bridges (white arrow). A forked bridge is indicated by a black arrow. MT polarities are indicated with a red (capped end), turquoise (flared end), blue (blunt end), or white circle (ambiguous end). **I)** Nuclear envelope with bridges (white arrows) connecting from the outer bilayer to the MT. **J)** Tomographic snapshot of a flared MT tip in direct contact with the PM. **K)** 3D model of protofilament structure at one MT end (each ~2 nm thick) **L)** An occasion where a capped MT end is connected to another MT by a strong electron dense bridge (white arrow). All MT snapshots are at the same scale: bar = 100 nm. White bar = 50 nm.

In fission yeast, the majority of capped (minus) MT ends (red spheres, figure 1A-F) were in close proximity to the nucleus. There was, however, no apparent object to serve as a point of MT nucleation; this made it difficult to fit this high resolution MT organization into the two anti-parallel bundles suggested by LM studies.

Interestingly, in some instances (n=10 of 70) MTs were completely disconnected from the nuclear region. These were typically short polymers and were oriented along other MTs. On these short polymers, clearly capped (minus) ends (n=3) were found oriented towards the cell center in two cases, but we also found one MT of opposite polarity (figure 1B-C and F; white arrowheads). However, the MT of opposite polarity was still within an iMTOC region that had shifted away from the nucleus (figure 1F).

Microtubules touch the plasma membrane

Microtubules are necessary for the correct positioning of the nucleus, as well as other organelles in the cell (Ayscough et al. 1993; Yaffe et al. 1996; Tran et al. 2001; Daga and Chang 2005). To push against cytoplasmic organelles, like the nucleus, the MTs must interact mechanically with the cell cortex. Additionally, polar growth of fission yeast cells depends on the cytoskeleton and a few gene products, like tea1 and tip1, that are delivered to the cell tip by the MTs (La Carbona et al. 2006; Sawin and Tran 2006). It was therefore of great interest to examine the exact subcellular location and structure of MTs as they made contact with the plasma membrane at the cell tips. We found six MTs in direct physical contact with the plasma membrane, each of which had a flared end (figure 3J). A 3D model of the MT tip was made on each computational slice of the tomogram (ca 2 nm thick) to exclude the possibility that the flared MT end was simply electron-dense noise (figure 3K). The presence of the density in each section confirmed the flared structure as a true MT end structure.

The flared structure has been associated with depolymerizing MT ends (Mandelkow et al. 1991). However, MT ends at the plasma membrane commonly continue to grow for ~1 min (D. Foetkhe, pers. communication). To correlate MT end morphology with the polymer's dynamic state at the time of freezing, we determined the fraction of total MT ends (n=88, figure 3M) that showed particular structures. Further, we

quantified the end types of the longest MT in each bundle separately (n=14; figure 3N), since this is the MT dynamic measured using fluorescence microscopy. We found that 79% of the longest MT's ends were flared. Since MT growth is slower than shrinkage, at steady state there should be more polymers growing than shrinking, so growing MTs in *S. pombe* may be flared (see discussion).

Microtubules are cross-bridged with each other and with the nuclear envelope

In order for MTs to push the nucleus to the center of the cell there must also be a physical connection between MTs and the nucleus. Studying the nuclear region in our tomograms (figure 3G) we found electron-dense filamentous bridges 25-30 nm long between the outer lipid bilayer of the NE and MTs (figure 3I; white arrows). Putative connecting bridges between MTs and the NE were found only on MTs that were closest to the nucleus. We suggest these structures might be physical links enabling the MTs to position the nucleus.

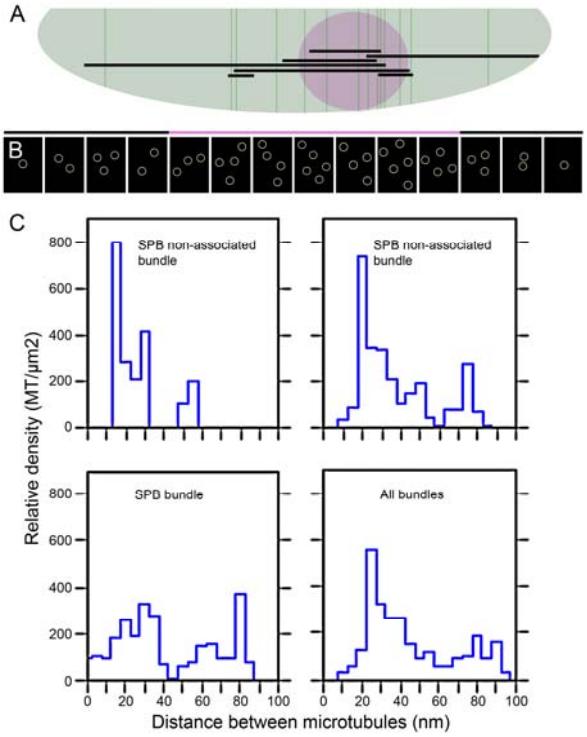

Figure 4 Neighbor density analysis shows the preferred distances between MTs
A) A schematic cell (green) containing a representative MT bundle, which is shown in transverse orientation (B) from the locations marked with green lines on (A). Nucleus is in pink. **B)** Frames from supplemental movie 3 indicating cross-sections through the cell schematized in A). Frames from the nuclear region are under the pink bar. **C)** Data from three similar models of individual bundles, preferred MT spacing is ~25 nm, surface to surface.

We saw no electron-dense area around the capped MT ends, but on one occasion a thick, electron-dense bridge was seen connecting the middle of one MT with the minus end of a parallel MT (white arrow in

figure 3L). In other cases filamentous structures were associated with the capped MT ends (white arrowhead in figure 3A and H). Some of the MTs in a bundle have similar electron-dense structures connecting them (figure 3H). These bridges are about one MT diameter long, and they are oriented at diverse angles relative to the MTs. Additionally, forked structures were seen (black arrow in figure 3H). Finally, bridges could be seen between both parallel and antiparallel MTs.

We hypothesized that the electron dense bridges might act as either spacers or bundlers of MTs. If so, one could predict the distance between the MTs to be constant. To examine whether the length of the filamentous bridges corresponds to the preferred minimum distance between MTs we performed a neighbor density analysis (nda). 3D models of bundles were used to determine the relative distances between MTs in regions with three or more MTs. Figure 4A shows a schematic representation of one such bundle that was analyzed (figure 4B; supplementary movie 3). The preferred minimum distance was 25-30 nm, surface to surface, with an additional small peak at around 50-60 nm (figure 4C).

Bundles associated with SPBs contain more MTs

We reconstructed 12 SPBs in their entirety, including all the attached MTs, which confirmed the lateral association of MT with both single and duplicated SPBs (figure 5A and E). In 11 cases, only one of the MTs in a bundle seemed in direct contact with the SPB (with no visible bridges), and this MT usually had no end close to this structure (figure 5B; supplementary movie 4). The other MTs in each bundle appeared to be stacked around this anchoring MT. Bundles were never in contact with both SPB and NE.

In one case out of 12, MTs radiated from the SPB with their minus ends towards that structure (figure 5C). Interestingly, almost all these MTs showed parallel polarity. This dissimilar cell's length was ~7μm. In all cases, SPB associated MTs were further from the NE than when not associated with the SPB (figure 5D).

In fluorescence images of cells expressing tubulin-GFP there is frequently one bundle that is brighter than the others; this is the one commonly assumed to be associated with the SPB. We examined the number of MTs in bundles associated with SPBs and found them to have a greater average number of MTs (5.7±1.5, n=12) than the bundles

that were not SPB-associated (3.25±2.5, n=16; figure 5F). However, there was no difference in the length of MTs in these two classes of bundles.

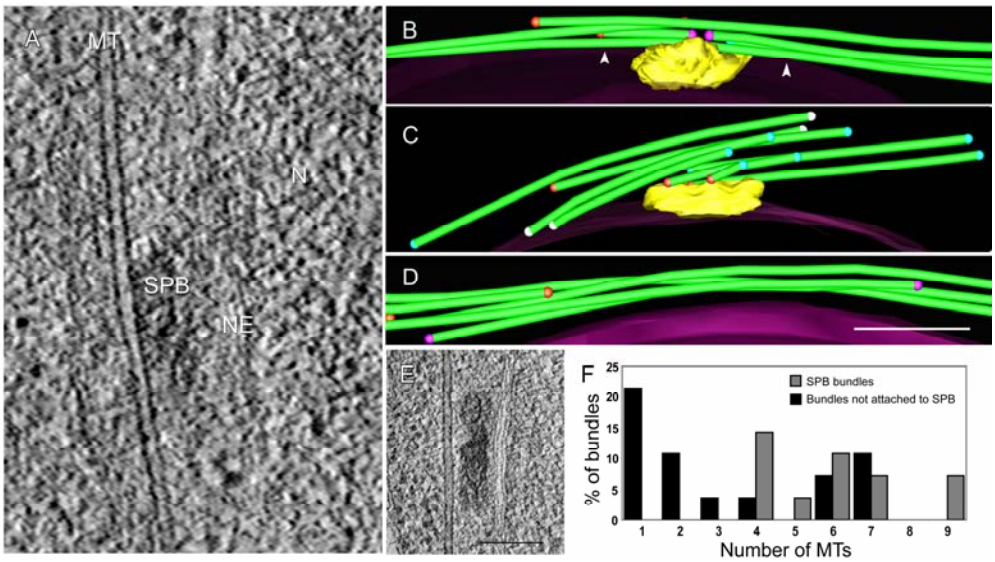

Figure 5 MT bundles associated with the SPB
A) Lateral association between the SPB, which is on the cytoplasmic side of the nuclear envelope (NE), and its closest MT. **B)** 3D model of a typical SPB (yellow) associated a MT bundle (green); the closest MT lies like a bar across the SPB (white arrowheads). MT capped minus ends (red) are not invariably directed towards the SPB; a few flared ends (turquoise) are near the centrosome equivalent. **C)** The sole example in which short MTs radiated from the SPB; their capped minus ends and a majority of the flared ends point to one side. (White caps = ambiguous end) **D)** Lateral MT association with a duplicated SPB (courtesy of Mary Morphew) **E)** Comparison of numbers of MTs in a SPB-associated bundle and in a non-associated bundle. White bar = 200 nm. Black bar = 100 nm.

Interaction of MT bundles and mitochondria

Connections between MTs and mitochondria have previously been described by fluorescence microscopy (Yaffe et al. 1996; Yaffe et al. 2003). These associations were, however, particularly clear in tomograms. We therefore examined these connections in more detail. Mitochondria and MTs co-cluster, with the mitochondria appearing to be stretched along the MTs (figure 6A-C). Further, mitochondria were often located between the MTs of a splayed bundle (figure 1A; red arrowheads; supplementary movie 5). In general, extensively branched mitochondrial networks were always associated with MTs (volume 0.23±0.16 μm^3, n=9; figure 6D-F and H), whereas non-MT-associated

mitochondria were smaller and unbranched (volume 0.02±0.03 μm^3, n=9). MTs were often bent around or towards mitochondria (figure 6I), suggesting a connection between them; however we did not detect any bridges like those found between MTs and the NE.

If MTs bind mitochondria one would expect there to be a preferred distance between the two (assuming one mechanism). In agreement with this hypothesis we found a peak of preferred minimal distance between MTs and mitochondria to be ~20 nm (figure 6J), comparable to the MT-MT distances described above (figure 4C).

In the full cell volume reconstruction we found 12 separate mitochondria of various sizes; these encompassed a total membrane area of 22 μm^2 and occupied 4% of the total cell volume. Comparatively, the nucleus occupied 9% of the cytoplasmic volume. Based on this evidence, we suggest that the MT bundles are connected to and shape this multicompartment organelle, which in turn, might influence the bundle architecture.

Most vesicles are not associated with MTs

Vesicle trafficking in mammalian cells is commonly dependent on MTs (Lippincott-Schwartz 1998). In yeast, however, there has been some indication of vesicle transport inside actin patches, which in turn are transported on actin cables (Marks et al. 1986; Kanbe et al. 1989; Motegi et al. 2001; Pelham and Chang 2001; Takagi et al. 2003; Gachet and Hyams 2005). We have analyzed the spatial relationships between vesicles and MTs in fission yeast to see if vesicle trafficking is likely to depend on them.

S. pombe contains three distinguishable vesicle morphologies that we treated as separate populations (figure 7). Interestingly, these categories of vesicles included the same fraction of the total vesicle population in each of the three (partial) cells examined. Circa 80% of all vesicles were small and electron dense (diameter 37±5.7 nm; n=197; figure 7A-C). This group also contained a structure that has been previously described as filasomes (figure 7C), a secretory vesicle surrounded by a thick ring of actin meshwork (Kanbe et al. 1989; Takagi et al. 2003). The two remaining types of vesicles included large, electron-dense vesicles (diameter 90±21.7 nm; n=28; figure 7D-F) and electron transparent vesicles (diameter 52±18.2 nm; n=25 figure 7G-I) each type comprised ~10%

of the total population. However, the average vesicle size within these categories varied significantly in different cells ($p < 0.001$; figure 7J). Vesicle sizes and numbers mentioned here were measured in the full cell volume.

Vesicles were modeled as spheres of representative diameters, and all three categories showed a clear preference for the cell ends (figure 7K; supplementary movie 6). To study the densely packed cytoplasm at a cell's end, we modeled a dual axis tomogram of a cell end with all its organelles (figure 7L). Here, small dense vesicles appeared to be more clustered around the Golgi apparatus, and large dark vesicles were found mostly in close approximation to the plasma membrane and the ER (figure 7M; supplementary movie 7). In this tip, only 1.6% of the vesicles were within 25 nm of a MT (n=128 vesicles; figure 7N; supplementary movie 8). Hence, we found no evidence for association with MTs. Furthermore, there was no apparent association between the MTs and other organelles such as vacuoles, Golgi and ER.

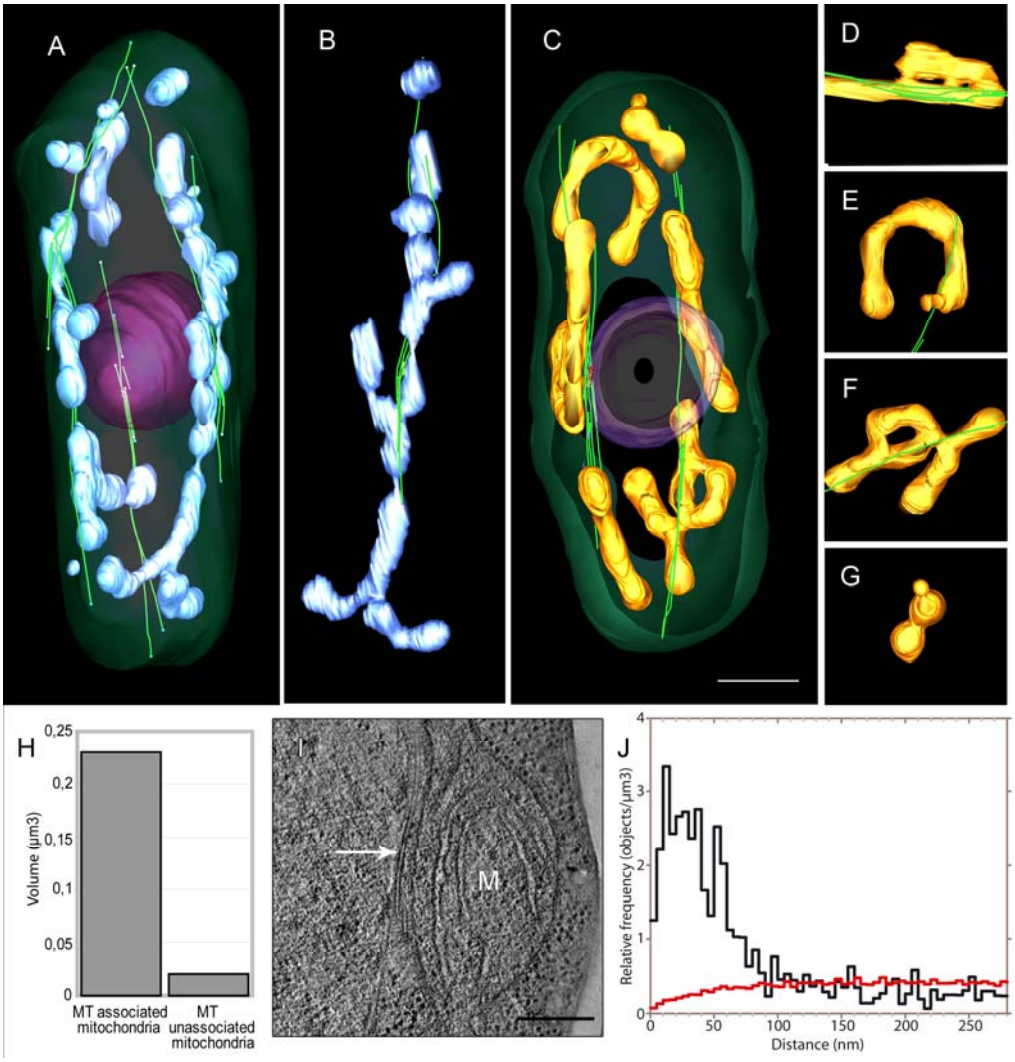

Figure 6 MT **bundles are intertwined with mitochondria**
A) 3D model of a full cell volume with MTs (green bundles) splaying around mitochondria (blue). **B)** Mitochondria that stretch along MTs are long and branched. **C)** Half the cell volume of a short cell (6.7 µm) with mitochondria (gold) arranged along MTs. **D-F)** Mitochondria associated with MTs are usually more branched and stretched than non-associated ones, e.g., the one shown in **G)**. **H)** Fractions of mitochondrial volume that are MT-associated or not. **I)** A tomographic slice where a MT (white arrow) is bending along a mitochondria (M). **J)** Spatial density analysis showing the preferred distances between MTs and mitochondria in the full cell volume (black line). The red line is a control where MTs were repeatedly shifted by random displacements, and the favored distances were recalculated (Marsh et al. 2001). The smoothness of the red line confirms that the black line's peak, achieved from measurements in the real model, is not likely to occur randomly. White bar = 1 µm. Black bar = 200 nm

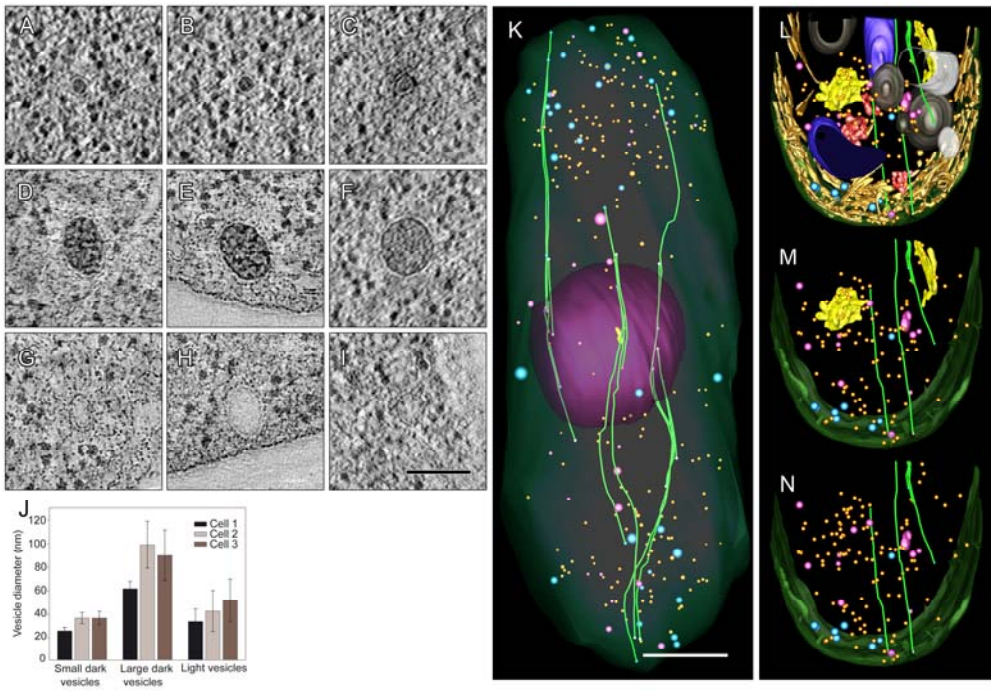

Figure 7 Vesicle trafficking in fission yeast appears to be MT independent
Vesicles were divided into three different populations: **A-C** small electron dense vesicles, **D-F** large electron dense vesicles, and electron transparent vesicles **G-I**. **J**) Vesicle sizes within the populations differ between cells. **K**) Small dark vesicles (orange), large dark vesicles (blue) and light vesicles (pink) localize to cell ends. **L**) Mitochondria (dark blue), Golgi (yellow), electron dense vacuoles (grey), light vacuoles (white), membrane clusters (red), endoplasmic reticulum (dark yellow), vesicles and MTs show a dense packing just below the plasma membrane (dark green) in a cell end. **M**) Small dark vesicles cluster slightly around the Golgi and large dark vesicles cluster below the PM. **N**) Vesicles show no preference for regions around MTs. White bar = 1 µm. Black bar = 100 nm.

Discussion

Microtubule bundle structure

A precise knowledge of MT length, polarity, and distribution in cells is essential for understanding how these filaments carry out their various functions. While a number of LM studies in conjunction with the use of GFP and other fluorescent protein tags provided good dynamic descriptions of MT arrays, sufficient spatial resolution has been lacking to identify several key parameters: 1. the number of MTs in a bundle; 2. MT polarity; 3. MT connections with each other and with other organelles. Drummond and

Cross (2000) presented evidence for an antiparallel arrangement of MT bundles, based on images of GFP-tubulin in live cells; dynamic MT ends (assumed plus ends) grew towards both cell ends. Here, we have used MT structure to determine polymer polarity. MT ends at or near the cell tip were generally flared, a characteristic usually associated with depolymerizing plus ends (Mandelkow et al. 1991; O'Toole et al. 2003). Capped (minus) ends were seldom found near the cell ends, confirming the MT polarities seen in previous work.

We also suggest that the flared end is a growing MT end morphology due to the following reasons: a) our cells are ~7 μm long. Thus, it should take the MTs ~1 min to grow half the cell's length but only about 30 s to depolymerize back to the cell's midplane (growth speed ~3 μm/min, shrinkage speed 8.5 μm/min, from Busch and Brunner, 2004). Therefore, about twice as many MTs should be growing as shrinking at steady state. b) Microtubules grow more slowly at the cell end for ~1 min, before they begin rapid shortening (Foetkhe, pers. communication). Hence, one would roughly expect 80% of the longest MTs in a bundle (since the dynamics of only these are measured in fluorescence microscopy) to be growing and the remaining 20% to be shrinking. We found only 7% sheets (usually assumed to be growing (Chretien et al. 1995)) and 79% flared MT ends in these bundles, indicating that this structure belongs to the growing population. This is in agreement with O'Toole et al. 1999 and 2003, who saw >70% flared end morphology at the MT plus ends in *Saccharomyces cerevisiae* and *Caenorhabditis elegans*. On the contrary, studies in *Arabidopisis* showed that only 1-2% of the phragmoplast MT plus ends were flared (Austin et al. 2005), illustrating possible differences in MT physiology between different cellular machines. Moreover, it is plausible that MTs visualized *in vitro* show morphologically distinct end structures from the equivalents captured *in situ*, due to the many proteins that associate with that part of the polymer (Carvalho et al. 2003).

Sagolla *et al*., (2005) provided arguments that the fluorescence seen at the tip of the cell was likely to correspond to only a single MT. Previous EM studies using serial sectioning in *S. pombe* cells had revealed some finer details about MT organization, but were not suitable to track MT bundles through the cytoplasm towards the cell end (Ding et al. 1997; Uzawa et al. 2004). In this study, we traced individual MTs through the

cytoplasm and found only single MTs in direct contact with the PM at the cell tip. Thus, deposition of proteins important for cell growth could occur directly at the PM.

Our approach based on large scale ET of plastic embedded sections (Höög and Antony, *in press*) provides an unprecedented way to visualize interphase MT arrays in full detail. From such data we have been able to provide the first 3D reconstruction of a full eukaryotic cell. Consequently, this is also the first study where a whole MT cytoskeleton has been described with precise length measurements (34.5 μm total polymer) on individual MTs of identified polarity. In the mitotic spindle this number varies between ~47 μm in the short spindle to over 70 μm in the long spindle (Ding et al. 1993). We also found that most MTs in an interphase bundle were short. In fact, 6% are below the resolution of conventional fluorescence microscopy (200 nm), and only few extended outside the nuclear overlap area in our 'snap-shot' view of the overall organization.

A new model of bundle architecture and nucleation

In the current view of interphase MTs in fission yeast two antiparallel bundles overlap near the cell's midplane, but our electron tomography data are not fully consistent with this model. In agreement with fluorescence studies we find capped MT ends (presumably minus) around the nucleus and along existing MTs further away from the iMTOC (Sawin et al. 2004; Janson et al. 2005; Zimmerman and Chang 2005). However, the minus ends show no spatial preference for two loci within the perinuclear area, as one would expect from the two anti-parallel bundles model; the overlap region does not show a discrete bipolarity. We suggest a novel model in which MT origins are scattered in the perinuclear region and along existing MTs. After a nucleation event the new MT would self-orient into a parallel or anti-parallel fashion and bundle with the existing MTs. The fast growing plus end would then naturally grow towards the cell end it faces, creating ONE linear bundle with scattered minus ends in the middle region and with plus ends more commonly at the cell tip.

Recently, it was found that MTs slide and nucleate along other MTs within the bundles (Carazo-Salas et al. 2005; Janson et al. 2005; Zimmerman and Chang 2005). We

found ten occasions where a short MT with a capped end (probably a γ-TURC complex) was present outside the nuclear area. Only one of these corresponded to a MT with its minus end pointing towards the nearer cell end. This single MT of opposite polarity was in an iMTOC region, away from the nucleus (figure 1D). From live-cell imaging, one would expect these short MTs to be transported back to the iMTOC region by the kinesin klp2 (Carazo-Salas et al. 2005).

Bundling of microtubules

We observed ~25 nm long, electron dense cross-bridges between MTs themselves and between MTs and the NE. Since this is similar to the preferred minimal distance between MTs (found by neighbour density analysis), we suggest that these visible cross-bridges are responsible for MT bundling. The components of these cross-bridges remain unknown, however ase1p has been shown to mediate antiparallel MT bundling in fission yeast (Loiodice et al. 2005; Yamashita et al. 2005). Further, the ase1 plant homologue, MAP65, bundles MTs by forming 25-30 nm long cross-bridges *in vitro* (Chan et al. 1999; Smertenko et al. 2004). Ase1p is therefore a likely candidate to form these electron dense bridges. However, a recent study has shown that ase1Δ mutant's ability to form bundles is decreased but not absent (Daga et al. 2006b), indicating the existence of more bundling factors. In a previous study proteins like tau and MAP2C were also shown to bundle MTs with longitudinal distances around 25-30 nm (Chen et al. 1992). Our nda analysis showed a second, smaller peak at around 55-60 nm distance. This could come from either a) MTs at twice the minimal preferred distance or b) a second MT bundler. Consistent with the theory of a second bundling protein, MAP2, bundles MTs at ~60 nm in neuronal dendrites (Chen et al. 1992).

SPB bundles differ from non-SPB bundles

When interphase MTs in fission yeast were de-polymerized and then allowed to regrow, they were initiated by 3-6 iMTOCs (Tran et al. 2001; Loiodice et al. 2005). Our data suggest that the cytoplasmic face of the SPB is one of these iMTOCs, since there was always a MT bundle attached to it. However, most MTs were laterally associated

with the SPB, so it is uncertain weather the SPB actively nucleates MTs in interphase (Masuda et al. 1992). Nonetheless, the SPB appears to provide a favorable environment for MT nucleation or stabilization during interphase, since we found an average of twice as many MTs in the bundles associated to it as in non-SPB bundles.

MT interactions with mitochondria and transport vesicles

It is known that large organelles such as the nucleus, mitochondria and the Golgi complex interact with cytoplasmic MTs (Ayscough et al. 1993; Yaffe et al. 1996; Tran et al. 2001). We often observed that MT bundles splayed apart, and almost invariably there was a mitochondrion at the site where the MTs diverged. Hence, mitochondria seem to influence MT bundle morphology. On the other hand, MTs appear to influence the shape of mitochondria, since mitochondria attached to MTs appear as more reticulated and stretched than those that are not attached. Moreover, non-attached mitochondria were smaller, and in general were positioned closer to the cell tips. It has previously been shown that the distribution of mitochondria in fission yeast is MT dependent (Yaffe et al. 1996; Yaffe et al. 2003). This attachment depended on the protein mmd1p (Weir and Yaffe 2004). However no electron-dense bridges between MTs and mitochondria, which could correspond to the mmd1p, could be identified in our tomograms. Still, a preferred minimum distance of around 20 nm, similar to the MT to MT distances, was found between MTs and mitochondria.

On the contrary, vesicles do not seem to be transported along MTs in fission yeast but are rather found in ribosome free areas, some of which contains a fuzzy structure that could be patches of actin, which have previously been suggested to transport vesicles (Takagi et al. 2003; Gachet and Hyams 2005). Secretion is not influenced by the loss of MTs in fission yeast (Ayscough et al. 1993). Similarly, in budding yeast secretion appears to be independent of cytoplasmic MTs (Huffaker et al. 1988). Here, vesicles were found in three different populations, the diameter of which changed between samples. This could possibly reflect the nutritional status of the culture at the time of freezing. The small electron dense vesicles had a diameter of only 26 nm in one cell. This is half of the diameter measured in mammalian cells (Marsh et al. 2001). However, small vesicles 20-

30 nm have also been found in budding yeast, that are thought to be part of the endocytic pathway (Mulholland et al. 1999). Therefore, we suggest these small vesicles to be possible yeast specific transport intermediates.

In summary the large volume ET approach developed here has unraveled several novel features of ultrastructural organization in the context of a whole eukaryotic cell.

Chapter 4

Mal3 Stabilizes Microtubule Growth and Might be Involved in SPB Maturation

Introduction

The end binding protein 1 (EB1) family is a group of conserved proteins, with homologues in yeasts, plant and humans. EB1 has been shown to be a regulator of MT stability, localizing to the MT plus ends during phases of growth and dissociating before MTs undergo catastrophe (Akhmanova and Hoogenraad 2005; Morrison 2007). It also recruits other proteins to the plus ends of MTs that are important for MT integrity and search and capture of the cytoplasm (Busch and Brunner 2004).

EB1 was first discovered as a protein that interacts with adenomatous polyposis coli (APC), a tumor suppressor protein that is mutated in most colon cancers (Su et al. 1995). Both proteins localize to the mitotic spindle, and their suppression cause defects in metaphase chromosomal alignment and anaphase segregation (Green et al. 2005; Draviam et al. 2006) . However, as a MT growth regulator, EB1 has been shown to be involved in many cellular interphase processes such as cell migration, formation of tight junctions and establishment of cell polarity (Akhmanova and Hoogenraad 2005; Shaw et al. 2007).

In fission yeast the EB1 homologue, Mal3, was found in a screen for mini-chromosome loss. If the *mal3* gene is removed, the cells grows bent since the MT bundles only grow to half the length of their WT equivalents (Beinhauer et al. 1997) Short microtubule bundles establish the growth site to the wrong position (Sawin and Snaith 2004). However, it is not known whether the short bundles in *mal3Δ* are due to a general decrease in MT filament length or change in bundle architecture. Moreover, it takes twice as long for MTs to perform rescue after a catastrophe (Busch and Brunner 2004). This could be due to both difficulties in MT nucleation or elongation.

Mal3 has also been shown to localize along MTs in fission yeast. A recent *in vitro* study showed a mechanism with which mal3 may stabilize MTs by binding to the MT seem (Sandblad et al. 2006). The seem is occurring on all 13 protofilament MTs, which is the most common MT structure found *in vivo* (Tilney et al. 1973). By stabilizing this interaction, Mal3 may alleviate the internal forces in the MT GDP-lattice and as such counter act catastrophe initiation.

EB1 homologues also has a less discussed localization to the centrosomes in *Dictyostelium*, human cells and to the SPB in budding yeast (Hestermann et al. 2002). It has been reported to preferentially localize to around the maternal centriole (Louie et al. 2004) and the old SPB in budding yeast (Hwang et al. 2003; Liakopoulos et al. 2003; Maekawa et al. 2003). EB1 is involved in MT anchoring to the centrosome (Askham et al. 2002) but the exact mechanism of action is unclear, and no ultra-structure localization of EB1 at the centrosome has been performed.

In this study, we have examined the role of Mal3 on interphase MT organization in fission yeast, visualizing mal3Δ cells using cellular electron tomography, conventional thin section EM and fluorescence microscopy. We show that mal3 is important for MT elongation but not nucleation. Further, we show an unforeseen phenotype of the SPB, the yeast centrosome equivalent.

MT bundle architecture in *mal3Δ*

To investigate the effects of Mal3p on the cytoplasmic microtubules we examined variable volumes of eight different cells where this protein had been deleted. A combination of single-axis montaged tomograms and single frame dual-axis tomograms were acquired. Most of the data was extracted from the four largest montaged volumes.

As previously shown, microtubule bundles in *mal3Δ* are about half the length of the WT bundles. These short MT bundles were less aligned along the cell's length axis than WT cells (figure 1A-B). Additionally, MT alignment within the bundle was often disturbed too. Short microtubules were often at an angle to the longer microtubules in that bundle (figure 1C). However, bundles with more linear MT arrangements are also found both in associations with the SPB and other iMTOCs (figure 1D).

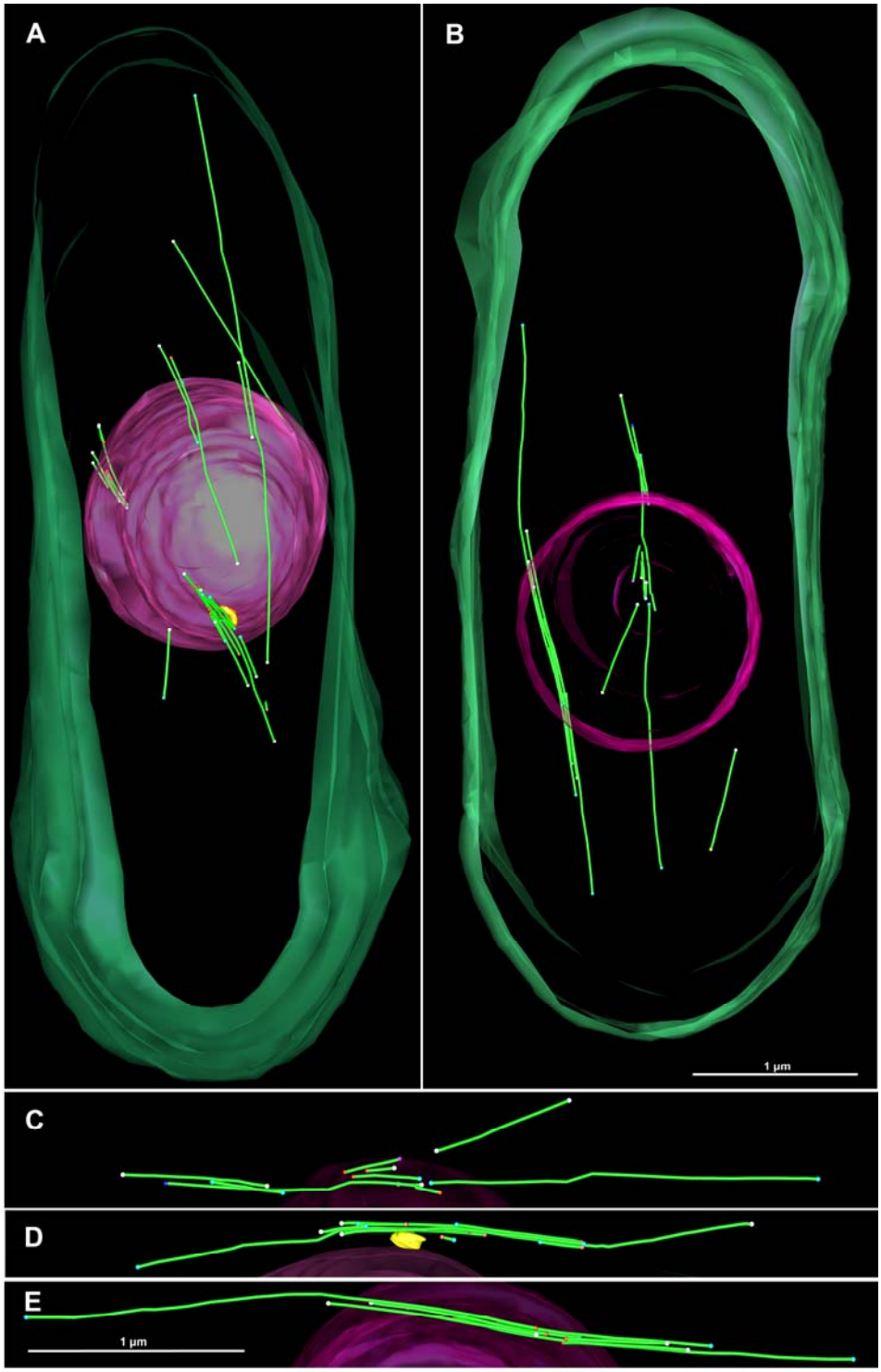
A
B
1 µm
C
D
E
1 µm

Figure 1 Architecture of the short MT bundles in *mal3Δ*
Microtubules (green) are short, only slightly extending outside the nuclear envelope (pink). Microtubule end structures are shown with colored caps, where red (capped end), turquoise (flared end), yellow (sheet), blue (blunt end) and white (ambiguous end). The plasma membrane is shown in transparent green. A-B) 3D reconstruction models of 2.25 μm thick volumes of two cells. C) A MT bundle where the MTs are at an angle to each other. D) A SPB associated bundle. E) A more linear MT bundle.

Microtubule lengths and numbers in a bundle

We measured individual microtubule lengths and found them ranging between 0.07 and 2.4 μm, with an average of 0.65 ± 0.55 μm (n=55) (figure 2A-E). Most microtubules measured were under 0.5 μm (figure 2E). Only microtubules with both ends inside the reconstructed volume were measured. Since Mal3Δ MTs are less well aligned to the cell's long axis, more of the longer MTs left the volume than in WT. This could cause a slight skew in the data towards more measured shorter MTs. However, if we include all the MTs in the volumes we found the average MT length to be almost identical; 0.66 ± 0.62 μm (n=107).

Since we were not able to reconstruct a complete cell volume of this mutant we can not compare total polymerized tubulin concentrations to that shown in WT.

Further, we show that there is on average 4.8 ± 4.1 MTs in a bundle (figure 2F). That is not significantly different from WT bundles, where each bundle had 4.4 ± 2.6 MTs. However, the bundles in this mutant showed an amount of MTs widely spreading from only one to a large bundle containing fifteen MTs.

We conclude that Mal3 is important for MT elongation, whereas it does not appear to affect MT nucleation.

Microtubules lacking Mal3 show kinks along the lattice

Fluorescence microscopy shows mal3-GFP localization to growing MT plus ends as well as faint staining along MT lattices. Further, *in vitro* data has shown that Mal3 seals the seam of the MT lattice (Sandblad et al. 2006). Therefore, deletion of mal3Δ could have an effect of MTs *in situ*.

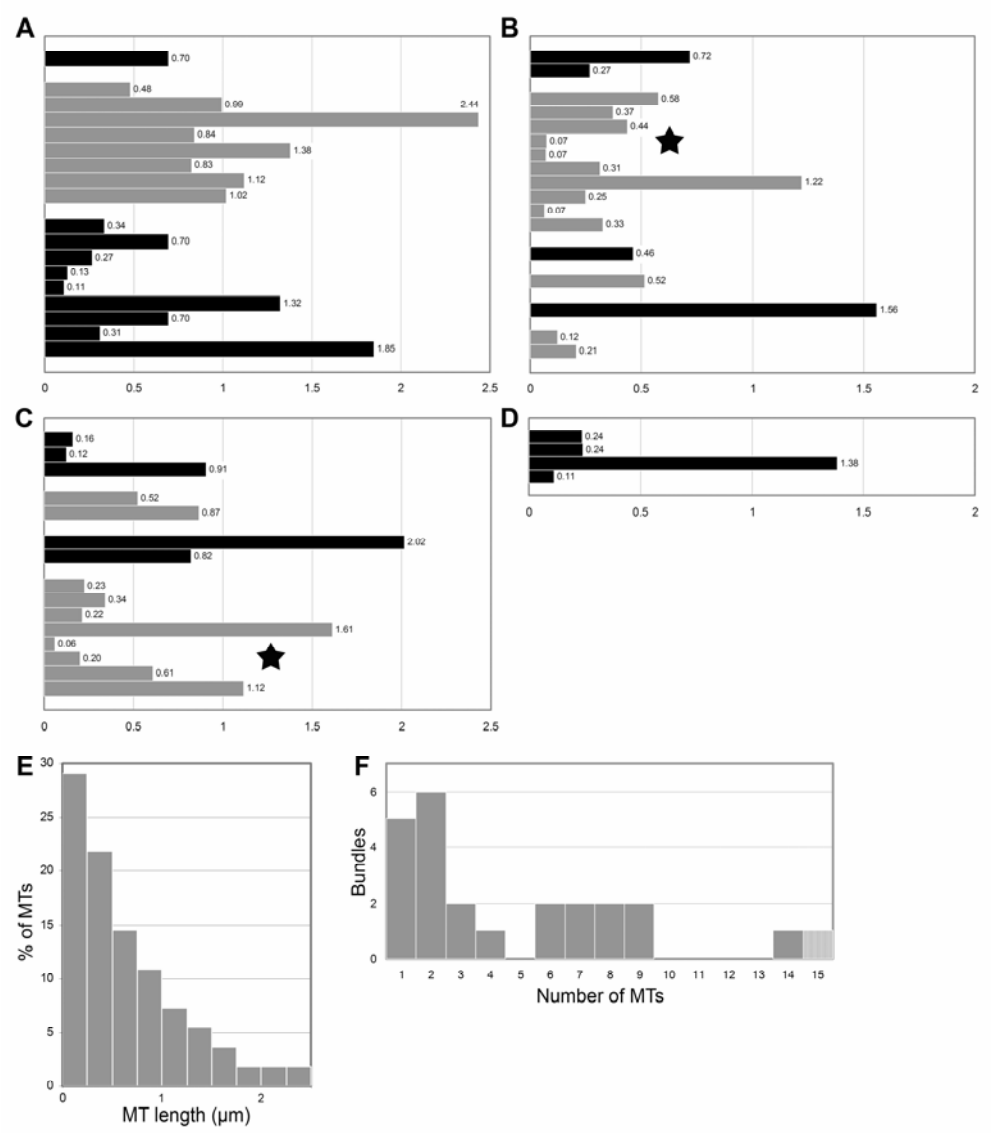

Figure 2 *mal3Δ* cell microtubules are shorter but there is the same amount of filaments in a bundle as in WT

Bundles of microtubules from four different cells are depicted as groups of black and grey bars. Cells are A) 7.0 μm B) 7.6 μm C) 7.6 μm and D) 6.6 μm in length. The * indicates SPB bundles. E) Histogram of MT lengths (all MTs in [A]-[D] pooled) showing that most bundles are shorten than 0.5 μm and none are longer than 2.5 μm. F) There is 1-15 MTs in a bundle, with an average of 4.8 MTs per bundle. The last bar in the histogram (striped) shows a bundle where the SPBs had separated.

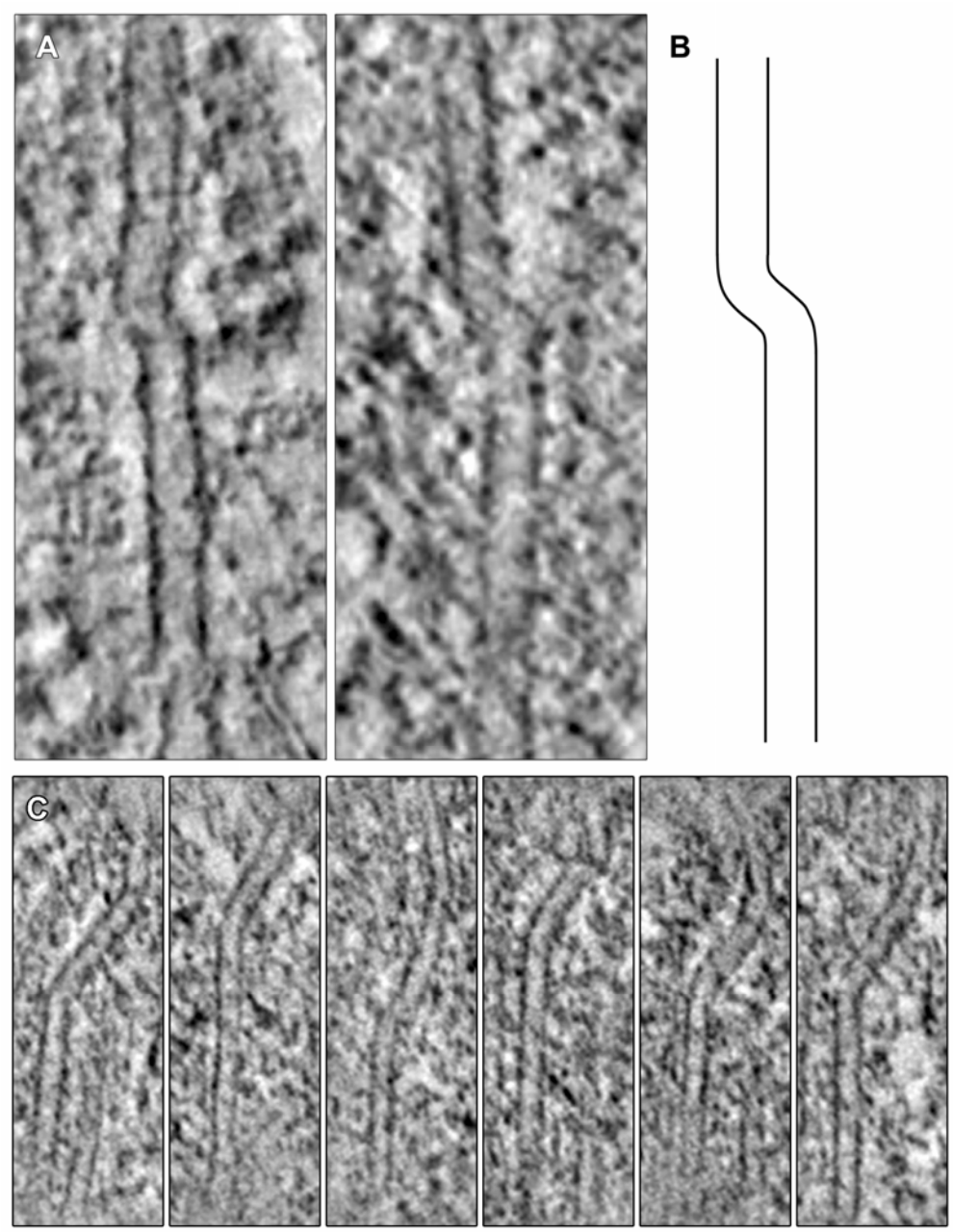

Figure 3 Microtubules lacking Mal3 have 'kinks' A) Interphase microtubules with 'kinked' lattice **B)** model of a kinked microtubule **C)** six different 'kinked' microtubules from a mitotic spindle.

The total of 120 MTs studied in *mal3Δ* cells, sums up to 78 μm polymer length. Four of these MTs contained a 'kink' in the lattice (figure 3). Hence, we had one kink per 19.5 μm polymer. In WT cells no such kinks were found, when studying a total polymer length of 121 μm spread over 87 filaments. We also observed adjacent MT ends facing each other as if they had been the same MT but broken in two parts in *mal3Δ*.

We have also reconstructed a *mal3Δ* metaphase spindle. In this spindle we saw kinks on almost all MTs in a particular region where many MT ends were found. Unfortunately, we can not see the kinetochores in fission yeast, but it would be probable that their presence is causing the MTs to end here. The 'kinks' of the mitotic MTs appear more pleomorphic than during interphase (figure 3C).

SPBs appear displaced, abnormal and only one binds to MTs

In WT, SPBs are normally closely fitted between a mitochondrion on one side and the face of the nuclear envelope closest to the PM on the other side. In mal3Δ cells SPBs were more difficult to detect than in WT and other mutants. We found a SPB-resembling electron dense structure sitting on the 'north pole' of the nucleus in one cell. The density was banana-shaped and had only one end attached to the nuclear envelope. The other end was extended out towards a bundle of MTs that passed the SPB at an angle (figure 4A-C).

We wanted to know if SPBs in mal3Δ bind to MTs in a normal way. For this, we studied two further SPBs that were duplicated and with apparently normal morphology. In both cases MTs were only in contact with one of the two SPBs, indicating one SPB to be functionally immature.

Therefore, SPB size was also measured by randomly measuring 35 SPBs in thin sections. This initial study showed that the SPBs, although appearing abnormal, were rather similar to what has been measured in WT previously (Ding et al. 1997; Hoog et al. 2007).

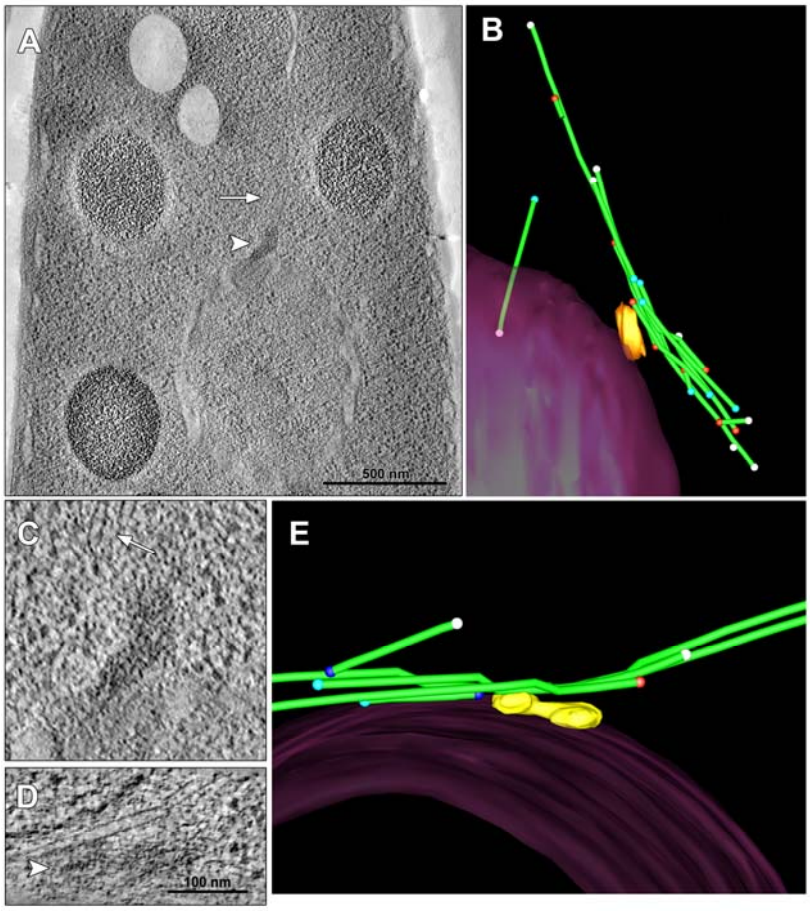

Figure 4 SPBs in Mal3Δ cells have a different morphology and MT interaction
A) A duplicated SPB with abnormal 'banana shape', sat on the cell's 'north pole' (arrowhead). Cross-sections of microtubules are indicated with the white arrow. **B)** The 3D model of the abnormal SPB with the attached MT bundle. Note that only one SPB is in contact with the MTs. **C)** Zoom in on the SPB in A) that sits outside the nuclear envelope. No intranuclear MTs were seen. **D)** Another duplicated SPB (arrowhead) where only one SPB is in contact with the MTs. **E)** The 3D model of the SPB in D).

However, we will redo this experiment with synchronized cells to enable easy measurements of large amounts of SPBs. The SPB size could then be correlated with the cell length and a delay in maturation, if any, would become obvious.

To ensure that every cell had a SPB we performed serial section reconstruction of 12 complete nucleus volumes in *mal3Δ* cells. We found SPBs in 9 cells, in two cells there were ambiguous structures that could possibly be SPBs but in the final cell we found

nothing resembling a SPB (figure 5). To get statistically more valid numbers we turned to fluorescence microscopy.

Fragmented SPBs during interphase in *mal3Δ* cells?

Nine different SPB proteins tagged with fluorescent proteins (GFP, CFP or YFP) were crossed into *mal3Δ* background. The brightest marker was Pcp1-GFP, which showed a 30% increase in cells containing more than one 'SPB' dot in *mal3Δ* cells (11% WT and 41% *mal3Δ*; n= 280 WT, 215 *mal3Δ*). Pcp1-GFP localized to two loci in most multi-dotted mutant cells, but up to four loci was observed (figure 6A-C).

10% of these dots seemed localized away from the nucleus (seen as a circle of less background fluorescence). We tracked three fluorescent dots in one cell and found one moving at a faster speed than the others (figure D), a further indication that this particle was free in the cytoplasm.

However, the same experiment counting cytoplasmic dots in cells expressing cut12-GFP showed no difference between SPB numbers in *mal3Δ* and WT (figure 6E). The other markers (cdc11-GFP, sid4-GFP and spg1-GFP) were only examined visually, and they appeared similar to cut12-GFP.

The extra dots in the pcp1-GFP cells were almost always less intense than the clear dot we assume to be the normal SPB. Therefore, we now want to study all the strains under a confocal microscope where possibly fainter extra dots could be visualized.

Are immature SPBs responsible for delay of mitosis onset in *mal3Δ* cells?

mal3Δ cells has a delay of entry into mitosis (Beinhauer et al. 1997; Asakawa and Toda 2006). Even though our study foremost involved interphase cells, an even stronger phenotype was noticed in mitotic pcp1-GFP *mal3Δ* cells. Here, we found up to six cytoplasmic dots instead of the normal two SPBs during mitosis (figure 7A-A'; n= 4 WT and 54 *mal3Δ*).

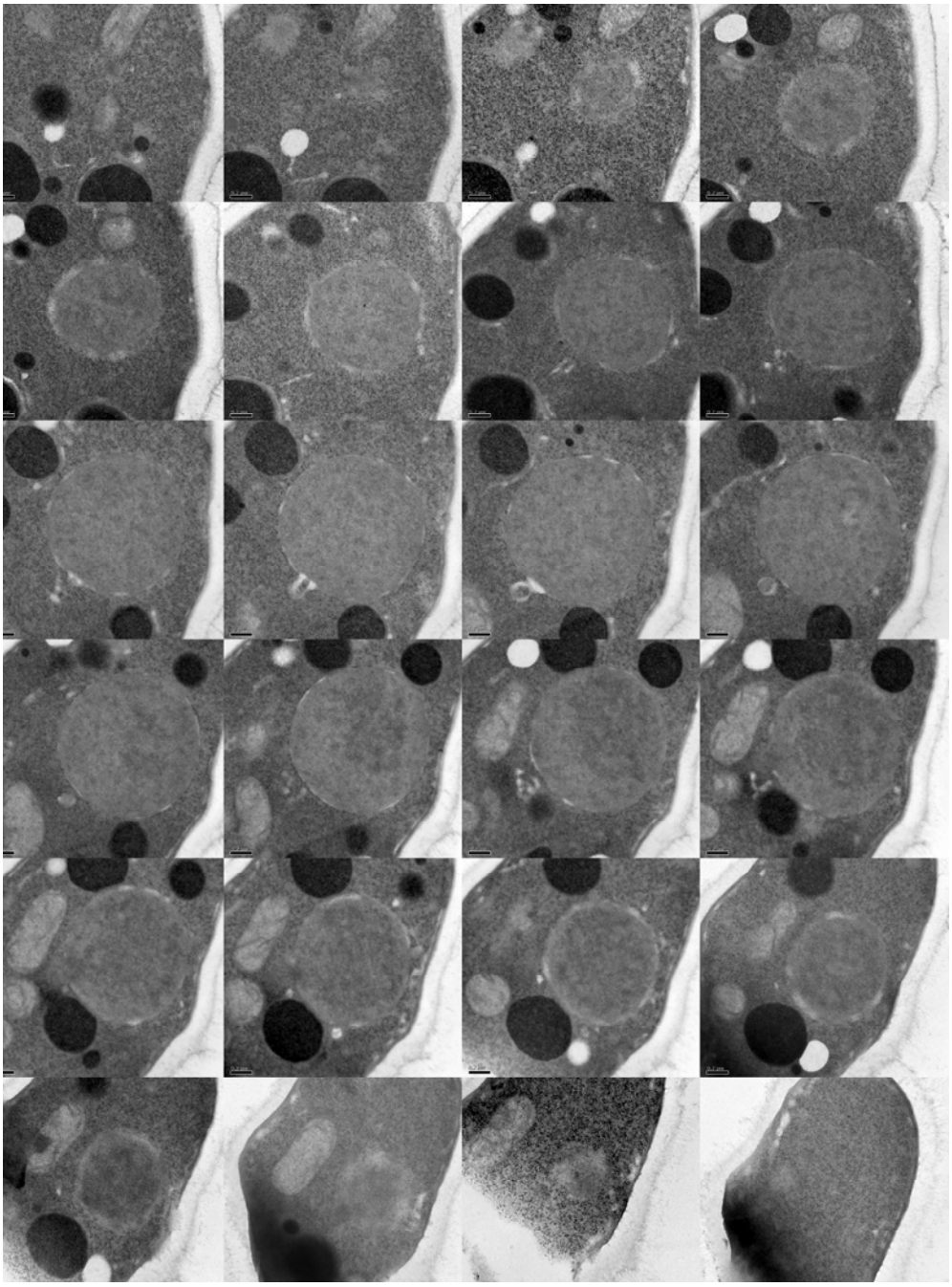

Figure 5 Serial sections from a whole nuclear volume in a *mal3Δ* cell lacking an SPB. Each section is 60 nm thick, which means an SPB should appear in 1-3 serial sections.

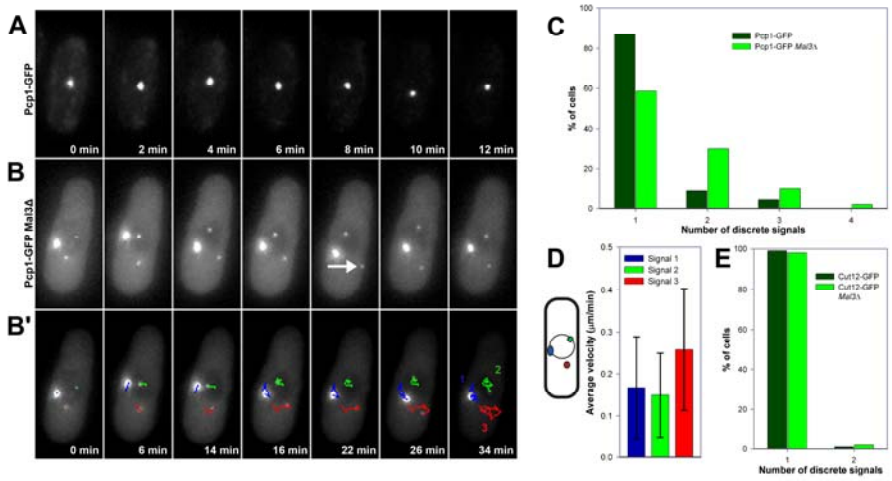

Figure 6 Fragmented SPBs during interphase in *mal3Δ* cells. A) WT cells with pcp1-GFP showing the SPB. **B)** Pcp1-GFP in time-lapse of *Mal3*Δ cells show multiple SPB dots of which some are not associated with the nuclear envelope (arrow). **B')** lines from particle tracking. **C)** The amount of discrete pcp1-GFP signals seen in *Mal3*Δ and WT cells. **D)** The speed with which the fluorescence signals in B) move are slightly different, probably due to disassociation from the nuclear envelope by the speckle color-coded in red. **E)** The amount of discrete cut12-GFP signals in *Mal3*Δ and WT cells.

Could the delay of mitotic onset be due to immature SPBs? A tomogram reconstruction of two newly separated SPBs in *mal3Δ* cells was made. The SPB separation characterizes the G2/M transition of the cell cycle. At this phase, the SPBs appeared normal in size and both were in contact with large bundle containing 15 MTs (figure 8 A-C).

However, when we reconstructed SPBs in a metaphase spindle, they appeared to have divided unequally. One SPB had an electron dense ellipsoid without the central plaque and the other appeared to only have a wide central plaque (figure 8D-E). Here, we also hope that thin plastic sections of synchronized cells will provide more illustrations, to enable better understanding of the mutant SPB morphology.

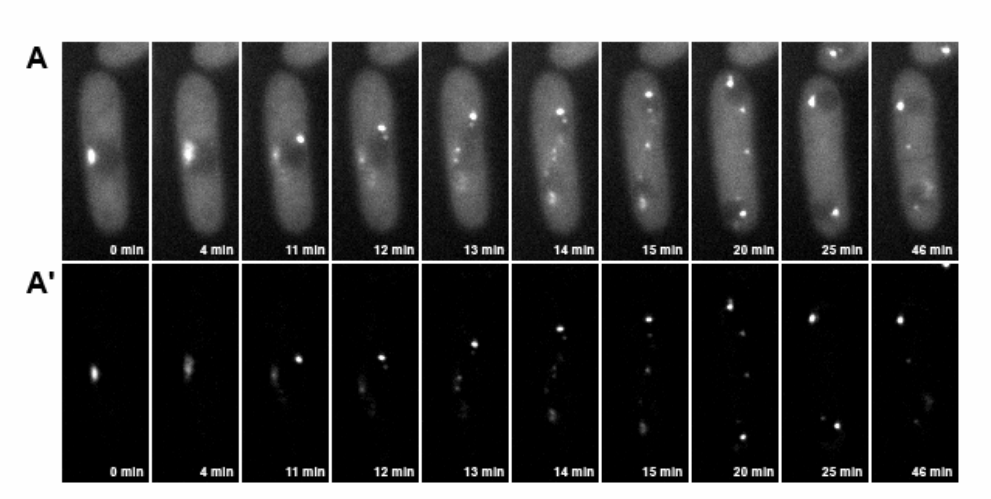

Figure 7 Fragmented SPBs during mitosis in *mal3*Δ cells. A) Frames from a time-lapse movie of *mal3*Δ cells expressing Pcp1-GFP. **A')** the same frames as in A) but with background subtracted (rolling ball radius: 5 pixel), to enhance visualization of the fragmented SPBs.

Immunolocalization of Mal3 in WT cells

We are currently trying to localize Mal3 to the SPB using immunocytochemsistry. Antigens are localized on thin lowicryl sections using antibodies and then visualized using protein A coated gold particles. However, only the antigens exposed on the surface of the section can be detected. Therefore, this experiment is better performed using a polyclonal antibody that can detect many epitopes. To enhance the signal a secondary antibody is used before the gold is applied. The outcome of this experiment will be crucial to confirm if Mal3 is a true SPB component, which might be necessary for SPB maturation.

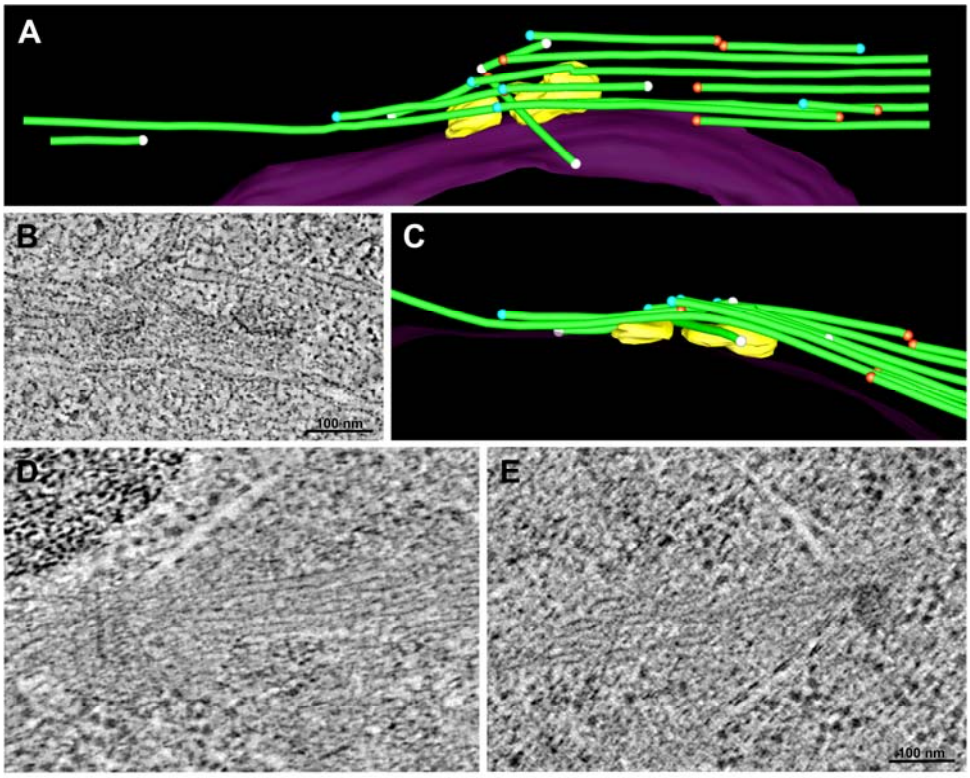

Figure 8 G2/M transition and mitotic SPBs in *mal3Δ* A) The microtubule bundle associated with the separated SPBs contains 15 microtubules. The SPBs are both outside the nuclear envelope. **B)** A tomographic slice of the separated SPBs, the central bridge remains associated with only one SPB. **C)** Microtubules are now associated with both SPBs. **D-E)** The SPBs of a metaphase spindle seems unevenly duplicated. One SPB appear reduced to only the central plaque and the other SPB merely has the electron dense material and no visible central plaque.

Discussion

The role of Mal3 in MT structure and bundle architecture

Light microscopy studies showed that MT bundles in *mal3Δ* cells are half as long as WT bundles (Busch and Brunner 2004), but due to the limited resolution individual MT can not be detected. Therefore, it could not be known weather this change in bundle length was due to a different organization within the bundle, because the MTs were just shorter or both.

Using electron tomography we could reconstruct the short bundles in 3D and see individual MT lengths and polarity. WT MTs were 1.64 ± 1.43 μm long, in contrast to *mal3Δ* that only had 0.65 ± 0.55 μm long MTs. This correlates well with the bundle lengths measured in light microscopy studies. *mal3Δ* bundles do not appear to a have different organization compared to WT. To confirm that the bundles do not show a difference in organization we should measure the spread of capped ends around the nuclear envelope and compare with WT. This would give an indication if closed (assumed minus) ends would be more or less spread in the mutant.

MT bundles in *mal3Δ* contained similar amounts of MTs as a WT bundle. Hence, we suggest that MT nucleation is normal without Mal3 present. Further, the delay in regrowth after catastrophe, shown by (Busch and Brunner 2004), is probably due to difficulties in elongation rather than nucleation. An alternative explanation would be that nucleation within an existing bundle is not affected but de novo bundle formation is made more difficult by the lack of Mal3.

We also describe a novel and rare 'kinked' MT morphology in the *mal3Δ* cells. Notably, such 'kinks' were generally not seen in WT cells, neither in tip1Δ cells that were cryoimmobilized alongside the *mal3Δ* mutants. These kinks could result from MTs having a less stable seem when lacking Mal3 (Sandblad et al. 2006). We assume that such 'kinks' could cause a lot of strain and possible breakage on the microtubule lattice and therefore be transient features. This observation could be a partial explanation of the short microtubules seen in *mal3Δ* cells.

Altered SPB location, morphology and function

This study has shown aberrant SPB structure in the absence of Mal3. SPBs were displaced, malformed and had an altered affinity to MTs. The displacement could be an indirect effect from having short cytoplasmic MTs, since long MTs would automatically align to the long axis of the cell and position the SPB at the side of the NE. The shorter MTs in *mal3Δ* will Accordingly, MTs have been shown to position the SPB during entry into mitosis (Vogel et al. 2007).

On the contrary, the malformation of SPBs is not easily explained. However, we give three hypotheses on how this may have occurred. Firstly, mal3 could be a structural

SPB component, which itself or through recruiting other proteins to the SPB, is important for its morphology. Secondly, MTs may usually be delivering components back to the SPB and this delivery is impaired in the absence of a normal interphase MT array. Thirdly, EB1 can be involved in the connecting the SPB to the nuclear envelope. By removing Mal3 the SPB would then be less well attached and what we observe as altered SPB morphology may be a result from other cytoplasmic components pulling on MTs and the SPB.

Is mal3 a structural SPB component?

Fluorescence microscopy studies have localized +TIPs such as EB1 and XMAP215 to the centrosome (Berrueta et al. 1998; Graf et al. 1998; Morrison et al. 1998; Askham et al. 2002). However, since this is the site of new MT outgrowth and accordingly one of high concentration of MT plus ends, this localization may be considered inevitable. More convincing evidence that EB1 is a centrosome component comes from studies using molecular truncations of EB1 and siRNA silencing of the gene product. When disrupting EB1 the focused interphase array dissolves, showing that EB1 plays a role in anchoring the MTs to this region (Askham et al. 2002; Yan et al. 2006). In agreement with this, EB1 has been shown to localize to the mother centrioles that is anchoring of MTs to the centrosome (Piel et al. 2000; Louie et al. 2004).

In fission yeast, both SPBs have been shown to bind the MTs during late interphase. In *mal3Δ*, MTs did not bind to one of the duplicated SPBs. This suggests a maturation problem with that SPB. We have no means to distinguish the old and new SPBs in the tomogram reconstructions once duplication is complete. However, previous studies in budding yeast have localized its EB1 homologue, Bim1, to the old SPB that is directed to the daughter bud during mitosis (Hwang et al. 2003; Liakopoulos et al. 2003; Maekawa et al. 2003). Localization of EB1 to the mother centriole has also been shown using fluorescence microscopy of mammalian cells (Louie et al. 2004).

With this knowledge one could make two hypotheses; firstly, the non-binding SPB is the mother SPB that has lost EB1 or EB1 interacting proteins responsible for the MT binding of this structure. This would assume that the daughter SPB has an alternative

mechanism for MT attachment. Alternatively, the non-binding SPB is the daughter SPB that has a delay in maturation due to the lack of EB1.

Our studies of late G2 and mitotic SPBs do not show conclusive evidence of such a maturation defect. Therefore, we will carry out fluorescence microscopy of different SPB components available in *mal3Δ* cells. A maturation defect could be seen by lower fluorescence intensity in one of the separating SPBs. If this was the case, a mother SPB specific marker could be used to determine which one of the SPBs lacks these proteins. Further, thin section electron microscopy of synchronized cells may shed more light on the SPB ultrastructure both in interphase and mitosis.

Chapter 5

Tip1 is a microtubule stabilizer involved in nucleation and attachment to the nuclear envelope

Introduction

Clip-170 (Cytoplasmic linker protein of 170 kDa molecular weight) was the first MT plus end tracking protein described (Rickard and Kreis 1990). Clip-170 binds directly to MTs by its two N-terminal CAP-Gly domains (Pierre et al. 1994). However, this binding is auto-inhibited by the C-terminal end which is folded back on to the N-terminus (Lansbergen et al. 2004). This autoinhibition is thought to compromise MT end binding and may provide a mechanism for local regulation of Clip-170 activity.

Clip-170 has been shown to regulate MT dynamics and link MTs to intracellular sites, such as endocytic vesicles (Pierre et al. 1992). Live cell imaging in HeLa cells showed localization of Clip-170 to comet like structures at all growing MT ends (Perez et al. 1999). Before depolymerization this comet disappears and reoccurs again upon rescue.

In fission yeast, the Clip-170 homologue Tip1 is involved in spatial organization of the MT cytoskeleton (Brunner and Nurse 2000). It is localized along the MT lattice and in particular at MT plus ends where it is transported by the kinesin Tea2. In this location Mal3 (EB1) is responsible for anchoring Tip1 (Busch et al. 2004).

In WT, over 90% of the MT bundles reach the cell ends before undergoing catastrophe. Tip1 is unloaded at the cell ends, and its localization to this region is dependent on the Tea1 landmark protein. However, in *tip1Δ* cells MTs depolymerize when touching the cell cortex anywhere along the length of the cell. Therefore, Tip1 is

thought to be an anti-catastrophe factor that locally regulates the MT dynamics, guiding them to the cell ends. Consequently, the MT bundles in *tip1Δ* are shorter and the cells grow bent and branched (Brunner and Nurse 2000).

It is not known how Tip1 stabilizes the MTs or what happens to the MT when it is unloaded before depolymerization. As in Mal3, the influence on the bundle ultrastructure of *tip1Δ* is not known. In this chapter, I describe a strong reduction of polymerized tubulin in *tip1Δ*, depending on both short MTs and fewer MTs in a bundle. This indicates a role for Tip1 in MT nucleation. Further, we found the MT attachment to NE and SPB weakened.

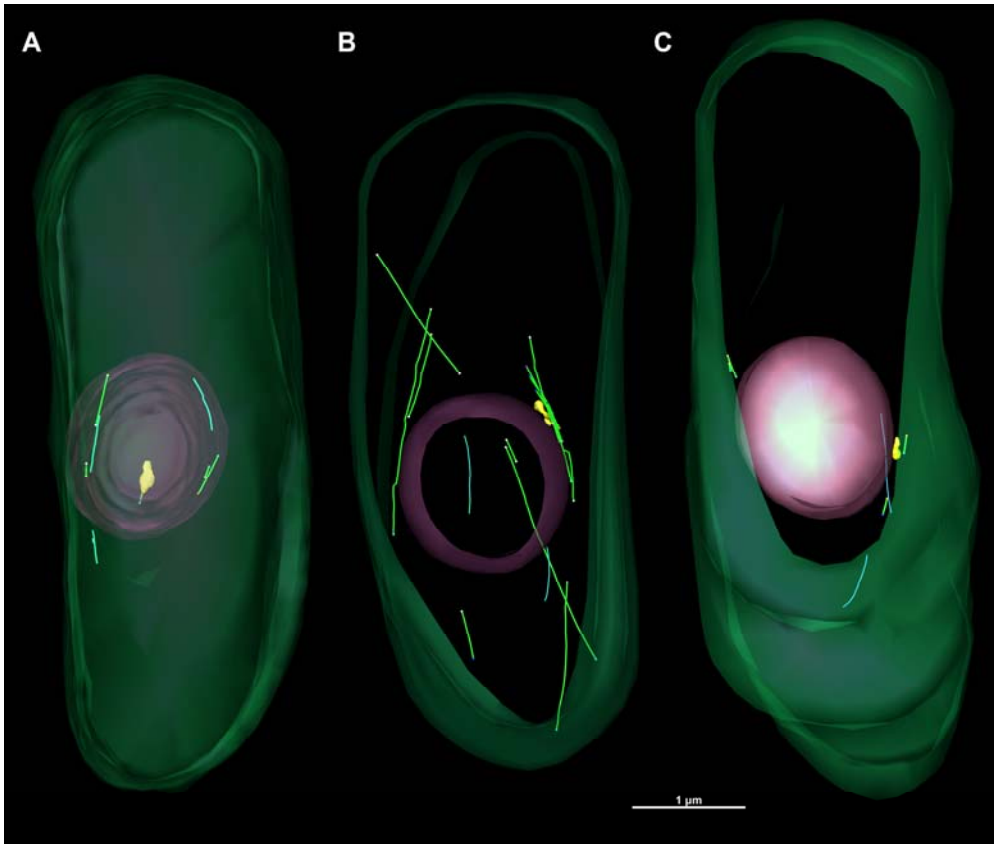

Figure 1 Architecture of the short MT bundles in *tip1Δ*
Microtubules (green) are very short and seldom extending outside the nuclear region. Thin filaments are shown in turquoise. The nuclear envelope is shown in pink. Microtubule end structures are shown with colored caps, where red (capped end), turquoise (flared end), yellow (sheet), blue (blunt end) and white (ambiguous end). The plasma membrane is shown in transparent green. **A)** 3D reconstruction model of a full cell volume. **B)** Reconstruction of 2 µm and **C)** 4.25 µm thick cell volumes.

tip1Δ causes an increase in thin filament prevalence

We have reconstructed tomograms from five different cells. Four of these were single axis montages and one was a whole nuclear volume reconstructed from dual axis tomograms. These cells contained bundles of short MTs. Mostly MTs were found alone in the cytoplasm (figure 1). Notably, the nuclear volume did not contain any MTs at all.

We have seen thin filaments that appear more flexible than normal MTs since they bend and fold on themselves, in both WT and *mal3Δ*. However, in *tip1Δ* these filaments became noticeably more abundant (turquoise filaments in figure 1 and 2). In WT these filaments were often inside MT bundles (63% n= 5 out of 8) and aligned to a MT (figure 2A-B). Their partial hollow structure, ability to fray into filaments and their association with other MTs made us consider them as a form of MTs (see discussion).

The thin filaments are 40 nm to 1.3 μm long, with an average length of 0.60 ± 0.35 μm (n = 24 from all three strains; figure 2C). They are often hollow tubes for a part of the length and then change to be just a filament or a couple of filaments. This makes their diameter variable. However, when measured on the widest point we found diameters from ~3 nm (single filament) to ~18 nm (the diameter of most MTs in our sections; figure 2D). The average thin filament diameter was 10.8 ± 4.1 nm (n=17).

In *tip1Δ* these thin 'MTs' represent 24% of the polymerized tubulin, whereas in *mal3Δ* and WT the same number was 1% and 4% respectively (figure 2E). This proportional increase of thin filaments could be due to a stabilizing function of Tip1 that causes filaments to assume this conformation when it is removed. Alternatively, it could be an indirect effect of a large decrease of 'normal' MTs in *tip1Δ* whilst these structures are left unaffected.

Figure 2 *tip1Δ* has an increased proportion of thin filaments A) A wild type MT bundle (green), containing two thin filaments (turquoise). The white arrowhead points indicates the filament shown in B. **B)** Slices from the tomogram (every 3 nm) showing a thin hollow filament next to a normal MT. The insert is a snapshot of the marked position (turquoise arrowhead) rotated 90 degrees in the x-axis, so that the filaments are visible in cross-section. This clearly shows that both filaments are hollow as well as they display different diameters. **C-D)** The lengths and widths of individual thin filaments **E)** The proportion of the total polymerized tubulin that represents thin filaments in WT, *mal3Δ* and *tip1Δ* clearly shows an increase in these filaments in *tip1Δ*.

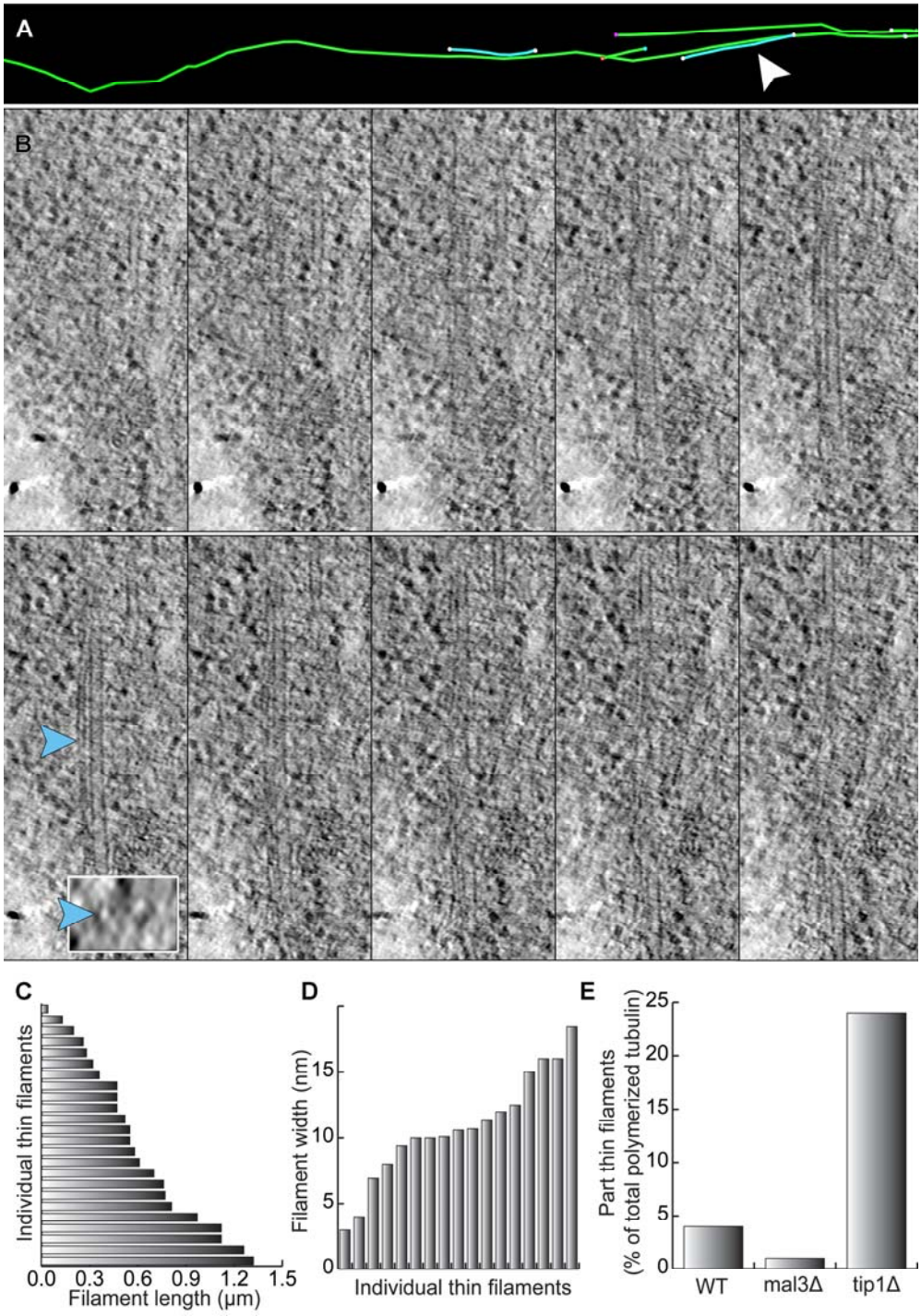
A
B
C
Individual thin filaments
0.0 0.3 0.6 0.9 1.2 1.5
Filament length (μm)
D
Filament width (nm)
0 5 10 15
Individual thin filaments
E
Part thin filaments
(% of total polymerized tubulin)
0 5 10 15 20 25
WT
mal3Δ
tip1Δ

tip1Δ shows a strong reduction of polymerized tubulin

Removing Tip1 causes a reduction both in the number of MTs and in their length. Using live cell imaging of GFP-tubulin, we measured the MT bundles to be 7.9 ± 1.4 μm long in WT and 2.4 ± 0.9 μm in *tip1Δ* cells (n= 220 WT, 198 *tip1Δ*). This corresponds to a bundle length reduction of 70% in *tip1Δ* cells.

Using tomography, individual MT polymer lengths were measured to be between 40 nm and 2.40 μm, with an average of 0.68 ± 0.57 μm (n=33, including nine thin filaments; figure 3A-E). If the thin filaments are excluded, the average length of MT polymer was 0.71 ± 0.63 μm. Interestingly, the average amount of fibers in a bundle decreases from 4.4 ± 2.6 in WT to 1.7 ± 1.6 in *tip1Δ* cells (including thin filaments; figure 3F).

In this mutant we were able to reconstruct a second full cell volume. This cell contained 9 MTs (of which 4 were thin filaments). The total length of polymerized tubulin was 2.81 μm, which is a 91% reduction from the reconstructed full cell volume of a WT cell.

Individual MT length can not be measured by light microscopy, however the length of large numbers of MT bundles can be determined easily. To exclude that this massive reduction of polymerized tubulin was caused by sample preparation, we compared bundle lengths measured by tomography and light microscopy of GFP-tubulin in WT and *tip1Δ* cells (figure 3G). Since we select for short cells when doing tomography, we used the bundle length as a ratio of the cell length to compare the two techniques.

In WT cells, bundles were 71 ±13 % (n=220) of the cell length when measured with light microscopy. The corresponding MT bundle lengths measured by tomography was 68 ± 20 % (n=14). In *tip1Δ* examined using light microscopy bundles measured an average of 24 ± 11%, whereas tomographically reconstructed bundles measured 14 ± 11% (n= 19).

The lengths of MT bundles as measured by the two methods are the same within the range of the errors. This implies that the observed reduction of MT length between WT and *tip1Δ* using tomography is not an artifact.

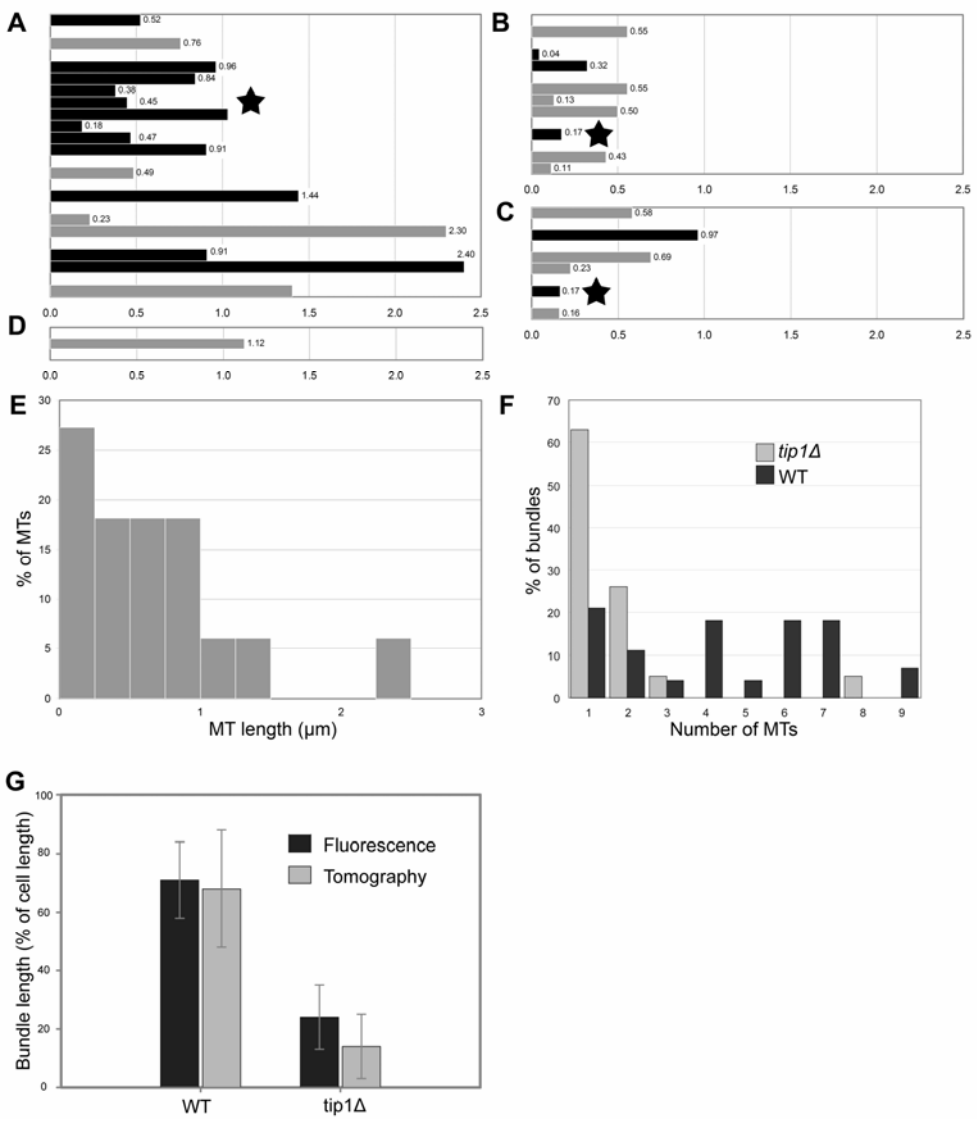

Figure 3 *tip1Δ* microtubules are shorter and bundles have fewer MTs
Bundles of microtubules from four different cells are depicted as groups of black and grey bars. Cells are **A)** 6.5 μm **B)** 6.9 μm **C)** 7.5 μm and **D)** 7.0 μm in length. The * indicates SPB bundles. **E)** Histogram of MT lengths (all MTs in [A]-[D] pooled) showing that most MTs are shorter than 1 μm and none are longer than 2.5 μm. **F)** Most MTs are single filaments and bundles contain in general only two to three MTs. Average in *tip1Δ* of MTs per bundle was 1.7 ± 1.6 MTs, less than half of WT. **G)** A control experiment where bundle length in WT and *tip1Δ* was measured using both light microscopy and tomography. Like this we could confirm that the measured decrease in *tip1Δ* is not a sample preparation artifact.

Microtubule attachment to the NE and SPB is weakened

In general, MTs were found close to the nucleus but we noticed weakened attachment to the NE. Eleven of the nineteen (58%) single MTs and bundles that we studied were apart from the NE in *tip1Δ* (figure 1). This is in comparison to WT where only two out of fourteen bundles (14%) were NE-disassociated. Of these disassociated fibers, six were thin filaments. Therefore, the loosening of the MT and NE connection is apparent in *tip1Δ*.

In the reconstructed *tip1Δ* cell volumes, four SPBs were reconstructed. Their morphology appears normal but only two had attached MTs (figure 4A-B). The third SPB had a MT at approximately 25 nm distance and the final SPB had no MTs attached at all (figure 4C-D). However, this was the cell where we found no MTs at all, so was this a real phenotype of *tip1Δ*?

We decided to examine MT-SPB association by live cell imaging. Cells expressing cherry-fused α-tubulin and cut12-GFP (SPB marker protein) were used to see if SPBs sometimes have no MTs associated with them in WT and *tip1Δ*. We found some evidence for SPBs without associated MTs in *tip1Δ* (figure 4E). However, the MTs in WT appeared short (figure 4F). This could be because cherry-tubulin is not bright enough to show single MTs extending towards the tip or because the cherry-tubulin molecules have altered polymerization properties. Therefore, we are not certain that single short MTs, like most *tip1Δ* MTs, would be visible. A change to GFP-tubulin with another SPB marker would solve this problem. This will be the next step in this investigation.

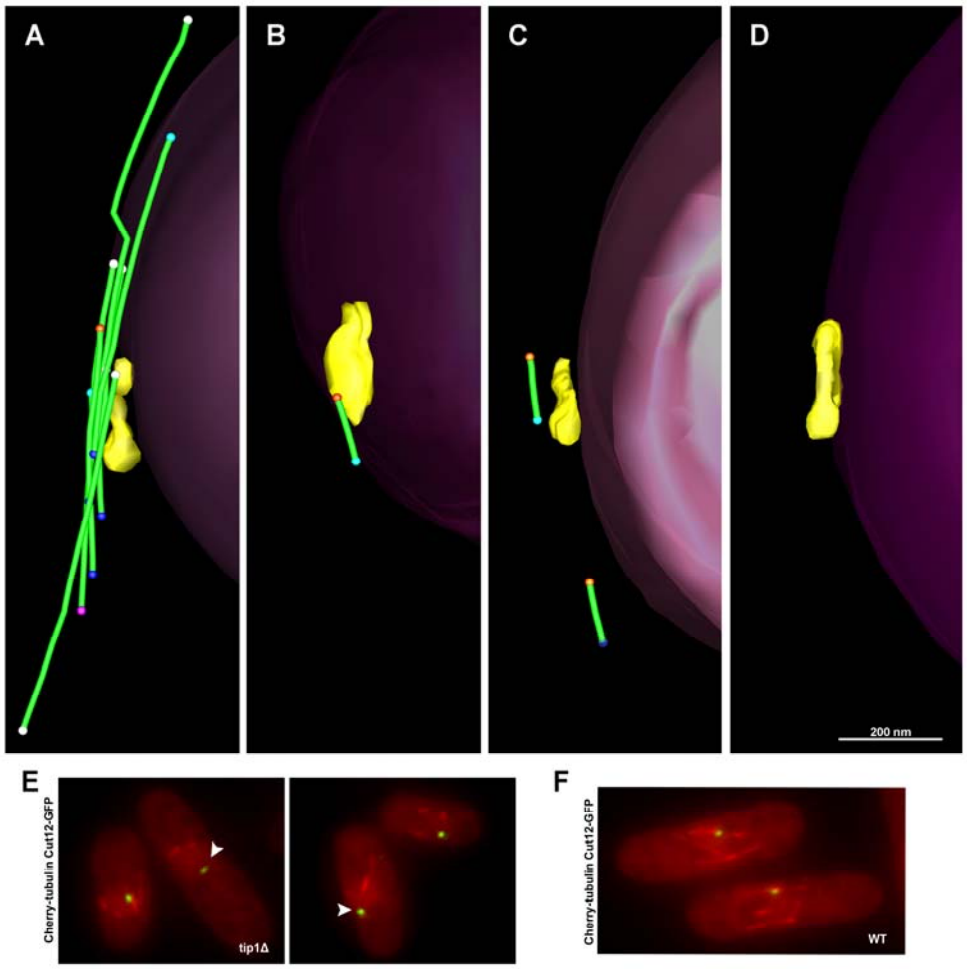

Figure 4 MT attachment to SPB is weakened in *tip1Δ* cells A-B) SPBs with attached MT bundles. **C)** A SPB with a MT adjacent but not touching **D)** A SPB without any MTs at all. **E)** *tip1Δ* cells expressing cherry-tubulin and cut12-GFP show some SPBs without a connecting MT bundle. However, WT bundles **F)** are appear shorter than when using GFP-tubulin, maybe single MTs are not visible.

Discussion

Tip1 affects MT stability, nucleation and NE attachment

We describe more severe MT defects in *tip1Δ* than those found in *mal3Δ*. Microtubules in *tip1Δ* are only half as long and MT bundles contain half as many MTs as in WT. A previous study measuring *tip1Δ* MT bundles using immunofluorescence showed a 30-

60% reduction in bundle length (Brunner and Nurse 2000). Tomography showed an 82% decrease in bundle length.

Therefore, a comparative measurement of WT and *tip1Δ* MT bundles was carried out using GFP-tubulin to visualize the bundles. The results showed a 70% reduction in MT bundle length, a number in between the published original measurement and the tomography data. Considering the small number of measurements feasible when using tomography, and the fact that the measurements from light microscopy and tomography are within each other's standard deviations we conclude that the tomography measurements are correct.

Tip1 prevents MTs to undergo catastrophe when they reach the cell cortex away from the cell ends (Brunner and Nurse 2000). That MTs are shorter when this protein is absent is therefore not surprising. However, we also show that there are fewer MTs in a bundle and that these are not connected to the NE to the same extent as in WT cells. This indicates functions of Tip1 in MT nucleation in addition to attachment of MTs to the nucleus.

Since most nucleation events occur in the nuclear area (Drummond and Cross 2000), it is possible that these two new functions of Tip1, MT nucleation and NE attachment, are related. For instance, proteins binding γ-TURCs might be contained in the NE. MTs detaching from the NE would then be less likely to find such a γ-TURC that would nucleate one further MT. This model would suggest that Tip1 may be involved in MT anchoring to the NE and that the observed nucleation defect was indirect.

The nature of the thin filaments

Thin filaments which appear more flexible than normal MTs were observed in all three strains that we worked with. We have considered them as MTs because of the following reasons:

1. They are often, but not exclusively, found in MT bundles and are then aligned with another MT.
2. They are hollow.

3. Some filaments have regions as thick as a normal MT but then transform into thinner filaments.
4. They frequently appear to be fraying into smaller filaments that could be protofilaments.
5. They are up to 1.3 μm long, making them very unlikely to be a random occurrence of electron dense material.
6. Deletion of a microtubule associated protein (Tip1) changes their prevalence.

The thin filaments are unlikely to be actin cables because these have been described to be ~ 60 nm thick in fission yeast (Kamasaki et al. 2005). Further, the long stretches of two parallel walls are unlike any known actin structure. Moreover, fission yeast has no described IFs and neither actin nor IF proteins form hollow filaments.

The thin filaments are therefore most likely a form of MT polymer. We speculate that they could be a sheet of polymerized tubulin protofilaments that did not form a proper MT cylinder. A reason for this defect could be the absence of a γ-TURC template. Alternatively, the thin filaments could be the remains of MTs that have depolymerized incompletely. A third hypothesis is that these are simply MTs composed of fewer protofilaments as has commonly been observed *in vitro* (Desai and Mitchison 1997).

It could also be possible that our cryoimmobilization method using high pressure freezing caused the already destabilized MTs in *tip1Δ* to form these structures. There is contradicting data as to whether pressure can depolymerize MTs, but at least two studies show that this is possible (O'Connor et al. 1974; Salmon 1975; Salmon et al. 1976). What contradicts this theory is the time frame (~25 ms) in which this cryoimmobilization is achieved. It is unlikely that a major structural reorganization can occur within this time, which is indeed the benefit of using this fixation method (Studer et al. 2001; Osumi et al. 2006).

Since these structures are difficult to visualize using tomography, it is impossible to observe them in thin sections. The only technique, to our knowledge, which could give final proof of the existence of this form of fiber, is cryotomography of frozen hydrated sections. The tomograms prepared of these samples have a resolution of around 2-3 nm, enough to see individual tubulin subunits (Lucic et al. 2005). A second approach to test if

these are real and conserved MT structure intermediates would be to acquire tomograms of for example *S. cerevisiae* and search for similar filaments.

Chapter 6

Discussion and Outlook

Many research groups which are striving to understand cell polarity and polar growth focus on the fission yeast interphase MTs. MT arrays are central in supporting these processes and readily imaged using light microscopy. Our knowledge about MT dynamics and the proteins involved in its regulation is consequentially increasing steadily (La Carbona et al. 2006; Sawin and Tran 2006). However, the detailed MT bundle architecture has remained elusive, since individual MTs can not be resolved using light microscopy. Attempts to reconstruct the MT bundles by electron microscopy have failed because of the long distances over which they extend. Additionally, tracking of MTs through serial sections is made difficult by MTs splaying apart since only parallel MTs can be followed.

A large part of this project was to establish a method to reconstruct and analyze the ultrastructural architecture of the MT cytoskeleton in WT, enabling both quantitative and qualitative description of the MT bundles. Our large-scale electron tomography approach proved to be efficient to describe a number of factors including bundle architecture, the polarity of MTs, the amount of filaments in a bundle, the contact of MTs at the cell end and MT interactions with the NE, SPB, mitochondria and vesicles. Having a large bank of reconstructions of WT was crucial to establish a reference for further tomographical investigations performed on +TIP mutants. This was particularly important since the MT organization is already so pleomorphic in WT cells.

I will first comment on the advantages and disadvantages of the technical and methodological aspects of this study, before discussing the main biological findings and future projects.

The benefits of using electron tomography

Electron tomography has been able to provide information that would not have been available from conventional serial thin section 3D reconstruction. This conventional method combines images of thin sections (60-80nm), which allows an investigator to follow microtubules through their characteristic cross-sectional appearance (Ding et al. 1993). It is limited in 3D resolution by the thickness of the sections and cannot give isotropic 3D information. In electron tomography, a semi-thick section is reconstructed in 3D and a model is built by digitally slicing the tomogram in any direction and drawing around the objects of interest. Using this method, microtubules that diverge from a bundle or bundles that change direction are not lost from the reconstruction. Furthermore, tomography provides a resolution of around 5-12 nm in computerized sections of about 1-2 nm thickness. This resolution is comparable with the resolution in images of thin sections, and almost the same resolution is obtained in the dimension perpendicular to the section's plane. Thus, a model created from a tomogram is of much higher accuracy than one made from serial sections. In addition, using the serial section method, bundles are very difficult and time-consuming to track, even using a goniometer and a rotation holder to tilt the sections so that the MTs of a given bundle are parallel to the electron beam axis. On the contrary, in a tomogram all bundles in the volume can be tracked through their entire length and eventually modelled. Thus, not only information about the bundles themselves but also their interactions can be described.

Plastic shrinkage can induce measurement errors

When a tilt series is being acquired in the electron microscope, the plastic that embeds the sample is being evaporated by the electrons. The resulting shrinkage occurs mostly along the axis perpendicular to the section, and it can be as dramatic as 30-50%. The process of fiducial alignment helps to correct most shrinkage effects in the other axes, and after calculation, an approximate correction of the major shrinkage distortions can be applied. However, the tomograms do not shrink uniformly. The higher the density of material that binds heavy metal stain, the lesser the shrinkage. Thus, joining tomograms of two adjacent sections so that cellular structures fit perfectly between the

sections is very difficult. This means that microtubules stretching over serial tomograms may appear kinked in the model. Consequentially, measurements made from a model include errors that may be considerable and are very hard to estimate.

This problem can be minimized by choosing a cell whose MTs lie as flat as possible, using the prescreen method described in the materials and methods chapter. MTs that lie approximately parallel to the plane of section should not stretch between many serial sections.

An alternative technique would be the use of frozen hydrated sections visualized using cryo-electron tomography. This is where the sample is first frozen at high pressure then sectioned directly at very low temperature. Ice does not evaporate under the electron beam, so the whole problem of shrinkage would be avoided. However, the ice-embedded sample heats up and may form crystals when hit by the electrons. Therefore, upon tomogram acquisition under these conditions the electron dose needs to be optimized to get high signal-to-noise ratio whilst avoiding beam damage. This makes montaging of tomograms impractical, since the overlapping regions used to 'glue' the frames together would get a double electron dose. Furthermore, serial sectioning of such frozen hydrated samples can only be carried out by rare experts. Therefore, reconstructions of large samples like our fission yeast cells using cryo-tomography would be very challenging.

Joining microtubules over serial section may introduce errors

Even larger errors might arise in the modelling process when it is not possible to determine which MTs should be joined at a boundary between sections. For this there is no cure except for careful examination of the model, using tools in *3dmod* like slicer.

For this study it was crucial to reconstruct large fractions of cell volumes. To accomplish this in a reasonable period of time, we compromised on image resolution. Dual axis tomograms were avoided by choosing cells whose orientation provided optimal resolution of the MTs under study, i.e., both the long axis of the cells and the MTs were parallel to the tilt axis. Furthermore, we combined a slightly lower magnification and higher tilt increments than commonly used in cellular tomography. Nonetheless, the MTs were still clearly visible and, sometimes, beautiful MT end structures were seen. These

enabled determination of MT polarity. Of course, such a compromise in resolution may lead to mistakes, such as incorrect classification of the MT ends or even missed MTs. Based on the quality of the obtained images, however, we believe that the likelihood of the latter problem is minute. Moreover, errors made as a consequence of lower-than-optimal resolution should be compensated by the larger sample size we have achieved by studying large volumes and looking at quite a few cells. For further verification we used complementary dual-axis tomograms of small areas for comparison with the single axis tomograms. For example, fine details visible in our single axis reconstructions, such as electron dense bridges between the nuclear envelope and MTs and between the MTs of a bundle, were seen in dual axis tomograms as well. These bridges have also been observed when imaging hydrated sections of the fission yeast mitotic spindle using cryo-electron tomography (D. Nicastro, personal communication). This suggests that the resolution in the single axis tomograms maintained an acceptable quality for our purposes.

The advantage of full cell volume reconstructions

From the studies of WT cells we could give the first complete view of MT bundle architecture and some of the intracellular interactions they make. By joining 15-17 serial tomograms we were able to reconstruct a full cell volume of one WT cell and one *tip1Δ* cell. These cells enabled us to give a snapshot view of a complete MT cytoskeleton. We showed the total length of MT polymer in the cell, number of MTs as well as other organelles, such as mitochondria and vesicles. Furthermore, the proportion of the total cell volume occupied by membrane-bound organelles such as the nucleus, mitochondria and vacuoles was reported. Naturally, additional full cell volumes would further validate our results. However, these were the first two full eukaryotic cell volumes reconstructed using electron tomography, and achieving this was a time-consuming effort. Therefore, the combination of large partial volumes of cells that are easy to acquire and the full cell volumes were the most effective way of describing fission yeast's large internal structures.

Microtubule structures visualized *in situ*

Numerous *in vitro* cryo electron microscopy studies have shown that growing, metastable and shrinking MT ends have different morphology (Mandelkow et al. 1991; Hyman et al. 1995; Muller-Reichert et al. 1998; Arnal et al. 2000). These studies have provided us with detailed models of how MTs grow and shrink. However, *in vitro* conditions do not necessary correspond to the situation in the cytoplasm where a number of different MAPs might affect the structure of MT ends.

Using plastic section tomography, we image MTs in physiological conditions inside the cell. From the parameters of MT dynamics measured by live cell imaging (Busch and Brunner 2004), we could estimate the proportion of MTs that are growing and shrinking at any one time in the cell. This was compared with the morphology of the longest MT in a bundle (this would have been measured using light microscopy) in our tomography reconstructions. The low number of MT end morphologies extracted from the tomograms was surprisingly close to the estimated proportions of MT dynamics, if both flared and sheeted MT ends were considered growing. Based on these results, we propose that growing ends are likely to be seen as both polymer sheets and flared ends *in situ*. However, we can not be sure that our suggestion is correct, since it is based on an indirect way of evaluating the MT dynamic state at the time of cryoimmobilization.

To more conclusively show the morphology of growing MT ends *in situ*, we performed an experiment where MTs were depolymerized using a MT depolymerizing drug and then cryoimmobilized during regrowth after wash out. After drug release, most MTs should be growing and their morphology can be readily identified using electron tomography. Regrettably, these data could not be completely processed and analyzed yet.

Additionally, we could show structural alterations of the MT lattice in both *tip1Δ* (thin filaments) and *mal3Δ* ('kinked' MTs) mutants. Yet, we know that MTs can grow without these proteins with no difficulty *in vitro* (Lee et al. 1974). This leads us to hypothesize that these alterations might be explained by the presence of organelles and macromolecular complexes in the cytoplasm. In the case of the 'kinked' MTs in mal3Δ, the MTs may be weakened by the lack of this protein or proteins interacting with it. A collision or interaction with cytoplasmic structures could then cause the shown lattice deformation.

We speculated that the thin filaments found in higher rates in *tip1Δ* could be incompletely depolymerized MTs, leaving sheets of protofilaments behind. If this was the case, the increase of thin filaments in *tip1Δ* would correspond well to the increased catastrophe rates observed in these cells (Brunner and Nurse 2000). We also suggested that they might be MTs with fewer protofilaments. This could be associated with the nucleation defect discussed in the next section. However, the nature of these thin filaments remains to be elucidated. Possibly, we could get clues about their formation when analyzing the tomograms of cells treated with a MT depolymerizing drug.

Our results prompt us to conclude that studying MTs *in situ* can give a more multi-facetted picture of MT structure than *in vitro* studies.

Electron tomography revealed new functions of the +TIP proteins Tip1 and Mal3

We followed the study of interphase MT organization by analyzing *tip1* and *mal3* deletion mutants. These genes encode proteins that localize to the plus ends of MTs. Mal3 has a general stabilizing effect on MTs, whereas Tip1 stabilizes MTs by locally inhibiting catastrophe at the central cell cortex (Brunner and Nurse 2000; Busch and Brunner 2004).

In both cases, we could confirm the previously described MT stabilizing functions, by measuring MT lengths about half of that seen in WT, as well as additional functions of these proteins. Firstly, we found structural changes in the MT lattice as mentioned above. Secondly, we found alterations in the association to the SPB in both mutants.

EB1 has been shown to be a centrosome component that anchors MTs to, most likely, the mother centriole (Askham et al. 2002; Louie et al. 2004; Yan et al. 2006). In our 3D snapshot view of the *mal3Δ* cells, we could see that MTs are in close association with only one of the SPBs. It is therefore important to ascertain whether this is the old or new SPB, and also if this is due to a maturation defect caused by the lack of Mal3. This will be examined using both light and electron microscopy approaches.

Firstly, we want to use fluorescently tagged SPB markers and compare the fluorescent intensity of just separated SPBs in *mal3Δ*. If we find unequal intensity fluorescence in *mal3Δ* cells, we will proceed to identify which SPB is concerned. For this we could, for example, use a SPB protein fused with the red fluorescent protein DsRed that takes several hours to fold into an actively fluorescing molecule. This property has been exploited previously to differentiate the new from the old SPB (Pereira et al. 2001; Tanaka et al. 2002; Grallert et al. 2004).

Since we showed that the brightest SPB marker Pcp1-GFP had a higher number of SPB dots in *mal3Δ* cells (see results in Chapter 3), more SPB markers will be imaged in *mal3Δ* cells using the spinning disk confocal microscope. The improved signal-to-noise ratio gained by the confocal sectioning of the sample could expose multiple dots using other less bright markers. Such a SPB fractionation would explain the abnormal SPB morphology we see in these mutants.

Secondly, localization of EB1 to the centrosome in vertebrate cells has been performed using light microscopy (Berrueta et al. 1998; Morrison et al. 1998; Askham et al. 2002). From these data it is not clear if EB1 labels a concentration of MT plus ends or the actual centrosomal structure itself. Therefore, we are trying to localize Mal3 to the SPB using Mal3 directed antibodies and on-section immunogold labelling. A specific gold localization to the SPB would be the final proof that Mal3 is actually a SPB component.

For the Clip-170 protein family, on the other hand, there are no previous indications that they might be centrosome components. However, we found *tip1Δ* to have a nucleation defect. It has been shown that satellite MTOCs nucleate MTs along the length of pre-existing MTs (Sawin et al. 2004; Zimmerman et al. 2004; Janson et al. 2005; Zimmerman and Chang 2005). It could therefore be predicted that shorter MTs could lessen the probability for new nucleations. If true, *mal3Δ* would also show a nucleation defect, which we did not observe. Therefore, this nucleation defect in *tip1Δ* is Tip1 specific.

Furthermore, we show that MTs in *tip1Δ* were predominantly found in the nuclear region distant from the NE and SPB. This suggests that Tip1 is important in anchoring the MT lattice or minus ends to the NE and also the SPB, which could be related with the

observed nucleation defect. The localization away from the NE would, in most cases, not be detectable using light microscopy, since MTs are still relatively close. However, the absence of MTs from the SPB can and will be addressed using this technique. Therefore, both +TIPs studied have shown important functions at or near the MT minus end.

Tip1 and Mal3 may localize to the growing plus end of MTs to provide a pool of 'building blocks' for new MT lattice formation

Tip1 localizes to the lattice of MTs and is transported by Tea2 to the end of MTs. Here, larger particles of Tip1 are anchored by Mal3 (Busch et al. 2004). Therefore, in *mal3Δ*, Tip1 is absent from MT plus ends but still present along the lattice. This provides a tool to dissect the function of Tip1 along the lattice from its role at the MT plus ends.

Due to the additional role of Mal3 in anchoring Tip1 to MT ends, one would expect the *mal3Δ* to cause a more severe MT phenotype than *tip1Δ*. However, we see a more severe reduction of polymerized tubulin in *tip1Δ*. This could be due to impaired nucleation in *tip1Δ* or interactions unknown to date. However, it could also be an indication that the major function of Tip1 is exerted along the MT lattice. Furthermore, the increased amount of thin flexible filaments in *tip1Δ* could also be an indication of Tip1 being a MT lattice stabilizer.

Additionally, the description of Mal3 as a molecular zipper along the MT lattice seam (Sandblad et al. 2006) as well as the MT lattice 'kinks' shown in this study, suggests that Mal3 have an important structural function along the lattice. We therefore hypothesise that these two +TIP proteins, and maybe others, localize to growing MT ends to provide a large pool of 'building blocks' necessary for stable MT growth. This large quantity of proteins at the growing MT end would increase the chance of proper MT sheet closure and stabilization of the seam.

In conclusion, tomography proved to be a powerful tool to show important new functions of proteins that can then be further examined using light microscopy to enlarge the sample size and provide the dynamic picture. This confirms that new insights in the

architecture of the fission yeast interphase cytoskeleton in particular, but also cellular architecture in general, is best achieved using a combination of methods.

References

Akhmanova A, Hoogenraad CC (2005) Microtubule plus-end-tracking proteins: mechanisms and functions. Curr Opin Cell Biol 17(1): 47-54.

Anders A, Lourenco PC, Sawin KE (2006) Noncore components of the fission yeast gamma-tubulin complex. Mol Biol Cell 17(12): 5075-5093.

Arai R, Nakano K, Mabuchi I (1998) Subcellular localization and possible function of actin, tropomyosin and actin-related protein 3 (Arp3) in the fission yeast Schizosaccharomyces pombe. Eur J Cell Biol 76(4): 288-295.

Arnal I, Karsenti E, Hyman AA (2000) Structural transitions at microtubule ends correlate with their dynamic properties in Xenopus egg extracts. J Cell Biol 149(4): 767-774.

Asakawa K, Toda T (2006) Cooperation of EB1-Mal3 and the Bub1 spindle checkpoint. Cell Cycle 5(1): 27-30.

Askham JM, Vaughan KT, Goodson HV, Morrison EE (2002) Evidence that an interaction between EB1 and p150(Glued) is required for the formation and maintenance of a radial microtubule array anchored at the centrosome. Mol Biol Cell 13(10): 3627-3645.

Austin JR, 2nd, Segui-Simarro JM, Staehelin LA (2005) Quantitative analysis of changes in spatial distribution and plus-end geometry of microtubules involved in plant-cell cytokinesis. J Cell Sci 118(Pt 17): 3895-3903.

Ayscough K, Hajibagheri NM, Watson R, Warren G (1993) Stacking of Golgi cisternae in Schizosaccharomyces pombe requires intact microtubules. J Cell Sci 106 (Pt 4): 1227-1237.

Ayscough KR, Winder SJ (2004) Two billion years of actin. Meeting on cytoskeletal dynamics: from cell biology to developmental disease. EMBO Rep 5(10): 947-952.

Bahler J, Nurse P (2001) Fission yeast Pom1p kinase activity is cell cycle regulated and essential for cellular symmetry during growth and division. Embo J 20(5): 1064-1073.

Basto R, Lau J, Vinogradova T, Gardiol A, Woods CG et al. (2006) Flies without centrioles. Cell 125(7): 1375-1386.

Baumeister W, Grimm R, Walz J (1999) Electron tomography of molecules and cells. Trends Cell Biol 9(2): 81-85.

Behrens R, Nurse P (2002) Roles of fission yeast tea1p in the localization of polarity factors and in organizing the microtubular cytoskeleton. J Cell Biol 157(5): 783-793.

Beinhauer JD, Hagan IM, Hegemann JH, Fleig U (1997) Mal3, the fission yeast homologue of the human APC-interacting protein EB-1 is required for microtubule integrity and the maintenance of cell form. J Cell Biol 139(3): 717-728.

Berrueta L, Kraeft SK, Tirnauer JS, Schuyler SC, Chen LB et al. (1998) The adenomatous polyposis coli-binding protein EB1 is associated with cytoplasmic and spindle microtubules. Proc Natl Acad Sci U S A 95(18): 10596-10601.

Bonifacino JS, Glick BS (2004) The mechanisms of vesicle budding and fusion. Cell 116(2): 153-166.

Braunfeld MB, Koster AJ, Sedat JW, Agard DA (1994) Cryo automated electron tomography: towards high-resolution reconstructions of plastic-embedded structures. J Microsc 174 (Pt 2): 75-84.

Brazer SC, Williams HP, Chappell TG, Cande WZ (2000) A fission yeast kinesin affects Golgi membrane recycling. Yeast 16(2): 149-166.

Browning H, Hackney DD (2005) The EB1 homolog Mal3 stimulates the ATPase of the kinesin Tea2 by recruiting it to the microtubule. J Biol Chem 280(13): 12299-12304.

Browning H, Hackney DD, Nurse P (2003) Targeted movement of cell end factors in fission yeast. Nat Cell Biol 5(9): 812-818.

Browning H, Hayles J, Mata J, Aveline L, Nurse P et al. (2000) Tea2p is a kinesin-like protein required to generate polarized growth in fission yeast. J Cell Biol 151(1): 15-28.

Brunner D, Nurse P (2000) CLIP170-like tip1p spatially organizes microtubular dynamics in fission yeast. Cell 102(5): 695-704.

Bu W, Su LK (2003) Characterization of functional domains of human EB1 family proteins. J Biol Chem 278(50): 49721-49731.

Bullitt E, Rout MP, Kilmartin JV, Akey CW (1997) The yeast spindle pole body is assembled around a central crystal of Spc42p. Cell 89(7): 1077-1086.

Busch KE, Brunner D (2004) The microtubule plus end-tracking proteins mal3p and tip1p cooperate for cell-end targeting of interphase microtubules. Curr Biol 14(7): 548-559.

Busch KE, Hayles J, Nurse P, Brunner D (2004) Tea2p kinesin is involved in spatial microtubule organization by transporting tip1p on microtubules. Dev Cell 6(6): 831-843.

Carazo-Salas RE, Nurse P (2006) Self-organization of interphase microtubule arrays in fission yeast. Nat Cell Biol 8(10): 1102-1107.

Carazo-Salas RE, Antony C, Nurse P (2005) The kinesin Klp2 mediates polarization of interphase microtubules in fission yeast. Science 309(5732): 297-300.

Carvalho P, Tirnauer JS, Pellman D (2003) Surfing on microtubule ends. Trends Cell Biol 13(5): 229-237.

Carvalho P, Gupta ML, Jr., Hoyt MA, Pellman D (2004) Cell cycle control of kinesin-mediated transport of Bik1 (CLIP-170) regulates microtubule stability and dynein activation. Dev Cell 6(6): 815-829.

Cassimeris L, Morabito J (2004) TOGp, the human homolog of XMAP215/Dis1, is required for centrosome integrity, spindle pole organization, and bipolar spindle assembly. Mol Biol Cell 15(4): 1580-1590.

Celton-Morizur S, Racine V, Sibarita JB, Paoletti A (2006) Pom1 kinase links division plane position to cell polarity by regulating Mid1p cortical distribution. J Cell Sci 119(Pt 22): 4710-4718.

Chan J, Jensen CG, Jensen LC, Bush M, Lloyd CW (1999) The 65-kDa carrot microtubule-associated protein forms regularly arranged filamentous cross-bridges between microtubules. Proc Natl Acad Sci U S A 96(26): 14931-14936.
Chang F, Peter M (2003) Yeasts make their mark. Nat Cell Biol 5(4): 294-299.
Chen J, Kanai Y, Cowan NJ, Hirokawa N (1992) Projection domains of MAP2 and tau determine spacings between microtubules in dendrites and axons. Nature 360(6405): 674-677.
Chretien D, Fuller SD, Karsenti E (1995) Structure of growing microtubule ends: two-dimensional sheets close into tubes at variable rates. J Cell Biol 129(5): 1311-1328.
Chretien D, Jainosi I, Taveau JC, Flyvbjerg H (1999) Microtubule's conformational cap. Cell Struct Funct 24(5): 299-303.
Daga RR, Chang F (2005) Dynamic positioning of the fission yeast cell division plane. Proc Natl Acad Sci U S A 102(23): 8228-8232.
Daga RR, Yonetani A, Chang F (2006a) Asymmetric microtubule pushing forces in nuclear centering. Curr Biol 16(15): 1544-1550.
Daga RR, Lee KG, Bratman S, Salas-Pino S, Chang F (2006b) Self-organization of microtubule bundles in anucleate fission yeast cells. Nat Cell Biol 8(10): 1108-1113.
Daunderer C, Schliwa M, Graf R (1999) Dictyostelium discoideum: a promising centrosome model system. Biol Cell 91(4-5): 313-320.
Desai A, Mitchison TJ (1997) Microtubule polymerization dynamics. Annu Rev Cell Dev Biol 13: 83-117.
Diamantopoulos GS, Perez F, Goodson HV, Batelier G, Melki R et al. (1999) Dynamic localization of CLIP-170 to microtubule plus ends is coupled to microtubule assembly. J Cell Biol 144(1): 99-112.
Ding R, McDonald KL, McIntosh JR (1993) Three-dimensional reconstruction and analysis of mitotic spindles from the yeast, Schizosaccharomyces pombe. J Cell Biol 120(1): 141-151.
Ding R, West RR, Morphew DM, Oakley BR, McIntosh JR (1997) The spindle pole body of Schizosaccharomyces pombe enters and leaves the nuclear envelope as the cell cycle proceeds. Mol Biol Cell 8(8): 1461-1479.
Donaldson AD, Kilmartin JV (1996) Spc42p: a phosphorylated component of the S. cerevisiae spindle pole body (SPD) with an essential function during SPB duplication. J Cell Biol 132(5): 887-901.
Draviam VM, Shapiro I, Aldridge B, Sorger PK (2006) Misorientation and reduced stretching of aligned sister kinetochores promote chromosome missegregation in EB1- or APC-depleted cells. Embo J 25(12): 2814-2827.
Drubin DG (1991) Development of cell polarity in budding yeast. Cell 65(7): 1093-1096.
Drubin DG, Nelson WJ (1996) Origins of cell polarity. Cell 84(3): 335-344.
Drummond DR, Cross RA (2000) Dynamics of interphase microtubules in Schizosaccharomyces pombe. Curr Biol 10(13): 766-775.
Erickson HP (1974) Microtubule surface lattice and subunit structure and observations on reassembly. J Cell Biol 60(1): 153-167.
Feierbach B, Chang F (2001) Roles of the fission yeast formin for3p in cell polarity, actin cable formation and symmetric cell division. Curr Biol 11(21): 1656-1665.

Feierbach B, Verde F, Chang F (2004) Regulation of a formin complex by the microtubule plus end protein tea1p. J Cell Biol 165(5): 697-707.

Folker ES, Baker BM, Goodson HV (2005) Interactions between CLIP-170, tubulin, and microtubules: implications for the mechanism of Clip-170 plus-end tracking behavior. Mol Biol Cell 16(11): 5373-5384.

Frank J (1992) electron tomography: Three Dimensional Imaging with Transmission Electron Microscope. New York: Plenum Press.

Fudge DS, Gosline JM (2004) Molecular design of the alpha-keratin composite: insights from a matrix-free model, hagfish slime threads. Proc Biol Sci 271(1536): 291-299.

Fujita A, Vardy L, Garcia MA, Toda T (2002) A Fourth Component of the Fission Yeast gamma -Tubulin Complex, Alp16, Is Required for Cytoplasmic Microtubule Integrity and Becomes Indispensable When gamma -Tubulin Function Is Compromised. Mol Biol Cell 13(7): 2360-2373.

Fukasawa K (2005) Centrosome amplification, chromosome instability and cancer development. Cancer Lett 230(1): 6-19.

Funabiki H, Hagan I, Uzawa S, Yanagida M (1993) Cell cycle-dependent specific positioning and clustering of centromeres and telomeres in fission yeast. J Cell Biol 121(5): 961-976.

Gachet Y, Hyams JS (2005) Endocytosis in fission yeast is spatially associated with the actin cytoskeleton during polarised cell growth and cytokinesis. J Cell Sci 118(Pt 18): 4231-4242.

Giddings TH, Jr., O'Toole ET, Morphew M, Mastronarde DN, McIntosh JR et al. (2001) Using rapid freeze and freeze-substitution for the preparation of yeast cells for electron microscopy and three-dimensional analysis. Methods Cell Biol 67: 27-42.

Glynn JM, Lustig RJ, Berlin A, Chang F (2001) Role of bud6p and tea1p in the interaction between actin and microtubules for the establishment of cell polarity in fission yeast. Curr Biol 11(11): 836-845.

Goldie KN, Wedig T, Mitra AK, Aebi U, Herrmann H et al. (2006) Dissecting the 3-D structure of vimentin intermediate filaments by cryo-electron tomography. J Struct Biol.

Goldstein LS, Yang Z (2000) Microtubule-based transport systems in neurons: the roles of kinesins and dyneins. Annu Rev Neurosci 23: 39-71.

Graf R, Euteneuer U, Ueda M, Schliwa M (1998) Isolation of nucleation-competent centrosomes from Dictyostelium discoideum. Eur J Cell Biol 76(3): 167-175.

Grallert A, Krapp A, Bagley S, Simanis V, Hagan IM (2004) Recruitment of NIMA kinase shows that maturation of the S. pombe spindle-pole body occurs over consecutive cell cycles and reveals a role for NIMA in modulating SIN activity. Genes Dev 18(9): 1007-1021.

Grallert A, Beuter C, Craven RA, Bagley S, Wilks D et al. (2006) S. pombe CLASP needs dynein, not EB1 or CLIP170, to induce microtubule instability and slows polymerization rates at cell tips in a dynein-dependent manner. Genes Dev 20(17): 2421-2436.

Green RA, Wollman R, Kaplan KB (2005) APC and EB1 function together in mitosis to regulate spindle dynamics and chromosome alignment. Mol Biol Cell 16(10): 4609-4622.
Griffiths G (1993) Fine structure immunocytochemistry; Griffiths G, editor. Berlin: Springer-verlag. 459 p.
Grishchuk EL, McIntosh JR (2006) Microtubule depolymerization can drive poleward chromosome motion in fission yeast. Embo J 25(20): 4888-4896.
Hagan I, Yanagida M (1990) Novel potential mitotic motor protein encoded by the fission yeast cut7+ gene. Nature 347(6293): 563-566.
Hagan I, Yanagida M (1997) Evidence for cell cycle-specific, spindle pole body-mediated, nuclear positioning in the fission yeast Schizosaccharomyces pombe. J Cell Sci 110 (Pt 16): 1851-1866.
Hagan IM (1998) The fission yeast microtubule cytoskeleton. J Cell Sci 111 (Pt 12): 1603-1612.
Hagan IM, Hyams JS (1988) The use of cell division cycle mutants to investigate the control of microtubule distribution in the fission yeast Schizosaccharomyces pombe. J Cell Sci 89 (Pt 3): 343-357.
Harris SD (2006) Cell polarity in filamentous fungi: shaping the mold. Int Rev Cytol 251: 41-77.
Hayashi I, Ikura M (2003) Crystal structure of the amino-terminal microtubule-binding domain of end-binding protein 1 (EB1). J Biol Chem 278(38): 36430-36434.
Hayashi I, Wilde A, Mal TK, Ikura M (2005) Structural basis for the activation of microtubule assembly by the EB1 and p150Glued complex. Mol Cell 19(4): 449-460.
Hayles J, Nurse P (2001) A journey into space. Nat Rev Mol Cell Biol 2(9): 647-656.
Heald R, Tournebize R, Habermann A, Karsenti E, Hyman A (1997) Spindle assembly in Xenopus egg extracts: respective roles of centrosomes and microtubule self-organization. J Cell Biol 138(3): 615-628.
Heckman DS, Geiser DM, Eidell BR, Stauffer RL, Kardos NL et al. (2001) Molecular evidence for the early colonization of land by fungi and plants. Science 293(5532): 1129-1133.
Heitz MJ, Petersen J, Valovin S, Hagan IM (2001) MTOC formation during mitotic exit in fission yeast. J Cell Sci 114(Pt 24): 4521-4532.
Helfand BT, Chang L, Goldman RD (2004) Intermediate filaments are dynamic and motile elements of cellular architecture. J Cell Sci 117(Pt 2): 133-141.
Herrmann H, Aebi U (2004) Intermediate filaments: molecular structure, assembly mechanism, and integration into functionally distinct intracellular Scaffolds. Annu Rev Biochem 73: 749-789.
Hestermann A, Rehberg M, Graf R (2002) Centrosomal microtubule plus end tracking proteins and their role in Dictyostelium cell dynamics. J Muscle Res Cell Motil 23(7-8): 621-630.
Holmes KC, Popp D, Gebhard W, Kabsch W (1990) Atomic model of the actin filament. Nature 347(6288): 44-49.
Holy TE, Leibler S (1994) Dynamic instability of microtubules as an efficient way to search in space. Proc Natl Acad Sci U S A 91(12): 5682-5685.

Honnappa S, John CM, Kostrewa D, Winkler FK, Steinmetz MO (2005) Structural insights into the EB1-APC interaction. Embo J 24(2): 261-269.

Hoog JL, Schwartz C, Noon AT, O'Toole ET, Mastronarde DN et al. (2007) Organization of interphase microtubules in fission yeast analyzed by electron tomography. Dev Cell 12(3): 349-361.

Höög JL, Antony C (*in press*) Analyzing Whole Cell Architecture by Electron Tomography: the interphase microtubule complex of *Schizosaccharomyces pombe*. In: McIntosh JR, editor. Methods in Cell Biology. San Diego: Elsevier Inc.

Horio T, Uzawa S, Jung MK, Oakley BR, Tanaka K et al. (1991) The fission yeast gamma-tubulin is essential for mitosis and is localized at microtubule organizing centers. J Cell Sci 99 (Pt 4): 693-700.

Howard J, Hyman AA (2007) Microtubule polymerases and depolymerases. Curr Opin Cell Biol 19(1): 31-35.

Howard WD, Timasheff SN (1986) GDP state of tubulin: stabilization of double rings. Biochemistry 25(25): 8292-8300.

Huckaba TM, Gay AC, Pantalena LF, Yang HC, Pon LA (2004) Live cell imaging of the assembly, disassembly, and actin cable-dependent movement of endosomes and actin patches in the budding yeast, Saccharomyces cerevisiae. J Cell Biol 167(3): 519-530.

Huffaker TC, Thomas JH, Botstein D (1988) Diverse effects of beta-tubulin mutations on microtubule formation and function. J Cell Biol 106(6): 1997-2010.

Hwang E, Kusch J, Barral Y, Huffaker TC (2003) Spindle orientation in Saccharomyces cerevisiae depends on the transport of microtubule ends along polarized actin cables. J Cell Biol 161(3): 483-488.

Hyman AA, Chretien D, Arnal I, Wade RH (1995) Structural changes accompanying GTP hydrolysis in microtubules: information from a slowly hydrolyzable analogue guanylyl-(alpha,beta)-methylene-diphosphonate. J Cell Biol 128(1-2): 117-125.

Irazoqui JE, Lew DJ (2004) Polarity establishment in yeast. J Cell Sci 117(Pt 11): 2169-2171.

Janson ME, Setty TG, Paoletti A, Tran PT (2005) Efficient formation of bipolar microtubule bundles requires microtubule-bound gamma-tubulin complexes. J Cell Biol 169(2): 297-308.

Janson ME, Loughlin R, Loiodice I, Fu C, Brunner D et al. (2007) Crosslinkers and motors organize dynamic microtubules to form stable bipolar arrays in fission yeast. Cell 128(2): 357-368.

Janulevicius A, van Pelt J, van Ooyen A (2006) Compartment volume influences microtubule dynamic instability: a model study. Biophys J 90(3): 788-798.

Jaspersen SL, Winey M (2004) The budding yeast spindle pole body: structure, duplication, and function. Annu Rev Cell Dev Biol 20: 1-28.

Jeong JW, Rhee DK, Cho SY, Hae KL, Kim DU et al. (2002) Cloning and characterization of the kinesin-related protein, Krp1p, in Schizosaccharomyces pombe. Mol Cells 13(3): 389-398.

Kabsch W, Vandekerckhove J (1992) Structure and function of actin. Annu Rev Biophys Biomol Struct 21: 49-76.

Kaksonen M, Toret CP, Drubin DG (2005) A modular design for the clathrin- and actin-mediated endocytosis machinery. Cell 123(2): 305-320.
Kamasaki T, Arai R, Osumi M, Mabuchi I (2005) Directionality of F-actin cables changes during the fission yeast cell cycle. Nat Cell Biol 7(9): 916-917.
Kanbe T, Kobayashi I, Tanaka K (1989) Dynamics of cytoplasmic organelles in the cell cycle of the fission yeast Schizosaccharomyces pombe: three-dimensional reconstruction from serial sections. J Cell Sci 94 (Pt 4): 647-656.
Keating TJ, Borisy GG (2000) Immunostructural evidence for the template mechanism of microtubule nucleation. Nat Cell Biol 2(6): 352-357.
Kerkhoff E (2006) Cellular functions of the Spir actin-nucleation factors. Trends Cell Biol 16(9): 477-483.
Kirschner MW, Honig LS, Williams RC (1975) Quantitative electron microscopy of microtubule assembly in vitro. J Mol Biol 99(2): 263-276.
Klenchin VA, Khaitlina SY, Rayment I (2006) Crystal structure of polymerization-competent actin. J Mol Biol 362(1): 140-150.
Komarova YA, Vorobjev IA, Borisy GG (2002) Life cycle of MTs: persistent growth in the cell interior, asymmetric transition frequencies and effects of the cell boundary. J Cell Sci 115(Pt 17): 3527-3539.
Konomi M, Ishiguro J, Osumi M (2000) Abnormal formation of the glucan network from regenerating protoplasts in Schizosaccharomyces pombe cps8 actin point mutant. J Electron Microsc (Tokyo) 49(4): 569-578.
Krebs A, Goldie KN, Hoenger A (2004) Complex formation with kinesin motor domains affects the structure of microtubules. J Mol Biol 335(1): 139-153.
Kremer JR, Mastronarde DN, McIntosh JR (1996) Computer visualization of three-dimensional image data using IMOD. J Struct Biol 116(1): 71-76.
La Carbona S, Le Goff C, Le Goff X (2006) Fission yeast cytoskeletons and cell polarity factors: connecting at the cortex. Biol Cell 98(11): 619-631.
Lansbergen G, Akhmanova A (2006) Microtubule plus end: a hub of cellular activities. Traffic 7(5): 499-507.
Lansbergen G, Komarova Y, Modesti M, Wyman C, Hoogenraad CC et al. (2004) Conformational changes in CLIP-170 regulate its binding to microtubules and dynactin localization. J Cell Biol 166(7): 1003-1014.
Lawrence CJ, Dawe RK, Christie KR, Cleveland DW, Dawson SC et al. (2004) A standardized kinesin nomenclature. J Cell Biol 167(1): 19-22.
Lee WL, Bezanilla M, Pollard TD (2000) Fission yeast myosin-I, Myo1p, stimulates actin assembly by Arp2/3 complex and shares functions with WASp. J Cell Biol 151(4): 789-800.
Lee YC, Samson FE, Jr., Houston LL, Himes RH (1974) The in vitro polymerization of tubulin from beef brain. J Neurobiol 5(4): 317-330.
Li R, Zheng Y, Drubin DG (1995) Regulation of cortical actin cytoskeleton assembly during polarized cell growth in budding yeast. J Cell Biol 128(4): 599-615.
Liakopoulos D, Kusch J, Grava S, Vogel J, Barral Y (2003) Asymmetric loading of Kar9 onto spindle poles and microtubules ensures proper spindle alignment. Cell 112(4): 561-574.
Lippincott-Schwartz J (1998) Cytoskeletal proteins and Golgi dynamics. Curr Opin Cell Biol 10(1): 52-59.

Loiodice I, Staub J, Setty TG, Nguyen NP, Paoletti A et al. (2005) Ase1p organizes antiparallel microtubule arrays during interphase and mitosis in fission yeast. Mol Biol Cell 16(4): 1756-1768.
Louie RK, Bahmanyar S, Siemers KA, Votin V, Chang P et al. (2004) Adenomatous polyposis coli and EB1 localize in close proximity of the mother centriole and EB1 is a functional component of centrosomes. J Cell Sci 117(Pt 7): 1117-1128.
Lowe J, Amos LA (1998) Crystal structure of the bacterial cell-division protein FtsZ. Nature 391(6663): 203-206.
Lowe J, Li H, Downing KH, Nogales E (2001) Refined structure of alpha beta-tubulin at 3.5 A resolution. J Mol Biol 313(5): 1045-1057.
Lucic V, Forster F, Baumeister W (2005) Structural studies by electron tomography: from cells to molecules. Annu Rev Biochem 74: 833-865.
Luther PK, Lawrence MC, Crowther RA (1988) A method for monitoring the collapse of plastic sections as a function of electron dose. Ultramicroscopy 24(1): 7-18.
Ma S, Chisholm RL (2002) Cytoplasmic dynein-associated structures move bidirectionally in vivo. J Cell Sci 115(Pt 7): 1453-1460.
Maccioni RB, Cambiazo V (1995) Role of microtubule-associated proteins in the control of microtubule assembly. Physiol Rev 75(4): 835-864.
Maekawa H, Usui T, Knop M, Schiebel E (2003) Yeast Cdk1 translocates to the plus end of cytoplasmic microtubules to regulate bud cortex interactions. Embo J 22(3): 438-449.
Magin TM, Reichelt J, Hatzfeld M (2004) Emerging functions: diseases and animal models reshape our view of the cytoskeleton. Exp Cell Res 301(1): 91-102.
Mandelkow EM, Mandelkow E, Milligan RA (1991) Microtubule dynamics and microtubule caps: a time-resolved cryo-electron microscopy study. J Cell Biol 114(5): 977-991.
Marks J, Hagan IM, Hyams JS (1986) Growth polarity and cytokinesis in fission yeast: the role of the cytoskeleton. J Cell Sci Suppl 5: 229-241.
Marsh BJ, Mastronarde DN, Buttle KF, Howell KE, McIntosh JR (2001) Organellar relationships in the Golgi region of the pancreatic beta cell line, HIT-T15, visualized by high resolution electron tomography. Proc Natl Acad Sci U S A 98(5): 2399-2406.
Mastronarde DN (1997) Dual-axis tomography: an approach with alignment methods that preserve resolution. J Struct Biol 120(3): 343-352.
Mastronarde DN (2005) Automated electron microscope tomography using robust prediction of specimen movements. J Struct Biol 152(1): 36-51.
Mastronarde DN, McDonald KL, Ding R, McIntosh JR (1993) Interpolar spindle microtubules in PTK cells. J Cell Biol 123(6 Pt 1): 1475-1489.
Masuda H, Sevik M, Cande WZ (1992) In vitro microtubule-nucleating activity of spindle pole bodies in fission yeast Schizosaccharomyces pombe: cell cycle-dependent activation in xenopus cell-free extracts. J Cell Biol 117(5): 1055-1066.
Mata J, Nurse P (1997) tea1 and the microtubular cytoskeleton are important for generating global spatial order within the fission yeast cell. Cell 89(6): 939-949.
Matsuyama A, Arai R, Yashiroda Y, Shirai A, Kamata A et al. (2006) ORFeome cloning and global analysis of protein localization in the fission yeast Schizosaccharomyces pombe. Nat Biotechnol 24(7): 841-847.

McCollum D, Feoktistova A, Morphew M, Balasubramanian M, Gould KL (1996) The Schizosaccharomyces pombe actin-related protein, Arp3, is a component of the cortical actin cytoskeleton and interacts with profilin. Embo J 15(23): 6438-6446.
McConnell SJ, Yaffe MP (1993) Intermediate filament formation by a yeast protein essential for organelle inheritance. Science 260(5108): 687-689.
McDonald K, Morphew MK (1993) Improved preservation of ultrastructure in difficult-to-fix organisms by high pressure freezing and freeze substitution: I. Drosophila melanogaster and Strongylocentrotus purpuratus embryos. Microsc Res Tech 24(6): 465-473.
McDonald KL, M. Morphew, P. Verkade and T. Mueller-Reichert (2006) Recent advances in high pressure freezing:equipment and speciment loading methods.; Kuo J, editor. Totowa, NJ, USA: Humana Press.
McIntosh JR, O'Toole ET (1999) Life cycles of yeast spindle pole bodies: getting microtubules into a closed nucleus. Biol Cell 91(4-5): 305-312.
McIntosh R, Nicastro D, Mastronarde D (2005) New views of cells in 3D: an introduction to electron tomography. Trends Cell Biol 15(1): 43-51.
Melki R, Carlier MF, Pantaloni D, Timasheff SN (1989) Cold depolymerization of microtubules to double rings: geometric stabilization of assemblies. Biochemistry 28(23): 9143-9152.
Miki H, Okada Y, Hirokawa N (2005) Analysis of the kinesin superfamily: insights into structure and function. Trends Cell Biol 15(9): 467-476.
Mitchison JM, Walker PM (1959) RNA synthesis during the cell life cycle of a fission yeast Schizosaccharomyces pombe. Exp Cell Res 16(1): 49-58.
Mitchison JM, Nurse P (1985) Growth in cell length in the fission yeast Schizosaccharomyces pombe. J Cell Sci 75: 357-376.
Mitchison T, Kirschner M (1984) Dynamic instability of microtubule growth. Nature 312(5991): 237-242.
Moreno S, Klar A, Nurse P (1991) Molecular genetic analysis of fission yeast Schizosaccharomyces pombe. Methods Enzymol 194: 795-823.
Moritz M, Braunfeld MB, Guenebaut V, Heuser J, Agard DA (2000) Structure of the gamma-tubulin ring complex: a template for microtubule nucleation. Nat Cell Biol 2(6): 365-370.
Morrison EE (2007) Action and interactions at microtubule ends. Cell Mol Life Sci 64(3): 307-317.
Morrison EE, Wardleworth BN, Askham JM, Markham AF, Meredith DM (1998) EB1, a protein which interacts with the APC tumour suppressor, is associated with the microtubule cytoskeleton throughout the cell cycle. Oncogene 17(26): 3471-3477.
Motegi F, Arai R, Mabuchi I (2001) Identification of two type V myosins in fission yeast, one of which functions in polarized cell growth and moves rapidly in the cell. Mol Biol Cell 12(5): 1367-1380.
Mulholland J, Konopka J, Singer-Kruger B, Zerial M, Botstein D (1999) Visualization of receptor-mediated endocytosis in yeast. Mol Biol Cell 10(3): 799-817.
Muller-Reichert T, Chretien D, Severin F, Hyman AA (1998) Structural changes at microtubule ends accompanying GTP hydrolysis: information from a slowly hydrolyzable analogue of GTP, guanylyl (alpha,beta)methylenediphosphonate. Proc Natl Acad Sci U S A 95(7): 3661-3666.

Muller-Reichert T, Sassoon I, O'Toole E, Romao M, Ashford AJ et al. (2003) Analysis of the distribution of the kinetochore protein Ndc10p in Saccharomyces cerevisiae using 3-D modeling of mitotic spindles. Chromosoma 111(7): 417-428.

Muller EG, Snydsman BE, Novik I, Hailey DW, Gestaut DR et al. (2005) The organization of the core proteins of the yeast spindle pole body. Mol Biol Cell 16(7): 3341-3352.

Murata T, Sonobe S, Baskin TI, Hyodo S, Hasezawa S et al. (2005) Microtubule-dependent microtubule nucleation based on recruitment of gamma-tubulin in higher plants. Nat Cell Biol 7(10): 961-968.

Nabeshima K, Nakagawa T, Straight AF, Murray A, Chikashige Y et al. (1998) Dynamics of centromeres during metaphase-anaphase transition in fission yeast: Dis1 is implicated in force balance in metaphase bipolar spindle. Mol Biol Cell 9(11): 3211-3225.

Nakayama J, Xiao G, Noma K, Malikzay A, Bjerling P et al. (2003) Alp13, an MRG family protein, is a component of fission yeast Clr6 histone deacetylase required for genomic integrity. Embo J 22(11): 2776-2787.

Niccoli T, Yamashita A, Nurse P, Yamamoto M (2004) The p150-Glued Ssm4p regulates microtubular dynamics and nuclear movement in fission yeast. J Cell Sci 117(Pt 23): 5543-5556.

Nogales E, Wang HW (2006a) Structural intermediates in microtubule assembly and disassembly: how and why? Curr Opin Cell Biol 18(2): 179-184.

Nogales E, Wang HW (2006b) Structural mechanisms underlying nucleotide-dependent self-assembly of tubulin and its relatives. Curr Opin Struct Biol 16(2): 221-229.

Nogales E, Wolf SG, Downing KH (1998) Structure of the alpha beta tubulin dimer by electron crystallography. Nature 391(6663): 199-203.

O'Connor TM, Houston LL, Samson F (1974) Stability of neuronal microtubules to high pressure in vivo and in vitro. Proc Natl Acad Sci U S A 71(10): 4198-4202.

O'Toole ET, Winey M, McIntosh JR (1999) High-voltage electron tomography of spindle pole bodies and early mitotic spindles in the yeast Saccharomyces cerevisiae. Mol Biol Cell 10(6): 2017-2031.

O'Toole ET, McDonald KL, Mantler J, McIntosh JR, Hyman AA et al. (2003) Morphologically distinct microtubule ends in the mitotic centrosome of Caenorhabditis elegans. J Cell Biol 163(3): 451-456.

Omary MB, Coulombe PA, McLean WH (2004) Intermediate filament proteins and their associated diseases. N Engl J Med 351(20): 2087-2100.

Osumi M, Konomi M, Sugawara T, Takagi T, Baba M (2006) High-pressure freezing is a powerful tool for visualization of Schizosaccharomyces pombe cells: ultra-low temperature and low-voltage scanning electron microscopy and immunoelectron microscopy. J Electron Microsc (Tokyo) 55(2): 75-88.

Osumi M, Yamada N, Kobori H, Taki A, Naito N et al. (1989) Cell wall formation in regenerating protoplasts of Schizosaccharomyces pombe: study by high resolution, low voltage scanning electron microscopy. J Electron Microsc (Tokyo) 38(6): 457-468.

Ou Y, Rattner JB (2004) The centrosome in higher organisms: structure, composition, and duplication. Int Rev Cytol 238: 119-182.

Padte NN, Martin SG, Howard M, Chang F (2006) The cell-end factor pom1p inhibits mid1p in specification of the cell division plane in fission yeast. Curr Biol 16(24): 2480-2487.
Page R, Lindberg U, Schutt CE (1998) Domain motions in actin. J Mol Biol 280(3): 463-474.
Pelham RJ, Jr., Chang F (2001) Role of actin polymerization and actin cables in actin-patch movement in Schizosaccharomyces pombe. Nat Cell Biol 3(3): 235-244.
Pelletier L, O'Toole E, Schwager A, Hyman AA, Muller-Reichert T (2006) Centriole assembly in Caenorhabditis elegans. Nature 444(7119): 619-623.
Pereira G, Tanaka TU, Nasmyth K, Schiebel E (2001) Modes of spindle pole body inheritance and segregation of the Bfa1p-Bub2p checkpoint protein complex. Embo J 20(22): 6359-6370.
Perez F, Diamantopoulos GS, Stalder R, Kreis TE (1999) CLIP-170 highlights growing microtubule ends in vivo. Cell 96(4): 517-527.
Piel M, Meyer P, Khodjakov A, Rieder CL, Bornens M (2000) The respective contributions of the mother and daughter centrioles to centrosome activity and behavior in vertebrate cells. J Cell Biol 149(2): 317-330.
Pierre P, Pepperkok R, Kreis TE (1994) Molecular characterization of two functional domains of CLIP-170 in vivo. J Cell Sci 107 (Pt 7): 1909-1920.
Pierre P, Scheel J, Rickard JE, Kreis TE (1992) CLIP-170 links endocytic vesicles to microtubules. Cell 70(6): 887-900.
Popov AV, Pozniakovsky A, Arnal I, Antony C, Ashford AJ et al. (2001) XMAP215 regulates microtubule dynamics through two distinct domains. Embo J 20(3): 397-410.
Pringle JR, Bi E, Harkins HA, Zahner JE, De Virgilio C et al. (1995) Establishment of cell polarity in yeast. Cold Spring Harb Symp Quant Biol 60: 729-744.
Pruyne D, Legesse-Miller A, Gao L, Dong Y, Bretscher A (2004) Mechanisms of polarized growth and organelle segregation in yeast. Annu Rev Cell Dev Biol 20: 559-591.
Radcliffe P, Hirata D, Childs D, Vardy L, Toda T (1998) Identification of novel temperature-sensitive lethal alleles in essential beta-tubulin and nonessential alpha 2-tubulin genes as fission yeast polarity mutants. Mol Biol Cell 9(7): 1757-1771.
Rehberg M, Graf R (2002) Dictyostelium EB1 is a genuine centrosomal component required for proper spindle formation. Mol Biol Cell 13(7): 2301-2310.
Rhee DK, Cho BA, Kim HB (2005) ATP-binding motifs play key roles in Krp1p, kinesin-related protein 1, function for bi-polar growth control in fission yeast. Biochem Biophys Res Commun 331(2): 658-668.
Rickard JE, Kreis TE (1990) Identification of a novel nucleotide-sensitive microtubule-binding protein in HeLa cells. J Cell Biol 110(5): 1623-1633.
Rickard JE, Kreis TE (1991) Binding of pp170 to microtubules is regulated by phosphorylation. J Biol Chem 266(26): 17597-17605.
Robbins E, Gonatas NK (1964) Histochemical and Ultrastructural Studies on Hela Cell Cultures Exposed to Spindle Inhibitors with Special Reference to the Interphase Cell. J Histochem Cytochem 12: 704-711.
Rogalski AA, Singer SJ (1984) Associations of elements of the Golgi apparatus with microtubules. J Cell Biol 99(3): 1092-1100.

Roos UP (1975) Fine structure of an organelle associated with the nucleus and cytoplasmic microtubules in the cellular slime mould Polysphondylium violaceum. J Cell Sci 18(2): 315-326.

Rose A, Manikantan S, Schraegle SJ, Maloy MA, Stahlberg EA et al. (2004) Genome-wide identification of Arabidopsis coiled-coil proteins and establishment of the ARABI-COIL database. Plant Physiol 134(3): 927-939.

Rossanese OW, Reinke CA, Bevis BJ, Hammond AT, Sears IB et al. (2001) A role for actin, Cdc1p, and Myo2p in the inheritance of late Golgi elements in Saccharomyces cerevisiae. J Cell Biol 153(1): 47-62.

Rusan NM, Fagerstrom CJ, Yvon AM, Wadsworth P (2001) Cell cycle-dependent changes in microtubule dynamics in living cells expressing green fluorescent protein-alpha tubulin. Mol Biol Cell 12(4): 971-980.

Sagolla MJ, Uzawa S, Cande WZ (2003) Individual microtubule dynamics contribute to the function of mitotic and cytoplasmic arrays in fission yeast. J Cell Sci 116(Pt 24): 4891-4903.

Salmon ED (1975) Pressure-induced depolymerization of brain microtubules in vitro. Science 189(4206): 884-886.

Salmon ED, Goode D, Maugel TK, Bonar DB (1976) Pressure-induced depolymerization of spindle microtubules. III. Differential stability in HeLa cells. J Cell Biol 69(2): 443-454.

Sandberg K, Mastronarde DN, Beylkin G (2003) A fast reconstruction algorithm for electron microscope tomography. J Struct Biol 144(1-2): 61-72.

Sandblad L, Busch KE, Tittmann P, Gross H, Brunner D et al. (2006) The Schizosaccharomyces pombe EB1 homolog Mal3p binds and stabilizes the microtubule lattice seam. Cell 127(7): 1415-1424.

Sandin S, Ofverstedt LG, Wikstrom AC, Wrange O, Skoglund U (2004) Structure and flexibility of individual immunoglobulin G molecules in solution. Structure 12(3): 409-415.

Sawin KE, Nurse P (1998) Regulation of cell polarity by microtubules in fission yeast. J Cell Biol 142(2): 457-471.

Sawin KE, Snaith HA (2004) Role of microtubules and tea1p in establishment and maintenance of fission yeast cell polarity. J Cell Sci 117(Pt 5): 689-700.

Sawin KE, Tran PT (2006) Cytoplasmic microtubule organization in fission yeast. Yeast 23(13): 1001-1014.

Sawin KE, Lourenco PC, Snaith HA (2004) Microtubule nucleation at non-spindle pole body microtubule-organizing centers requires fission yeast centrosomin-related protein mod20p. Curr Biol 14(9): 763-775.

Schuyler SC, Pellman D (2001) Microtubule "plus-end-tracking proteins": The end is just the beginning. Cell 105(4): 421-424.

Schwartz C, Nicastro D, Ladinsky MS, Mastronarde D, O'Toole E et al. (2003) Cryo-Electron Tomography of Frozen-Hydrated Sections of Eukaryotic Cells. Microsc Microanal. pp. 1166-1167.

Shaw RM, Fay AJ, Puthenveedu MA, von Zastrow M, Jan YN et al. (2007) Microtubule plus-end-tracking proteins target gap junctions directly from the cell interior to adherens junctions. Cell 128(3): 547-560.

Sieberer BJ, Ketelaar T, Esseling JJ, Emons AM (2005) Microtubules guide root hair tip growth. New Phytol 167(3): 711-719.
Simon JR, Salmon ED (1990) The structure of microtubule ends during the elongation and shortening phases of dynamic instability examined by negative-stain electron microscopy. J Cell Sci 96 (Pt 4): 571-582.
Smertenko AP, Chang HY, Wagner V, Kaloriti D, Fenyk S et al. (2004) The Arabidopsis microtubule-associated protein AtMAP65-1: molecular analysis of its microtubule bundling activity. Plant Cell 16(8): 2035-2047.
Snaith HA, Sawin KE (2003) Fission yeast mod5p regulates polarized growth through anchoring of tea1p at cell tips. Nature 423(6940): 647-651.
Snaith HA, Samejima I, Sawin KE (2005) Multistep and multimode cortical anchoring of tea1p at cell tips in fission yeast. Embo J.
Snell V, Nurse P (1994) Genetic analysis of cell morphogenesis in fission yeast--a role for casein kinase II in the establishment of polarized growth. Embo J 13(9): 2066-2074.
Srayko M, O'Toole E T, Hyman AA, Muller-Reichert T (2006) Katanin disrupts the microtubule lattice and increases polymer number in C. elegans meiosis. Curr Biol 16(19): 1944-1949.
Steinbrecht RA (1993) Freeze-substitution for morphological and immunocytochemical studies in insects. Microsc Res Tech 24(6): 488-504.
Steinbrecht RAaM, M. (1987) Freeze substitution and freeze drying; Steinbrecht RA, editor. berlin: springer verlag. 149-172 p.
Steinmetz MO, Stoffler D, Hoenger A, Bremer A, Aebi U (1997) Actin: from cell biology to atomic detail. J Struct Biol 119(3): 295-320.
Studer D, Graber W, Al-Amoudi A, Eggli P (2001) A new approach for cryofixation by high-pressure freezing. J Microsc 203(Pt 3): 285-294.
Su LK, Burrell M, Hill DE, Gyuris J, Brent R et al. (1995) APC binds to the novel protein EB1. Cancer Res 55(14): 2972-2977.
Takagi T, Ishijima SA, Ochi H, Osumi M (2003) Ultrastructure and behavior of actin cytoskeleton during cell wall formation in the fission yeast Schizosaccharomyces pombe. J Electron Microsc (Tokyo) 52(2): 161-174.
Takamori S, Holt M, Stenius K, Lemke EA, Gronborg M et al. (2006) Molecular anatomy of a trafficking organelle. Cell 127(4): 831-846.
Takeda T, Chang F (2005) Role of fission yeast myosin I in organization of sterol-rich membrane domains. Curr Biol 15(14): 1331-1336.
Tanaka TU, Rachidi N, Janke C, Pereira G, Galova M et al. (2002) Evidence that the Ipl1-Sli15 (Aurora kinase-INCENP) complex promotes chromosome bi-orientation by altering kinetochore-spindle pole connections. Cell 108(3): 317-329.
Tanenbaum ME, Galjart N, van Vugt MA, Medema RH (2006) CLIP-170 facilitates the formation of kinetochore-microtubule attachments. Embo J 25(1): 45-57.
Tilney LG, Bryan J, Bush DJ, Fujiwara K, Mooseker MS et al. (1973) Microtubules: evidence for 13 protofilaments. J Cell Biol 59(2 Pt 1): 267-275.
Toda T, Umesono K, Hirata A, Yanagida M (1983) Cold-sensitive nuclear division arrest mutants of the fission yeast Schizosaccharomyces pombe. J Mol Biol 168(2): 251-270.

Tolic-Norrelykke IM, Sacconi L, Stringari C, Raabe I, Pavone FS (2005) Nuclear and division-plane positioning revealed by optical micromanipulation. Curr Biol 15(13): 1212-1216.

Tran PT, Doye V, Chang F, Inoue S (2000) Microtubule-dependent nuclear positioning and nuclear-dependent septum positioning in the fission yeast Schizosaccharomyces [correction of Saccharomyces] pombe. Biol Bull 199(2): 205-206.

Tran PT, Marsh L, Doye V, Inoue S, Chang F (2001) A mechanism for nuclear positioning in fission yeast based on microtubule pushing. J Cell Biol 153(2): 397-411.

Troxell CL, Sweezy MA, West RR, Reed KD, Carson BD et al. (2001) pkl1(+)and klp2(+): Two kinesins of the Kar3 subfamily in fission yeast perform different functions in both mitosis and meiosis. Mol Biol Cell 12(11): 3476-3488.

Tuszynski JA, Carpenter EJ, Huzil JT, Malinski W, Luchko T et al. (2006) The evolution of the structure of tubulin and its potential consequences for the role and function of microtubules in cells and embryos. Int J Dev Biol 50(2-3): 341-358.

Uzawa S, Li F, Jin Y, McDonald KL, Braunfeld MB et al. (2004) Spindle pole body duplication in fission yeast occurs at the G1/S boundary but maturation is blocked until exit from S by an event downstream of cdc10+. Mol Biol Cell 15(12): 5219-5230.

Vardy L, Toda T (2000) The fission yeast {gamma}-tubulin complex is required in G1 phase and is a component of the spindle assembly checkpoint. EMBO J 19(22): 6098-6111.

Venkatram S, Jennings JL, Link A, Gould KL (2005) Mto2p, a novel fission yeast protein required for cytoplasmic microtubule organization and anchoring of the cytokinetic actin ring. Mol Biol Cell 16(6): 3052-3063.

Verde F, Mata J, Nurse P (1995) Fission yeast cell morphogenesis: identification of new genes and analysis of their role during the cell cycle. J Cell Biol 131(6 Pt 1): 1529-1538.

Vogel SK, Raabe I, Dereli A, Maghelli N, Tolic-Norrelykke I (2007) Interphase Microtubules Determine the Initial Alignment of the Mitotic Spindle. Curr Biol.

Wachtler V, Rajagopalan S, Balasubramanian MK (2003) Sterol-rich plasma membrane domains in the fission yeast Schizosaccharomyces pombe. J Cell Sci 116(Pt 5): 867-874.

Walker RA, O'Brien ET, Pryer NK, Soboeiro MF, Voter WA et al. (1988) Dynamic instability of individual microtubules analyzed by video light microscopy: rate constants and transition frequencies. J Cell Biol 107(4): 1437-1448.

Walther P, Ziegler A (2002) Freeze substitution of high-pressure frozen samples: the visibility of biological membranes is improved when the substitution medium contains water. J Microsc 208(Pt 1): 3-10.

Wang PJ, Huffaker TC (1997) Stu2p: A microtubule-binding protein that is an essential component of the yeast spindle pole body. J Cell Biol 139(5): 1271-1280.

Wehland J, Henkart M, Klausner R, Sandoval IV (1983) Role of microtubules in the distribution of the Golgi apparatus: effect of taxol and microinjected anti-alpha-tubulin antibodies. Proc Natl Acad Sci U S A 80(14): 4286-4290.

Weir BA, Yaffe MP (2004) Mmd1p, a novel, conserved protein essential for normal mitochondrial morphology and distribution in the fission yeast Schizosaccharomyces pombe. Mol Biol Cell 15(4): 1656-1665.

Wiese C, Zheng Y (2000) A new function for the gamma-tubulin ring complex as a microtubule minus-end cap. Nat Cell Biol 2(6): 358-364.

Wiese C, Zheng Y (2006) Microtubule nucleation: gamma-tubulin and beyond. J Cell Sci 119(Pt 20): 4143-4153.

Wilson PD (1997) Epithelial cell polarity and disease. Am J Physiol 272(4 Pt 2): F434-442.

Wood V, Gwilliam R, Rajandream MA, Lyne M, Lyne R et al. (2002) The genome sequence of Schizosaccharomyces pombe. Nature 415(6874): 871-880.

Yaffe MP, Stuurman N, Vale RD (2003) Mitochondrial positioning in fission yeast is driven by association with dynamic microtubules and mitotic spindle poles. Proc Natl Acad Sci U S A 100(20): 11424-11428.

Yaffe MP, Harata D, Verde F, Eddison M, Toda T et al. (1996) Microtubules mediate mitochondrial distribution in fission yeast. Proc Natl Acad Sci U S A 93(21): 11664-11668.

Yamaguchi M, Biswas SK, Suzuki Y, Furukawa H, Sameshima M et al. (2002) The spindle pole body duplicates in early G1 phase in the pathogenic yeast Exophiala dermatitidis: an ultrastructural study. Exp Cell Res 279(1): 71-79.

Yamamoto A, West RR, McIntosh JR, Hiraoka Y (1999) A cytoplasmic dynein heavy chain is required for oscillatory nuclear movement of meiotic prophase and efficient meiotic recombination in fission yeast. J Cell Biol 145(6): 1233-1249.

Yamashita A, Yamamoto M (2006) Fission yeast Num1p is a cortical factor anchoring dynein and is essential for the horse-tail nuclear movement during meiotic prophase. Genetics 173(3): 1187-1196.

Yamashita A, Sato M, Fujita A, Yamamoto M, Toda T (2005) The roles of fission yeast ase1 in mitotic cell division, meiotic nuclear oscillation, and cytokinesis checkpoint signaling. Mol Biol Cell 16(3): 1378-1395.

Yan X, Habedanck R, Nigg EA (2006) A complex of two centrosomal proteins, CAP350 and FOP, cooperates with EB1 in microtubule anchoring. Mol Biol Cell 17(2): 634-644.

Zigmond SH (2004) Beginning and ending an actin filament: control at the barbed end. Curr Top Dev Biol 63: 145-188.

Zimmerman S, Chang F (2005) Effects of {gamma}-tubulin complex proteins on microtubule nucleation and catastrophe in fission yeast. Mol Biol Cell 16(6): 2719-2733.

Zimmerman S, Tran PT, Daga RR, Niwa O, Chang F (2004) Rsp1p, a J domain protein required for disassembly and assembly of microtubule organizing centers during the fission yeast cell cycle. Dev Cell 6(4): 497-509.

Supplementary table: Length of major bundles in wild type fission yeast

Cell	Major bundle length (µm)	Major bundle length (% of cell length)
Cell 1 (6,7 µm)	5.62	84
	6.05	90
	5.03	75
	2.38	35
Cell 2 (7,7 µm)	5.16	67
	7.03	91
	4.75	62
Cell 3 (7,9 µm)	5.27	67
	4.46	56
	2.31	29
Cell 4 (7,4 µm)	5,68	77
	5,86	79
Average	**4.97**	**68**
Standard deviation	**1.39**	**20**

Acknowledgements

First and foremost I want to thank my supervisor Claude Antony for supporting me throughout this work.

I am also very grateful to Damian Brunner and Richard McIntosh for scientific input and inspiration. Additional thanks to Damian also for organizing great retreats!

Special thanks go to Cindi Schwartz for believing in my ideas and providing practical solutions, as well as convincing the people that needed to be convinced. Also, to Daniela Nicastro who provided strong support on many occasions but especially on the last night on the microscope when I still had not been able to acquire a full cell volume.

Thanks also to:

Uta Haselmann-Weiß, Helio Roque, Xavier Heiligengeist, Charlotta Funaya, Wandrille Amaury-George, Catarina Resende and Diana Scholz for being very nice lab colleagues.

David Mastronarde for developing the software to our needs; Eileen O'Toole for sharing her experience in using iMOD; Mark Ladinsky and Garry Morgan for showing me tricks in serial sectioning and Mary Morphew for sharing her data and spending her Saturdays with me in the lab,

The undergraduate students who have been participating in this work: Angela Noon, Christopher Bleck and Abhay Kotecha,

The TAC committee: Claude Antony, Harald Herrmann-Lerdon, Damian Brunner, Andreas Hönger

The thesis defense committee: Harald Herrmann-Lerdon, Damian Brunner, John Briggs and Elmar Schiebel

The pompom club, the most relaxed, cake-eating, fun, board-game playing bunch of pombe colleagues around! Linda Sandblad, Emanuel Busch, Dietrich Foethke, Lindsay Murrells, Helio Roque, Tanja Georg, Andréia Feijão, Paulo Alves, Tatyana Makushok and Aynur Kaya,

Matthew Betts, Diana Scholz, Vienna Leigh and Lindsay Murrells for proof reading sections of this work, and to Diana Scholz again for translating the German introduction,

My family and grandparents who have helped me by taking care of my house and being very supportive through this time: Annika, Greger, Ann-Britt, Therese, Victor, Adam, Mona, Morgan, Ylva, Lars, Yvonne, Stabben and Siv,

Marianne Uteng, Malgosia Dusczcyk, Vienna Leigh, Matthew Betts, Cameron Mackereth, Sean Hooper and Chris Creevey for a thousand times sushi and beer!

The E-STAR program for financial funding and EMBL, the best employer ever.